Thesis for the degree of Doctor of Philosophy

Phase-Sensitive Fiber Optic Parametric Amplifiers and Their Applications in Optical Communication

Carl Lundström

Photonics Laboratory,
Department of Microtechnology and Nanoscience (MC2),
Chalmers University of Technology
Göteborg, Sweden, 2012

Phase-Sensitive Fiber Optic Parametric Amplifiers and Their Applications in Optical Communication

Carl Lundström

Göteborg, August 2012

ISBN 978-91-7385-730-7

Technical Report MC2-233
ISSN 1652-0769

Doktorsavhandling vid Chalmers Tekniska Högskola
Ny serie 3411
ISSN 0346-718X

Photonics Laboratory,
Department of Microtechnology and Nanoscience (MC2)
Chalmers University of Technology, SE-412 96 Göteborg, Sweden
Phone: +46 (0) 31 772 1000

Front cover illustration: Experimentally measured complex-space trajectories of the signal output in a phase-insensitive, unsaturated phase-sensitive and saturated phase-sensitive FOPA.

Printed by Bibliotekets reproservice, Chalmers University of Technology
Göteborg, Sweden, August, 2012

Phase-Sensitive Fiber Optic Parametric Amplifiers and Their Applications in Optical Communication

Carl Lundström

Photonics Laboratory,
Department of Microtechnology and Nanoscience (MC2)
Chalmers University of Technology, SE-412 96 Göteborg, Sweden

Abstract

This thesis deals with experimental and theoretical aspects of the phase-sensitive fiber optic parametric amplifier (FOPA) and their applications. FOPAs can be operated as both phase-insensitive and phase-sensitive amplifiers (PSAs), with the latter requiring phase-locked input waves, which, until recently, has limited their practical use. Based on the realization that a phase-insensitive FOPA, called the copier, can generate the phase-locked waves required, several applications of a copier-PSA configuration are proposed and demonstrated. These include phase excursion amplification, ultra-low noise amplification, and, by using the copier for carrier recovery, black-box all-optical phase- and amplitude regeneration.

A large part of this thesis deals with characterization of the PSA. The copier-PSA configuration is useful in this regard, since, by modulating the signal in between the copier and PSA, the phase-response of the PSA can be studied. The output signal was investigated both in terms of amplitude and phase, using a coherent receiver.

Finally, methods to suppress stimulated Brillouin scattering (SBS) in highly nonlinear fibers (HNLFs) are investigated. Without suppression, SBS will severely limit the available pump power for parametric amplification. The most common way to suppress the SBS is to increase the spectral width of the pump, but this is undesirable in phase-sensitive amplification and many other applications. Therefore, the application of a strain gradient to the fibers to decrease the SBS is studied, together with the resulting trade-offs. A cascade of HNLFs with strain gradients, separated by low-loss and low-dispersion isolators is proposed and evaluated, with a large increase in the SBS threshold demonstrated.

Keywords: fiber nonlinearities, fiber optic parametric amplification, four-wave mixing, phase-sensitive amplification, nonlinear optical signal processing, phase regeneration, stimulated Brillouin scattering

List of papers

This thesis is based on the following appended papers:

[A] J. Kakande, **C. Lundström**, P.A. Andrekson, Z. Tong, M. Karlsson, P. Petropoulos, F. Parmigiani, and D.J. Richardson, "Detailed characterization of a fiber-optic parametric amplifier in phase-sensitive and phase-insensitive operation," *Opt. Exp.*, vol. 18, no. 5, pp. 4130-4137, Jan. 2010. (Also presented at the European Conference on Optical Communication (ECOC), Vienna, Austria, Paper Mo.1.1.1, 2009.)

[B] **C. Lundström**, Z. Tong, M. Karlsson, and P.A. Andrekson, "Phase-to-phase and phase-to-amplitude transfer characteristics of a nondegenerate-idler phase-sensitive amplifier," *Opt. Lett.*, vol. 36, no. 22, pp. 4356-4358, Nov. 2011. (Also presented at the European Conference on Optical Communication (ECOC), Torino, Italy, Paper Th.10.C.1, 2010.)

[C] Z. Tong, **C. Lundström**, C.J. McKinstrie, P.A. Andrekson, M. Karlsson, and A. Bogris, "Ultralow noise, broadband phase-sensitive optical amplifiers and their applications" (Invited paper), *IEEE J. Select. Topics Quantum Electron.*, vol. 18, no. 2, pp. 1016-1032, March 2012.

[D] **C. Lundström**, B. Corcoran, M. Karlsson, and P.A. Andrekson, "Phase and amplitude characteristics of a phase-sensitive amplifier operating in gain saturation," Submitted to *Opt. Exp.*, June 2012. (Also presented at the European Conference on Optical Communication (ECOC), Geneva, Switzerland, Paper Th.11.LeCervin.4, 2011.)

[E] R. Slavík, F. Parmigiani, J. Kakande, **C. Lundström**, M. Sjödin, P.A. Andrekson, R. Weerasuriya, S. Sygletos, A.D. Ellis, L. Grüner-Nielsen, D. Jakobsen, S. Herstrøm, R. Phelan, J. O'Gorman, A. Bogris, D. Syvridis, S. Dasgupta, P. Petropoulos, and D.J. Richardson, "All-optical phase and amplitude regenerator for next-generation telecommunications systems," *Nat. Photon.*, vol. 4, pp. 690-695, Oct. 2010.

[F] **C. Lundström**, Z. Tong, and P.A. Andrekson, "Optical modulation signal enhancement using a phase sensitive amplifier," *Optical Fiber Communication Conference (OFC)*, Los Angeles, CA, Paper OWL6, 2011.

[G] **C. Lundström**, B. Corcoran, S.L.I. Olsson, Z. Tong, M. Karlsson, and P.A. Andrekson, "Short-pulse amplification in a phase-sensitive amplifier," *Optical Fiber Communication Conference (OFC)*, Los Angeles, CA, Paper OTh1C.1, 2012.

[H] Z. Tong, **C. Lundström**, P.A. Andrekson, C.J. McKinstrie, M. Karlsson, D.J. Blessing, E. Tipsuwannakul, B.J. Puttnam, H. Toda, and L. Grüner-Nielsen, "Towards ultrasensitive optical links enabled by low-noise phase-sensitive amplifiers," *Nat. Photon.*, vol. 5, pp. 430-436, June 2011.

[I] **C. Lundström**, E. Myslivets, A.O.J. Wiberg, N. Alic, S. Radic, M. Karlsson, and P.A. Andrekson, "Tension-optimized highly nonlinear fibers for parametric applications," Accepted to *European Conference on Optical Communication (ECOC)*, Amsterdam, The Netherlands, 2012.

[J] **C. Lundström**, R. Malik, L. Grüner-Nielsen, B. Corcoran, S.L.I. Olsson, M. Karlsson, and P.A. Andrekson "Fiber optic parametric amplifier with 10 dB net gain without pump dithering" To be submitted to *IEEE Photon. Technol. Lett.*, August 2012.

Related papers by the author not included in the thesis:

[K] J.M. Chavéz Boggio, **C. Lundström**, J. Yang, H. Sunnerud, and P.A. Andrekson "Double-pumped FOPA with 40 dB flat gain over 81 nm bandwidth," European Conference on Optical Communication (ECOC), Brussels, Belgium, Paper Tu.3.B.5, 2008.

[L] E. Myslivets, **C. Lundström**, J. Aparicio, S. Moro, A.O.J. Wiberg, C.-S. Brès, N. Alic, P.A. Andrekson, and S. Radic Spatial equalization of zero-dispersion wavelength profiles in nonlinear fibers *IEEE Photon. Technol. Lett.*, vol. 21, no. 24, pp. 1807-1809, Oct. 2009.

[M] Z. Tong, **C. Lundström**, A. Bogris, M. Karlsson, P.A. Andrekson, and D. Syvridis, "Measurement of sub-1 dB noise-figure in a non-degenerate cascaded fibre parametric amplifier," *European Conference on Optical Communication (ECOC)*, Vienna, Austria, Paper M.1.1.2, Sept. 2009.

[N] E. Myslivets, **C. Lundström**, S. Moro, A. Wiberg, C.-S, Brès, N. Alic, P.A. Andrekson and S. Radic, "Dispersion fluctuation equalization of nonlinear fibers

by spatially controlled tension," Optical Fiber Communications Conference (OFC), San Diego, CA, USA, Paper OTuA5, March 2010.

[O] F. Parmigiani, R. Slavík, J. Kakande, **C. Lundström**, M. Sjödin, P.A. Andrekson, R. Weerasuriya, S. Sygletos, A.D. Ellis, L. Grüner-Nielsen, D. Jakobsen, S. Herstrom, R. Phelan, J. O'Gorman, A. Bogris, D. Syvridis, S. Dasgupta, P. Petropoulos, and D.J. Richardson, "All-optical phase regeneration of 40 Gbit/s DPSK signals in a black-box phase sensitive amplifier," Optical Fiber Communications Conference (OFC), San Diego, CA, USA, Post-Deadline Paper PDPC3, March 2010.

[P] Z. Tong, A. Bogris, **C. Lundström**, C.J. McKinstrie, M. Vasilyev, M. Karlsson, and P.A. Andrekson, "Noise-figure measurement in phase-insensitive and phase-sensitive fiber parametric amplifier cascade," Optical Fiber Communications Conference (OFC), San Diego, CA, USA, Paper OWT4, March 2010.

[Q] Z. Tong, **C. Lundström**, E. Tipsuwannakul, M. Karlsson, and P.A. Andrekson, "Phase-sensitive amplified DWDM DQPSK signals using free-running lasers with 6-dB link SNR improvement over EDFA-based systems," European Conference on Optical Communication (ECOC), Torino, Italy, Post-deadline paper PDP1.3, 2010.

[R] P.A. Andrekson, **C. Lundström**, and Z. Tong, "Phase-sensitive fiber-optic parametric amplifiers and their applications" (Invited paper), European Conference on Optical Communication (ECOC), Torino, Italy, Paper We.6.E.1, 2010.

[S] Z. Tong, A. Bogris, **C. Lundström**, C.J. McKinstrie, M. Vasilyev, M. Karlsson, and P.A. Andrekson, "Modeling and measurement of the noise figure of a cascaded non-degenerate phase-sensitive parametric amplifier," *Opt. Exp.*, vol. 18, no. 14, pp. 14820-14835, July 2010.

[T] Z. Tong, C.J. McKinstrie, **C. Lundström**, M. Karlsson, and P.A. Andrekson, "Noise performance of optical fiber transmission links that use non-degenerate cascaded phase-sensitive amplifiers," *Opt. Exp.*, vol. 18, no. 15, pp. 15426-15439, July 2010.

[U] Z. Tong, **C. Lundström**, M. Karlsson, M. Vasilyev, and P.A. Andrekson, "Noise performance of a frequency nondegenerate phase-sensitive amplifier with unequalized inputs," *Opt. Lett.*, vol. 36, no. 5, pp. 722-724, March 2010.

[V] Z. Tong, **C. Lundström**, M. Karlsson, and P.A. Andrekson, "Impact of zero-dispersion-wavelength distributions on the noise figure nonreciprocity of a fiber parametric amplifier," *IEEE Photon. Technol. Lett.*, vol. 23, no. 6, pp. 365-367, March 2011.

[W] S.L.I. Olsson, B. Corcoran, **C. Lundström**, E. Tipsuwannakul, S. Sygletos, A.D. Ellis, Z. Tong, M. Karlsson, and P.A. Andrekson, Optical injection-locking-based pump recovery for phase-sensitively amplified links, Optical Fiber Communications Conference (OFC), Los Angeles, CA, USA, Paper OW3C.3, March 2012.

[X] B. Corcoran, S.L.I. Olsson, **C. Lundström**, M. Karlsson, and P.A. Andrekson,, Phase-sensitive optical pre-amplifier implemented in an 80km DQPSK link, Optical Fiber Communications Conference (OFC), Los Angeles, CA, USA, Post-deadline paper PDP5A.4, March 2012.

[Y] S.L.I. Olsson, B. Corcoran, **C. Lundström**, M. Sjödin, M. Karlsson, and P.A. Andrekson, "Phase-sensitive amplified optical link operating in the nonlinear transmission regime," Accepted to *European Conference on Optical Communication (ECOC)*, Amsterdam, The Netherlands, 2012.

[Z] T. Richter, B. Corcoran, S.L.I. Olsson, **C. Lundström**, M. Karlsson, C. Schubert, and P.A. Andrekson, "Experimental characterization of a phase-sensitive four-mode fiber-optic parametric amplifier," Accepted to *European Conference on Optical Communication (ECOC)*, Amsterdam, The Netherlands, 2012.

Acknowledgement

Many people around the world have been instrumental in supporting and guiding me during the five years of work upon which this thesis is based, and it should in part be considered a product of their efforts. First of all, I want to thank my supervisors, Prof. Peter A. Andrekson and Prof. Magnus Karlsson for accepting me as a Ph.D. student and continuously supporting and assisting me from the start and all the way until the completion of this thesis. Good supervisors makes a world of difference during one's studies, and I have been very fortunate in this regard.

Dr. Zhi Tong, with whom I had the privilege to work a great deal with deserves a very special thanks for being so helpful in the lab, and for many stimulating and fruitful discussions. Thanks also to Bill Corcoran, Pontus Johannisson, Henrik Sunnerud, Per-Olof Hedekvist and the many other current and former fiber group members who have worked with me or helped me in many ways. All the people at the Photonics Lab deserves a mention for the many memorable times on and off work. Thanks especially to my great office-mates Martin Sjödin and Ekawit Tipsuwannakul. Other fellow Ph.D. students I would be remiss not to mention include Krzysztof Szczerba, Samuel Olsson, and Tobias Eriksson.

We have had many visitors here at Chalmers who have helped and taught me a lot. I am grateful to all of them and especially would like to acknowledge José Manuel Chavez Boggio, Hiroyuki Toda and Ben Puttnam.

I would also like to thank Prof. Stojan Radic, Nikola Alic, Andreas Wiberg, Evgeny Myslivets and the others at the University of California at San Diego for having me as a two-time visitor, both very exciting stays.

Many thanks are due to Lars Grüner-Nielsen of OFS Fitel Denmark for being so helpful with our very specific wishes for highly nonlinear fibers, and for inviting me for several visits to their labs in Copenhagen. Another group I want to thank for great collaboration is Prof. David J. Richardson's at the Optoelectronics Research Centre, University of Southampton, especially Joseph Kakande, with whom I have collaborated a lot during mutual visits. Indeed, thanks to Radan Slavík, Adonis Bogris, Andrew Ellis, and everyone else involved in the successful PHASORS project. I feel very fortunate to have participated in it!

Last, but not least, I would like to thank my friends and family.

Carl Lundström

Göteborg
August 2012

This work was financially supported by the European Comission STREP Project PHASORS (FP7-ICT-2007-2 22457), the Air Force Office of Scientific Research, Air Force Material Command, USAF, under grant number FA8655-09-1-3076, the European Research Council (ERC) Advanced Grant PSOPA (291618), the Swedish Foundation for International Cooperation in Research and Higher Education (STINT), and also by the Swedish Research Council (VR).

OFS Fitel Denmark ApS and Sumitomo Electric Industries, Ltd are gratefully acknowledged for providing highly nonlinear fibers.

Abbreviations used in the text

AN	Amplitude Noise
ASE	Amplified Stimulated Emission
AQN	Amplified Quantum Noise
CW	Continuous Wave
DFG	Difference-Frequency Generation
DSP	Digital Signal Processing
EDFA	Erbium-Doped Fiber Amplifier
FOPA	Fiber Optic Parametric Amplifier
FWM	Four-Wave Mixing
GAWBS	Guided Acoustic-Wave Brillouin Scattering
GVD	Group-Velocity Dispersion
HNLF	Highly Nonlinear Fiber
NF	Noise Figure
NLSE	Noonlinear Schrödinger Equation
OBPF	Optical Bandpass Filter
OSNR	Optical Signal-to-Noise Ratio
PCF	Photonic Crystal Fiber
PI	Phase-Insensitive
PM	Phase Modulation/Modulator
PMD	Polarization-Mode Dispersion
PN	Phase Noise
PS	Phase-Sensitive
PSA	Phase-Sensitive Amplification/Amplifier
PSK	Phase-Shift Keying
PZT	Piezo-Electric Transducer
QAM	Quadrature Amplitude Modulation
RF	Radio Frequency
SBS	Stimulated Brillouin Scattering
SFG	Sum-Frequency Generation

SHG	Second Harmonic Generation
SMF	Single-Mode Fiber
SNR	Signal-to-Noise Ratio
SOP	State of Polarization
SPM	Self-Phase Modulation
SRS	Stimulated Raman Scattering
WDM	Wavelength Division Multiplexing/Multiplexer
XPM	Cross-Phase Modulation
ZDW	Zero-Dispersion Wavelength

Table of contents

Chapter 1

Introduction

The advent of the low-loss optical fiber proposed in 1966 [1] and realized in the early seventies [2, 3] not only ushered in a revolution in human communication, but also spurred much fundamental research into their properties and how light behaves as it propagates through them. Optical communication (telecom, datacom) is the most important application for optical fibers and much of the research work regarding optical fibers was and is conducted in the context of communications. Indeed, the work upon which this thesis is based also concerns a fiber property, namely the Kerr nonlinearity (also called the third-order nonlinearity), the parametric nonlinear interactions it gives rise to, and their use for optical communications-applications.

The field of modern optics, including the studies of most optical nonlinearities, started in 1960 with the invention of the laser [4]. Normally, the photons that make up an optical wave can propagate without interacting with each other, but when the number of photons per unit time (i.e. the optical intensity) become very large, the nonlinear response of the medium will start playing a role, which can couple the optical waves and make them interact with one another. Such nonlinearities can be extremely fast, with response times on the scale of femtoseconds, which opens up the possibility for ultrafast all-optical applications that are typically not possible in electronic devices, which are limited by the much slower speed of the electronics.

Parametric nonlinear effects in nonlinear optical media (crystals) was studied soon after the first laser was realized [5–7] and fiber-based parametric effects have been a topic of active research since the availability of low-loss optical fibers [8, 9]. In fiber-optical communications systems, fiber nonlinearities can be a detrimental effect, but the nonlinearities can also be exploited for many different applications. Parametric effects in either nonlinear crystals or in fibers can be used for signal

amplification as well as for many different all-optical signal processing applications. However, fiber-based nonlinear devices are more easily made compatible with existing fiber-based communications systems. Hence, for telecommunications, parametric effects in fibers have long been one of the main focuses for research on nonlinear signal processing, with many pioneering demonstrations in the 1990s of applications of parametric effects in fibers, such as demultiplexing [10], sampling [11], phase conjugation [12] and wavelength conversion [13]. However, the efficiency of those devices was often not good, until advances in nonlinear fibers around the turn of the century [14–17] made them more practical and capable of large and broadband net gains [18,19]. Many new signal processing applications in fibers have since emerged, such as signal amplitude regeneration [20–22], multicasting [23], all-optical tunable delays [24] and format conversion through phase erasure [25], to name a few.

In particular, parametric amplification offers the possibility of phase-sensitive amplification (PSA), something of the holy grail in amplification, because of their ability to amplify without adding excess noise, whereas all other amplifiers add noise to the signal, thereby degrading its signal-to-noise ratio (SNR) [26]. Phase-sensitive amplification means amplification that is dependent on the phase of the optical signal. Signal photons with a certain phase will be amplified while photons in the opposite quadrature will be de-amplified. PSAs are based on the parametric nonlinearity in a nonlinear medium and can thus be implemented in both nonlinear crystals and in optical fibers of various kinds, as well as optical waveguides (e.g. silicon). PSAs have long been considered an exotic type of amplifier mainly because of the difficult requirement of having phase-synchronized waves at the input, and thus not so excessively studied experimentally previously, beyond simpler proof-of-concept experiments.

In addition to noiseless amplification, another important application for PSAs is the regeneration of the optical phase, i.e. since only certain phase states will be amplified, deviations from this state (i.e. phase noise) will be reduced. Phase regeneration have been a topic of interest in telecommunications, as phase-encoded signals have become more common, with phase noise often being a limiting factor for the performance of optical communications links. Phase regeneration is not easy to accomplish otherwise, without first converting the phase information to amplitude, and subsequently regenerating the amplitude. This additional step is undesirable, and PSAs make it possible to regenerate the phase directly.

Fiber-based PSAs, unlike those based on nonlinear crystals, can be operated in two fundamentally different ways; either being sensitive to the absolute signal phase and thus regenerate the signal phase, or being insensitive to the absolute phase which enables noiseless amplification of all phase-states of the signal. In this thesis, both kinds are studied.

The PSA is a new type of optical amplifier, and thus fundamental studies of its properties and abilities are a prerequisite for further, more applications-oriented, research and development. In this thesis, PSAs are studied in a communications context, and applications in optical communications are discussed and evaluated. However, other large fields where optics play an important role include sensing, test-and-measurement and spectroscopy. Additionally, fields such as photon counting and quantum communications are other potential use-cases for ultralow-noise amplification. Moreover, since PSAs can be implemented in a number of different nonlinear media, they can be made to operate over different wavelength ranges, dictated only by the dispersive properties of the chosen medium. The potential of e.g. low-noise amplification in essentially arbitrary wavelength ranges offered by PSAs may prove useful in the applications mentioned above, or in any application where low levels of light need to be amplified and/or detected with high fidelity. With PSAs being the immature technology it is today, an increase in the general understanding of their potential performance and what is required to reach this performance in practice should be beneficial regardless of intended application or wavelength range of interest.

1.1 This thesis

This thesis is based on ten appended papers. The driving motivation for the work in Papers [A-H] has been to understand the fundamental behavior and performance of phase-sensitive parametric amplifiers and to identify and demonstrate possible applications and benefits in a communications context, but also to realize PSAs with performance comparable or better in many important aspects than other state-of-the-art optical amplifiers. To this end, an experimental configuration which we refer to as the copier - mid-stage - PSA is used. The "copier" generates a phase-correlated idler wave that is needed to ensure phase-sensitivity in the PSA. Essentially, this configuration is phase-insensitive as a whole, but phase-sensitive to any phase-shifts or phase decorrelations that is introduced in the mid-stage. We investigate the phase-to-phase and phase-to-amplitude transfer functions of the PSA by introducing a phase modulation in the mid-stage, and investigate the noise properties of the PSA by decorrelating the waves by a large loss in the mid-stage. The exception is Paper [E], in which a black-box PSA-based phase regenerator was constructed. Black-box here means that the regenerator was sensitive to the phase of the incoming signal, and that the free-running signal is the only input needed to the regenerator. Finally, Papers [I-J] concerns the suppression of another nonlinear effect, stimulated Brillouin scattering (SBS), which is a large limiting factor for the performance of

fiber-based parametric amplifiers, as it will significantly limit the available pump power. It can be suppressed by spectral broadening of the pump; however, this is very problematic for phase-sensitive amplifiers that require very good control of the phases of the interacting waves. Hence, new, passive, methods are needed to suppress the SBS.

Outline

This thesis is organized as follows: Chapter 2 introduces the fundamental theory of optical propagation through a fiber that is relevant for this work, and its physical origin. This includes linear effects and the nonlinear effects of self- and cross-phase modulation, four-wave mixing (the basis of parametric effects in fibers), as well as nonlinear scattering effects. Chapter 3 delves into further detail on one of the scattering nonlinearities, stimulated Brillouin scattering, as well as a discussion on how to suppress it and the trade-offs involved. An overview of phase-sensitive amplification in fibers, and various implementations, including the copier-PSA structure follows in Chapter 4. In Chapter 5, we discuss potential applications of PSAs, both in communications and in other fields, as well as other potential nonlinear media that may be developed and used to implement PSAs. We also discuss practical implementation issues that should be addressed, as well as topics in need of further investigation. Finally, in Chapter 6, the appended papers are summarized.

Chapter 2

Fiber dispersion and nonlinearities

SINCE this work deals with fiber-based devices, we describe the propagation effects affecting a light wave in optical (silica-based) fibers in this chapter. Fundamentally, these effects can be divided into linear and nonlinear effects. While nonlinear effects are the main topic of this thesis, the interplay between linear and nonlinear effects form the basis of many of the investigated phenomena. Linear effects include attenuation and chromatic dispersion (the spreading out in time of different frequency components), but also polarization-mode dispersion (PMD). Common for the linear effects is that they occur independently for each frequency component in the fiber, and are not affected by other waves (at other frequencies) also present. The nonlinear effects are so-called since they are dependent on the optical power of the wave(s) in the fiber, meaning that one wave can affect the properties of another, and that power can be transferred between optical waves of different frequencies during propagation, and even introduce components at frequencies not originally present. Throughout this thesis, we concern ourselves only with *single-mode fibers*, in which only one spatial mode can propagate (at least at the frequencies we consider). The modes represent different solutions to the Maxwell equations with the boundary conditions given by the physical properties of the fiber.

The nonlinear effect that we mostly concern ourselves with in this work is the *Kerr nonlinearity*, which modifies the index of refraction in response to the intensity (i.e. power) in the fiber. The refractive index is usually written as

$$n(\omega, I) = n(\omega) + n_2 I, \tag{2.1}$$

where ω and I is the frequency and intensity of the optical wave, respectively. The linear (dispersive) part of the refractive index is 1 in free space, and approximately 1.5 in optical fibers. The nonlinear refractive index n_2 is on the order of 10^{-20} m^2/W in silica-based optical fibers, and can be increased somewhat by doping the silica with GeO_2 [27, p. 17]. The large difference in magnitude of the linear and nonlinear part means that large intensities are required for nonlinear effects to play a significant role.

From Eq. 2.1 it is also evident how the aforementioned interplay between linear and nonlinear effects arises. Since the propagation speed of an optical wave is given by the refractive index, which changes with frequency and power of the wave, the change in phase of the wave as it propagates is also dependent on its frequency and power. The phase-shifts a wave imposes on itself and on other waves are called *self-phase modulation* and *cross-phase modulation* (SPM and XPM), respectively. The coupling between several waves through this nonlinearity is called *four-wave mixing* (FWM). FWM can be described as the the periodic modulation of the refractive index by the beating frequency of two waves, since the local intensity in the fiber varies at this beat note. Thus, the relative phase of the interacting waves become important, leading to both the concept of phase-matching as well as the phase-sensitive effects that are important parts of this thesis.

As the nonlinearities are dependent on the intensity and thus the area of the optical beam, the *nonlinearity coefficient* is commonly used as a measure of how strong the nonlinear effects of a particular fiber are. It is denoted by γ and written as

$$\gamma = \frac{2\pi n_2}{\lambda A_{\text{eff}}}, \tag{2.2}$$

where λ represents the signal wavelength, and A_{eff} is the effective area of the mode of the optical wave in the fiber. Conventional single-mode fibers (SMFs) used in transmission usually have a γ of around 1-3 $W^{-1}km^{-1}$ [27, p. 424].

There is also another class of nonlinear effects in optical fibers, namely the inelastic scattering processes, in which the optical wave transfers part of its energy to a phonon (vibrational quantum) in the fiber. *Raman scattering* describes scattering against optical phonons, while *Brillouin scattering* describes scattering against acoustic phonons. Especially Brillouin scattering can be a detrimental effect for building fiber-based devices based on the Kerr nonlinearity; hence, we devote Chapter 3 to further describing the phenomenon, its adverse effect in these cases, and how it can be suppressed.

Nonlinear fibers

It should be noted that in optical communications systems, fiber nonlinearities are typically considered an unwanted effect that should be minimized. On the other hand, nonlinearities can also be exploited for e.g. amplification and signal processing applications. In those cases, so-called *highly nonlinear fibers* (HNLFs) are often used in purpose-built nonlinear devices (rather than in the transmission fiber). They are fibers designed to have a large nonlinearity coefficient, between 10-20 $\mathrm{W^{-1}km^{-1}}$, usually achieved by decreasing the effective area of the fiber. This increases the magnitude of both the Kerr and the scattering nonlinearities, however.

There is also a large ongoing effort in developing other types of nonlinear fibers with even larger nonlinearity coefficients, for example fibers based on materials other than SiO_2, such as BiO_2 [28, 29], which have a larger nonlinear index, and also Photonic Crystal Fibers (PCFs), sometimes called holey fibers [30–32], in which there are holes along the propagation direction, making the effective area very small. Very high nonlinearities ($\gamma \approx 100 - 1000$ $\mathrm{W^{-1}km^{-1}}$) can be achieved in such fibers [33], allowing short lengths of fiber to be used and thus avoiding non-uniformity problems such as varying dispersion. However, there are other issues with such novel fibers, most notably the attenuation, which can be very large, sometimes several dB/m. Another problem is that it can be difficult to achieve a low splice or coupling loss to conventional single-mode fibers, something that is not a major problem with conventional HNLFs.

The most commonly used figure-of-merit for nonlinear media is γ/α, i.e. nonlinearity coefficient divided by attenuation coefficient. This quantity is still highest for conventional silica HNLFs, and in that coupling losses are not even considered, further making the case for conventional HNLFs as the best platform for nonlinear devices at the moment.

This chapter

This chapter is intended to serve as an introduction to optical nonlinearities and define the quantities and concepts necessary for the discussion in subsequent chapters in this thesis, as well as in the appended papers. It begins with a brief introduction to the linear propagation effects in section 2.1. In section 2.2 we discuss the physical origin for the nonlinear effects described in the rest of this chapter. In section 2.3 the concepts of self- and cross-phase modulation are introduced. Four-wave mixing is a central part of this thesis and is introduced in section 2.4. FWM is the nonlinear effect that is exploited in parametric amplifiers, but for them to be efficient and produce any significant gain, the FWM process need to be phase-matched. This concept is explained in section 2.4.1, and parametric amplification is discussed in

section 2.5. Finally, the scattering nonlinearities are briefly described in section 2.6.

2.1 Linear effects

Attenuation

Attenuation of the optical wave is one of the fundamental propagation effects that is always present, though in many cases it can be neglected. The majority of attenuation in silica fibers (at low-loss wavelengths) originate from Rayleigh scattering against the silica molecules, though some material absorption is also present, and dominates outside the low-loss window. In conventional single-mode fibers, the attenuation can be as low as $0.16-0.20$ dB/km, and in typical HNLFs the attenuation is usually around $0.8-1.2$ dB/km. Since a nonlinear device implemented in HNLF often needs only a few hundreds of meters of fiber, the total attenuation is often only a few tenths of a dB. In connection with fiber nonlinearities, attenuation is usually accounted for via the effective length, defined as

$$L_{\text{eff}} \equiv \frac{1-\exp(-\alpha L)}{\alpha}, \tag{2.3}$$

where α is the attenuation coefficient in m^{-1} and L is the length of the fiber. By using the effective length instead of the actual length L, the effects of attenuation can be accounted for. We can also deduce that the effective length grows increasingly slower with the physical length, meaning that in practice there is a length after which there is little or no gain to be had from increasing the physical length, with the effective length finally reaching a maximum of $1/\alpha$ when $L >> 1/\alpha$. For an HNLF with $\alpha = 1$ dB/km, the maximal effective length is about 4.3 km, however, about 11 km of physical length is required to reach 4 km of effective length. Fortunately, in most applications only a few hundred meters of HNLF is sufficient, and for such short sections of HNLF, the effective length is not much shorter than the physical length.

Chromatic dispersion

The first term in Eq. 2.1 is the linear part of the refractive index, and since it is frequency dependent, it is the term that is responsible for the chromatic dispersion, or group-velocity dispersion (GVD). Fundamentally, it means that the speed of light (the group velocity) is different for different frequencies, and thus different frequencies will experience a relative phase shift as they propagate through a dispersive medium. We usually express this through the propagation constant,

$\beta(\omega) = n(\omega) \cdot \omega/c$ (here, we ignore the intensity-dependent part of the refractive index). The second derivative with respect to frequency of $\beta(\omega)$ is responsible for the difference in propagation speed among frequency components and hence is known as the GVD parameter. It is written as

$$\beta_2(\omega) = \frac{d^2\beta(\omega)}{d\omega^2}. \tag{2.4}$$

Often, the dispersion parameter D, defined as

$$D = -\frac{2\pi c}{\lambda^2}\beta_2, \tag{2.5}$$

and expressed in units of ps/(nm·km), is used instead.

GVD causes dispersive broadening (spreading out in time) of pulses, since a pulse with a limited duration in time will contain a spectrum of frequencies. GVD is also responsible for dispersive walk-off meaning that two pulses at different center frequency will only overlap for a limited time, known as the dispersive walk-off time. This is an important limiting factor in applications where it is desired to have two distinct pulses interact through some nonlinear effect.

The case of $\beta_2 > 0$, where higher frequencies will propagate with lower speed, is said to be normal dispersion, while the opposite case is known as anomalous dispersion. The third-order derivative of $\beta(\omega)$, or alternatively $S = dD/d\lambda$, represents the frequency (wavelength) dependence of the dispersion. This parameter becomes important for phase-matching, as it dictates the difference in dispersion and thus relative phase-shift between two waves of different frequencies as they propagate through a fiber.

Polarization effects

Even a single-mode fiber supports two separate polarization modes at each frequency. Generally, these modes will have different propagation speeds, because the fiber does not have perfect cylindrical symmetry and/or it might be bent or twisted. This leads to polarization-mode dispersion (PMD). The time-domain manifestation of PMD is pulse splitting, which occurs if an input pulse excites both polarization modes. In nonlinear devices, the main impact of PMD is usually the frequency-domain manifestation, namely that waves of different frequencies will change their polarization states as they propagate, often reducing the efficiency of nonlinear interaction between the waves. This is because many nonlinear effects usually require that the interacting waves are co-polarized for maximal efficiency. To overcome this problem, usually one tries to find a *principal axis* of propagation of the fiber,

meaning an input state of polarization (SOP) for which different frequencies do not change their relative SOP significantly.

Furthermore, the output SOP and principal axis of a fiber usually changes with mechanical and thermal perturbations. There are so-called polarization-maintaining fibers for which this is not the case, but usually polarization-maintaining HNLFs are much worse in other aspects, such as nonlinearity and dispersion uniformity. Thus, conventional HNLFs are most often used and need to be in a controlled environment for the nonlinear device to operate stably.

2.2 Origins of nonlinear effects

$\chi^{(2)}$- and $\chi^{(3)}$-nonlinearities

We have already established that the Kerr nonlinearity fundamentally means the intensity-dependence of the refractive index. But how does this dependence arise? The answer lies in the higher-order susceptibilities of a material. When light propagates through a dielectric medium, its (time-varying) electric field $\mathbf{E}$ causes some amount of (time-varying) electric polarization in the medium, i.e. a shift in distribution of the electrically charged particles of the medium, typically the loosely bound valence electrons. Normally, this polarization field, $\mathbf{P}$, follows the electrical field, i.e. has the same direction and time variance. The proportionality constant describing this relation is called the *susceptibility*, χ, with

$$\mathbf{P} = \epsilon_0 \chi \mathbf{E}. \tag{2.6}$$

However, in the case of very large electrical field strengths, this relation saturates. We thus have to resort to a more general relation (assuming an isotropic medium where $\tilde{\mathbf{P}}$ and $\tilde{\mathbf{E}}$ are parallel, so that the relation can be reduced to the scalar):

$$P = \epsilon_0 \left(\chi E + \chi^{(2)} E^2 + \chi^{(3)} E^3 + ... \right). \tag{2.7}$$

Clearly, the polarization field (and thus the reradiated light) now contains new frequencies at integer multiples of the original frequency. Moreover, if the initial field contains multiple frequencies, new frequencies at the sum and difference frequencies of (integer multiples of) the original frequencies will appear. In typical cases, in media without inversion symmetry, such as many crystals, the $\chi^{(2)}$-term (2nd-order susceptibility) dominates over the $\chi^{(3)}$- (3rd-order susceptibility) and subsequent terms. In isotropic media, e.g. gases, liquids and amorphous solids such as silica glass, the even-order terms vanish, and the $\chi^{(3)}$-term dominates [34, pp. 2-3]. We can thus talk about $\chi^{(2)}$- and $\chi^{(3)}$-media. Finally, it should be noted that we have

significantly simplified things here, by ignoring the fact that the susceptibilities are in fact tensors, and the nonlinear response depends on the direction of the electrical field (i.e. the polarization) as well as any symmetry axes of the medium. The non-instantaneous response, which will be discussed later in this section, has been ignored as well. We also note that the real part of the first-order (linear) susceptibility of Eq. 2.7 is responsible for GVD and the imaginary part is responsible for attenuation.

Some effects that arise in $\chi^{(2)}$-media are second-harmonic generation (SHG), i.e. frequency-doubling, and sum- and difference-frequency generation (SFG, DFG) [34, pp. 4-9]. In $\chi^{(3)}$-media, the refractive index becomes intensity-dependent, which is what we call the Kerr nonlinearity, leading to intensity-dependent phase-shifts [27, pp. 14-15]. Moreover, both $\chi^{(2)}$- and $\chi^{(3)}$-media support parametric amplification [34, pp. 9-13], where energy from one wave is transferred to another, which thus is amplified. Besides glasses, silicon is another media that can be used for $\chi^{(3)}$-nonlinearities [35].

Scattering nonlinearities

All the effects that have been described so far are *elastic*, meaning that no energy is exchanged between the propagating lightwave and the medium. In the quantum-mechanical picture, they thus amount to the annihilation and creation of photons of different frequencies (energies), while the total energy of the light is conserved. The other class of nonlinearities are *inelastic* [27, pp. 15-16], and the lightwave exchanges energy with the medium, specifically through vibrational excitation modes of the medium, i.e. phonons. In the quantum-mechanical picture, an incident photon is annihilated and a new is created at a lower frequency, together with a phonon, making the total energy conserved. Raman scattering involves optical phonons, while Brillouin scattering involves acoustic phonons [27, p. 16].

Raman scattering can also be described classically in terms of the nonlinear polarization field [34, p. 372]. The Raman effect is a consequence of its non-instantaneous response. Often, the Kerr nonlinearity is considered to be the purely electronic (and hence instantaneous) part of the of the third-order-nonlinearity, originating in the real part of $\chi^{(3)}$, while the delayed response (Raman) part originate in the imaginary part of $\chi^{(3)}$ and form the remaining contributions to the nonlinear susceptibility. (Compare the real (dispersion) and imaginary (attenuation) parts of the linear susceptibility). Brillouin scattering on the other hand, occurs via the electrostriction effect that causes the medium to compress in the presence of an electrical field, and thereby couples optical and acoustic (sound) waves in the nonlinear medium.

2.3 Self- and cross-phase modulation

We have established that the refractive index, and thus the speed of light, is dependent on the optical intensity in the fiber, as described by Eq. 2.1, meaning that the phases of propagating waves will change dependent on the power of the waves in the fiber. This effect is called self-phase modulation (SPM) when the wave affects its own phase, and cross-phase modulation (XPM) when the phase of a wave is affected by other waves. The accumulated phase shift along a fiber of length L due to this effect is called the nonlinear phase shift, and when m frequency components are propagating through a fiber, it is written for frequency component n as [27, p. 230]

$$\Delta\Phi_{NL,n} = \gamma L \left(2P_1 + ... + 2P_{n-1} + P_n + 2P_{n+1} + ... + 2P_m\right), \tag{2.8}$$

where P_n is the optical power at frequency component n. Note in particular that the effect on the phase from other frequency components (XPM), is twice as large as the effect a frequency component has on its own phase (SPM). This is true if the waves are parallel-polarized. Otherwise, XPM is between one and two times as strong as SPM [36]. For XPM, one must also consider the dispersive walk-off if the interacting waves are pulses. SPM causes spectral broadening of pulses, or SPM-induced frequency chirp. XPM can be exploited in signal-processing applications for e.g. switching/demultiplexing [37].

An interesting phenomenon arises when the nonlinear phase shift and the dispersive phase shift cancel each other. This can give rise to pulses that propagate without being broadened in time, so-called solitons [27, 38]. Balancing nonlinear and dispersive phase shifts in a certain way is also the condition that maximizes the efficiency of nonlinear effects such as FWM, discussed further in section 2.4.1. Note, however, that since the the nonlinear phase shift is always positive, solitons can normally only occur for waves in the anomalous dispersion regime ($\beta_2 < 0$).

2.4 Four-wave mixing

Four-wave mixing (FWM), or synonymously four-photon mixing, is a process originating from the $\chi^{(3)}$-nonlinearity. As can be deduced from the name, it involves the nonlinear coupling of four distinct waves at different frequencies, but there is also a degenerate FWM, in which two of these frequencies are identical.

A classical description of FWM is as follows: two optical waves at different frequencies ω_1 and ω_2 co-propagate in an optical fiber. The local field intensity at a specific coordinate in the fiber thus varies by the beating frequency $\omega_2 - \omega_1$ of these two waves. Through the Kerr nonlinearity, the index of refraction will be modulated

by this beat note. Now, if a third wave at frequency ω_3 is introduced, it will be phase modulated with the frequency $\omega_2 - \omega_1$ by propagating in the fiber with modulated refractive index. As a result, sidebands at frequencies $\omega_3 \pm (\omega_2 - \omega_1)$ are generated. The wave at ω_3 will also beat with the wave at ω_1, which phase modulates the wave at ω_2 and introduces sidebands at $\omega_2 \pm (\omega_3 - \omega_1)$. Considering all possible non-degenerate and degenerate combinations in a system with three frequencies at the input, new frequency components will be generated at frequencies

$$\omega_{jkl} = \omega_j + \omega_k - \omega_l. \tag{2.9}$$

In the degenerate combinations, two of the waves are identical, e.g. $j = k$. Fig. 2.1 shows all frequencies. Note that some of the generated frequency components overlap with each other, or with the original waves. The latter is the origin of parametric gain. Some frequency components, e.g. at $\omega_{321} = \omega_{231}$, are stronger than the others and are usually referred to as the *idlers*. Often, all other generated components are neglected. As follows from this discussion, in the typical case, FWM will generate one new frequency of significance (an idler) from each combination of either two or three input waves, forming either a triplet (degenerate FWM) or quadruplet (non-degenerate FWM) of coupled waves.

Just like the $\chi^{(2)}$-phenomena of SHG, SFG and DFG, the process is called *parametric* since the medium does not actively participate in the process, like in the scattering nonlinearities, but rather participates as a passive catalyst. It involves the modulation of a medium parameter, specifically the susceptibility, or the refractive index, in the case of $\chi^{(3)}$-nonlinearities.

FWM can also be interpreted from a quantum mechanical point of view, in which two photons annihilate and two photons are created at new frequencies, under energy (i.e. frequency) and momentum conservation. The momentum conservation is the quantum-mechanical manifestation of phase-matching, which is what dictates the efficiency of each FWM process, and will be discussed in the next section.

When there are many different frequency components present from the start, such as in a wavelength division-multiplexing (WDM) system, there are of course many FWM processes acting simultaneously, and a very large number of new frequency components can be created. Depending on the frequency allocation, some of these can overlap with each other, or with the original frequency components, thus causing crosstalk. Indeed, FWM is often a major limitation in WDM systems [39]. However, it is important to note that each FWM process involves only three (degenerate) or four (nondegenerate) waves, as in Eq. 2.9.

Now, consider the case in which only a strong wave at ω_p, called the pump, and a weak wave at ω_s, called the signal, is injected into a fiber. Then, in the dominating process, sidebands of the pump wave will appear at ω_s and the idler

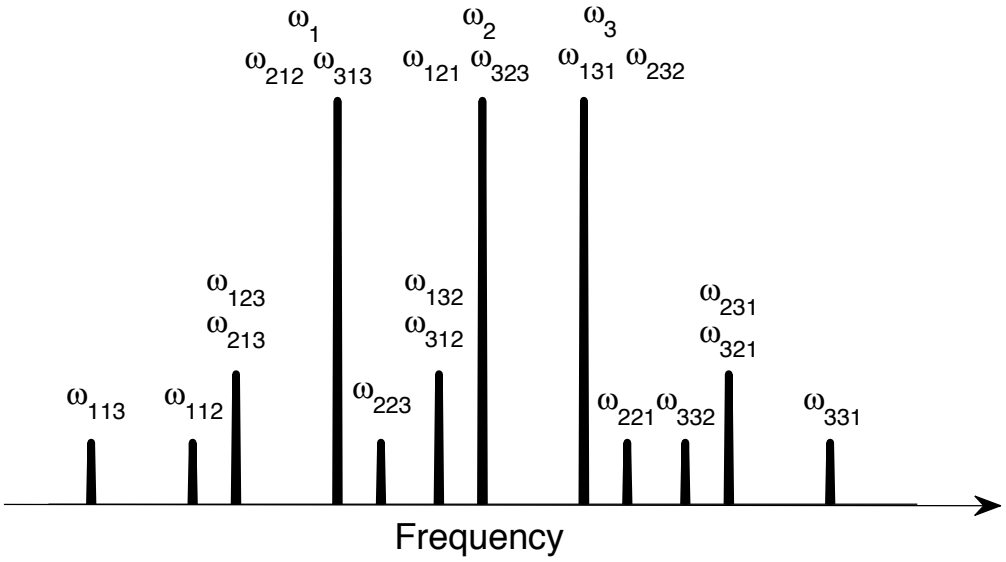

Figure 2.1: All frequency components that are generated through FWM in all possible degenerate and nondegenerate combinations when three waves (ω_1, ω_2 and ω_3) are present at the input. Nine new frequencies are generated.

frequency $\omega_i = 2\omega_p - \omega_s$. Since the pump wave is much stronger than the signal, the process in which sidebands from the signal at ω_p and $2\omega_s - \omega_p$ are generated can be neglected. The case described above is what is commonly referred to as degenerate or single-pumped FWM, in which a pump provides gain to a signal, while at the same time an idler wave is generated.

This case can also be extended to nondegenerate, or dual-pumped, FWM in which two strong pumps at frequencies ω_{p1} and ω_{p2} provides gain to an initially weak signal at ω_s and creates an idler at $\omega_i = \omega_{p1} + \omega_{p2} - \omega_s$.

FWM is highly polarization dependent, and the analysis in this thesis normally assumes that all interacting waves are co-polarized. It is, however, possible to make FWM polarization independent in principle, by using two orthogonally polarized pump waves [40, 41], but this is a much less efficient process, and is also difficult to maintain in practice.

Moreover, since FWM originates from the Kerr nonlinearity, it has a response time on the order of femtoseconds, making it instantaneous for most purposes. This property is what makes FWM interesting for ultrafast signal processing applications.

Finally, it is also important to understand that FWM also will occur between

actual waves and vacuum fluctuations (quantum fluctuations of the vacuum state, sometimes referred to as virtual photons) in the fiber. This phenomenon is the source of parametrically generated noise, so-called amplified quantum noise (AQN), sometimes also called parametric amplified spontaneous emission (ASE) or parametric fluorescence. This is the fundamental origin of noise in parametric amplification.

2.4.1 Phase-matching

Many of the nonlinear processes discussed above, both $\chi^{(2)}$- and $\chi^{(3)}$-based nonlinearities, require *phase-matching* to be efficient. Phase-matching essentially means that the *relative phase*, θ_{rel} between interacting waves is maintained during propagation through the nonlinear medium. If this is the case, the contribution to the nonlinearly generated wave(s) will be the same, i.e. in phase, throughout the propagation in the medium. If the process is not phase-matched, the contributions from different locations in the medium will not add constructively, resulting in a weak nonlinear interaction. A properly phase-matched nonlinearity, on the other hand, will result in exponential growth of the generated wave along the propagation direction.

This can be understood by realizing that the transfer of power between frequencies is proportional to some product of the fields (or complex conjugate fields) of the interacting waves, since the nonlinear polarization field in the medium (and thus the reradiated field, i.e. the generated wave) is proportional to such a product. This product of complex fields should be kept maximal for maximum power transfer efficiency, and with the correct sign to get power transfer in the desired direction (i.e. from the pump rather than vice versa). This puts a requirement on the phase of the complex field product and hence on the phases of the interacting waves. Phase-matching thus means keeping waves, usually of different frequencies, in phase. In other words, the phase-shifts that they experience during propagation should cancel out so the relative phase is kept constant. The phase-matching condition is usually expressed in terms of the propagation constants of the interacting waves, which may have different contributions (linear and nonlinear).

In the perfectly phase-matched case, the relative phase remains constant throughout propagation. Then, the complex field-product is dependent only on the power of the interacting waves, and the power of the generated wave grows exponentially (as long as its power is small compared to that of the pumps). In near-phase matched cases, the relative phase changes somewhat over propagation, but only by so little that the field product never changes its sign. Thus, good efficiency is still possible in the near-phase matched case. In the absence of phase matching, the relative phase will change rapidly, and thus, the sign of the field product and direction

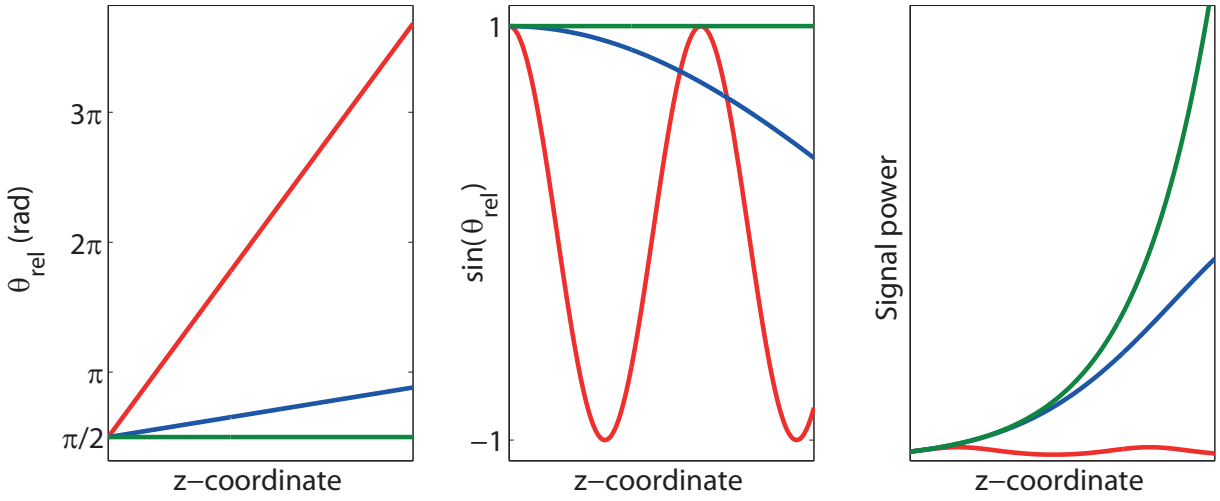

Figure 2.2: The evolution of the relative phase in a perfectly phase-matched case (green line), an near-phase-matched case (blue line) and an un-phase-matched case (red line).

of power flow, will change, possibly many times, over the propagation. This will lead to an initial growth of the generated wave that subsequently changes direction, resulting in an oscillation, rather than monotonous growth, of the generated wave. Fig. 2.2 illustrates the concept of phase-matching and shows how the relative phase, the sine of the relative phase (which is related to and sometimes proportional to the field product), and the power of the generated wave evolves in the corresponding cases. Note that the power initially grows at the same rate in all three cases.

Clearly, in phase-matching, chromatic dispersion must always be considered, since it means different phase-shifts for different frequencies. Nonlinear phase-shifts from SPM and XPM are always present in $\chi^{(3)}$-media, and must be taken into account. Birefringence can also be used for phase-matching, and is the usual phase-matching technique for many nonlinear crystals, but is not so common to use in fibers.

Notably SPM and XPM themselves do not require phase-matching to be efficient (or can be considered to be automatically phase-matched), since they are dependent only on the intensity, though they are very important for phase-matching of other nonlinearities via their induced phase-shifts. The above discussion is general in the sense that it can concern both $\chi^{(2)}$- and $\chi^{(3)}$-nonlinearities, and the generated wave can originate from e.g. SHG, SFG/DFG or be the parametric gain of a signal wave.

In the remainder of this section, we discuss phase-matching of FWM in optical fibers, achieved by balancing SPM/XPM and chromatic dispersion.

Phase-matching of fiber FWM

Let us consider the dual-pumped FWM case with four distinct interacting waves, two pumps at frequencies ω_{p_1,p_2} and signal and idler at frequencies $\omega_{s,i}$. The sum of the electrical fields is written as [27, p. 369]:

$$\begin{aligned} E(x,y,z) = f(x,y)\frac{1}{2}[&A_{p_1}(z)\exp(i\beta(\omega_{p_1})z - i\omega_{p_1}t) + \\ &A_{p_2}(z)\exp(i\beta(\omega_{p_2})z - i\omega_{p_2}t) + \\ &A_s(z)\exp(i\beta(\omega_s)z - i\omega_s t) + \\ &A_i(z)\exp(i\beta(\omega_i)z - i\omega_i t)] + c.c. \end{aligned} \tag{2.10}$$

Here, *c.c.* is the complex conjugate that is usually omitted in calculations and $f(x,y)$ is the transverse mode profile, assumed to be the same for all waves. Each wave is represented by the slowly varying complex field amplitude, A(z), and have a propagation constant denoted by β.

By inserting the expression above into the basic propagation equation, i.e. the nonlinear Schrödinger equation (NLSE), which in turn can be derived from Maxwell's Equations, the following coupled equations can be derived, (ignoring fiber attenuation, higher-order dispersion, any wavelength dependence in γ and the Raman effect) [9, 27, 42]:

$$\begin{aligned} \frac{dA_{p_1}}{dz} &= i\gamma[\left(|A_{p_1}|^2 + 2\left(|A_{p_2}|^2 + |A_s|^2 + |A_i|^2\right)\right)A_{p_1} \\ &\quad +2A_{p_2}^* A_s A_i \exp(i\Delta\beta z)], \end{aligned} \tag{2.11}$$

$$\begin{aligned} \frac{dA_{p_2}}{dz} &= i\gamma[\left(|A_{p_2}|^2 + 2\left(|A_{p_1}|^2 + |A_s|^2 + |A_i|^2\right)\right)A_{p_2} \\ &\quad +2A_{p_1}^* A_s A_i \exp(i\Delta\beta z)], \end{aligned} \tag{2.12}$$

$$\begin{aligned} \frac{dA_s}{dz} &= i\gamma\left(|A_s|^2 + 2\left(|A_{p_1}|^2 + |A_{p_2}|^2 + |A_i|^2\right)\right)A_s \\ &\quad +2A_{p_1} A_{p_2} A_i^* \exp(-i\Delta\beta z)], \end{aligned} \tag{2.13}$$

$$\frac{dA_i}{dz} = i\gamma[\left(|A_i|^2 + 2\left(|A_{p_1}|^2 + |A_{p_2}|^2 + |A_s|^2\right)\right) A_i + 2A_{p_1}A_{p_2}A_s^* \exp(-i\Delta\beta z)], \tag{2.14}$$

where

$$\Delta\beta = \beta(\omega_{p_1}) + \beta(\omega_{p_2}) - \beta(\omega_s) - \beta(\omega_i), \tag{2.15}$$

is the propagation constant mismatch. Looking at Eqs. 2.11-2.14, the first four terms on the right hand side represent SPM- and XPM-induced phase shifts, and the last term represents the power transfer between frequencies due to FWM. The maximization of this term leads to the phase-matching condition for FWM. If it is fulfilled, the signal and idler powers will grow exponentially as the waves propagate through the fiber.

Defining $A(z) = \sqrt{P(z)}\exp\left(i\theta(z)\right)$, with P and θ being the power and phase of the wave, respectively, we can rewrite Eq. 2.11-2.14 in terms of the power and phases, by multiplying them with the corresponding field conjugate:

$$\frac{dP_{p_1}}{dz} = \frac{dP_{p_2}}{dz} = -2\gamma\sqrt{P_{p_1}P_{p_2}P_sP_i}\sin(\theta_{\text{rel}}), \tag{2.16}$$

$$\frac{dP_s}{dz} = \frac{dP_i}{dz} = 2\gamma\sqrt{P_{p_1}P_{p_2}P_sP_i}\sin(\theta_{\text{rel}}), \tag{2.17}$$

$$\frac{d\theta_{rel}}{dz} = \Delta\beta + \gamma(P_{p_1} + P_{p_2} - P_s - P_i) + 2\gamma\sqrt{P_{p_1}P_{p_2}P_sP_i}\left(\frac{1}{P_s} + \frac{1}{P_i} - \frac{1}{P_{p_1}} + \frac{1}{P_{p_2}}\right)\cos(\theta_{\text{rel}}). \tag{2.18}$$

Here, θ is the relative phase between the waves, defined as

$$\theta_{\text{rel}} \equiv \theta_{p_1} + \theta_{p_2} - \theta_s - \theta_i. \tag{2.19}$$

From Eq. 2.16-2.17 it is evident that the total power is conserved, and that the power growth in signal and idler is the same and corresponds to an equal reduction in power of the two pumps (or vice versa, depending on the sign of the relative phase), i.e. $P_s - P_i = \text{constant}$ and $P_{p_1} - P_{p_2} = \text{constant}$. This is often referred to as the Manley-Rowe relation [42, p. 33] for FWM.

Notably, the last term in Eq. 2.18 can be neglected as long as we operate close to the phase-matched condition. The relative phase normally (in the absence of an

input idler) sets itself to $\pi/2$ at the start, so this term is initially zero, and will remain so in the case of ideal phase-matching.

The relative phase among the waves thus govern the magnitude, and indeed the direction of the power flow, as is readily seen from Eqs. 2.16-2.17. The change in relative phase as the waves propagate are influenced by the linear phase shifts due to the different propagation constants (the first term on the right hand side of Eq. 2.18), and the nonlinear phase shifts, due to SPM and XPM (the second term).

In the single-pumped case, $\omega_{p_1} = \omega_{p_2} = \omega_p$ and the relative phase $\theta_{rel} \equiv 2\theta_p - \theta_s - \theta_i$, and Eqs. 2.16-2.18 become:

$$\frac{dP_p}{dz} = -4\gamma\sqrt{P_p^2 P_s P_i}\sin(\theta_{\text{rel}}), \tag{2.20}$$

$$\frac{dP_s}{dz} = \frac{dP_i}{dz} = 2\gamma\sqrt{P_p^2 P_s P_i}\sin(\theta_{\text{rel}}), \tag{2.21}$$

$$\begin{aligned}\frac{d\theta_{rel}}{dz} &= \Delta\beta + \gamma(2P_p - P_s - P_i) \\ &+2\gamma\sqrt{P_p^2 P_s P_i}\left(\frac{1}{P_s} + \frac{1}{P_i} - \frac{2}{P_p}\right)\cos(\theta_{\text{rel}}).\end{aligned} \tag{2.22}$$

Following from the requirement that the relative phase should remain constant at $\pi/2$ throughout propagation, the condition for perfect phase matching is (if the pump powers remain much larger than that of the signal and idler):

$$\kappa \equiv \Delta\beta + \gamma(P_{p_1} + P_{p_2}) = 0, \tag{2.23}$$

or in the single-pumped case:

$$\kappa \equiv \Delta\beta + 2\gamma P_p = 0. \tag{2.24}$$

The first term represents the linear propagation mismatch, and the second term the nonlinear phase shift, and they need to cancel out in order for the phase-matching condition to be fulfilled, and the FWM efficiency maximized.

It can be shown [19,42] that in the single-pumped case, when operating the pump close to the-zero-dispersion frequency ω_0 of the fiber, the phase matching condition can be written as

$$\kappa = \beta_3(\omega_p - \omega_0)\cdot(\omega_s - \omega_p)^2 + 2\gamma P_p = 0, \tag{2.25}$$

where β_3 is the third derivative of the propagation constant at the zero-dispersion frequency. In the dual-pumped case, the phase-matching condition can similarly be shown to be [42, p. 117]

$$\kappa = \beta_3(\omega_c - \omega_0) \cdot \left[(\omega_s - \omega_c)^2 - \omega_d^2\right] + \gamma(P_{p_1} + P_{p_2}) = 0, \tag{2.26}$$

where $\omega_c = (\omega_{p_1} + \omega_{p_2})/2$ and $\omega_d = (\omega_{p_1} - \omega_{p_2})/2$.

Much can be learned about FWM from these equations. In order for the linear propagation mismatch and nonlinear phase shift to cancel out, $\Delta\beta$ must be negative. From the above equations, it is clear that this can only occur when the pump frequency or average pump frequency is in the anomalous dispersion regime[1].

In the single-pump case, we can see that there is only two signal frequencies for each given pump frequency that maximizes the efficiency. However, in the dual-pumped case, a wide spectrum of signal/idler frequencies between the pumps can fulfill good phase matching. Another observation is that fibers with low dispersion slopes give the largest FWM bandwidths since that reduces the dependency on the signal frequency. If the nonlinear phase shift dominates, i.e. if the pump powers are very large, the dispersive phase shifts play a smaller role, which is why the FWM bandwidth increases with pump power.

If the powers change considerably during propagation, the nonlinear phase shift will also change. This is the phenomenon behind saturation of FWM [42, 43]. As the signal and idler powers increase, and the pump powers decrease, the FWM efficiency is decreased, and eventually a point at which the relative phase changes sign is reached, thus the direction of the power flow is reversed, i.e. power flows from signal/idler to pump.

Finally, we have up until this point assumed that the idler was not present at the input, but generated in the FWM process. If this is the case, the idler will automatically obtain a phase so that the efficiency is maximized. Since the FWM efficiency is maximized for $\theta_{\text{rel}} = \pi/2$, the idler phase will set itself so that this condition is achieved after an infinitesimally short length of the fiber. The idler can be thought of as being initially generated with the "correct" phase. This can also be seen by considering the last term of Eq. 2.14. This explains why a generated idler phase carries a dependence on the pump phases and conjugated signal phase, as the relative phase at the input (or, more precisely, after the infinitesimal length after which the idler has formed) should be a constant. If, however, an idler at the correct frequency is present at the input, the initial generation of the idler does not take

[1]Phase matching is also possible over very narrow bandwidth regions far from the pump frequency when the pump is in the normal dispersion regime, when taking higher order dispersion into account.

place, leading to the FWM process to become dependent on the relative phase at the input, and the process is said to be phase sensitive. This is the topic of Chapter 4.

2.5 Parametric amplifiers

Previously in this chapter, we have established that both $\chi^{(2)}$- and $\chi^{(3)}$-nonlinearities can result in the conversion of energy from one frequency to others, and that this conversion can, in the case of good phase-matching be very efficient. When energy is converted from a pump wave to a weak signal present at the input (as opposed to e.g. SHG where only the pump is present at the input), we call this phenomenon parametric amplification. This conversion of pump photons to signal photons is also accompanied by the generation of an idler wave. Normally, we consider non-degenerate idler parametric amplification, in which the signal and idler are two distinct waves. Conversely, in degenerate-idler parametric amplification they are indistinguishable. Degenerate-idler parametric amplification is always phase-sensitive. In section 2.4, the case in which a strong pump wave and a weak signal wave interact through FWM, leading to amplification of the signal and the generation of an idler wave, was discussed. In section 2.4.1, we discussed the concept of phase matching, and its importance for the efficiency of FWM. A fiber device with one or two high-power pumps, in which phase-matched FWM can take place is commonly referred to as a *fiber optic parametric amplifier* (FOPA) [27, p. 387].

In second-order-nonlinear media, non-degenerate idler parametric amplification occurs between a pump, a signal and an idler fulfilling the frequency relation $\omega_p = \omega_s + \omega_i$. This is closely related to DFG. In the degenerate case, the pump frequency must be exactly two times the signal frequency. In third-order-nonlinear media such as optical fibers, parametric amplification is essentially phase-matched FWM. Therefore, we can have either single-pumped or dual-pumped parametric amplification in fibers. Single-pumped parametric amplification can only be of the non-degenerate idler variety, as it needs to fulfill the frequency relation $2\omega_p = \omega_s + \omega_i$, unless interferometers are used to separate the pump from the signal, since in that case all three waves need to have the same frequency. Single-pumped parametric amplification is only phase-sensitive if a wave triplet fulfilling the frequency relation is present at the input. Dual-pumped parametric amplification fulfills the frequency relation $\omega_{p1} + \omega_{p2} = \omega_s + \omega_i$, and can thus operate in the degenerate idler mode if the signal frequency is exactly the average of the two pump frequencies. Therefore, both single-pumped non-degenerate idler and dual-pumped degenerate idler parametric amplification are cases of degenerate FWM, involving only three waves. Fully non-

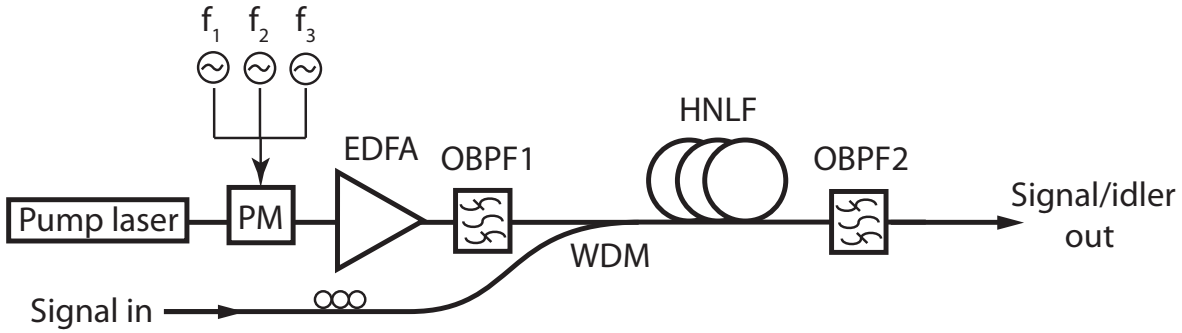

Figure 2.3: Typical construction of a single-pumped FOPA. PM: Phase modulator, EDFA: Erbium-doped fiber amplifier, OBPF: optical bandpass filter, WDM: Wavelength division multiplexing coupler, HNLF: highly nonlinear fiber.

degenerate FWM (i.e. non-degenerate idler dual-pumped parametric amplification) can also be made phase-sensitive, if all four waves are present at the input.

In the remainder of this section, we will discuss how fiber-optic parametric amplifiers usually are implemented, and how their gain and gain spectrum can be described mathematically. This will form the basis for the remainder of the thesis, and in Chapter 4, we will extend the discussion to phase-sensitive cases, where the performance and applications of phase sensitive amplifiers will be reviewed.

2.5.1 Implementation of fiber-optic parametric amplifiers

A typical FOPA is constructed around an HNLF of length around 0.1-1 km with a zero-dispersion wavelength (ZDW) in the low-loss regime of the fiber around 1550 nm. The pump power required is then usually in the 0.5-10 W-range, meaning that Erbium-doped fiber amplifiers (EDFAs) are normally required to boost the pump to this range. In Fig. 2.3, a typical construction for a phase-insensitive single-pumped continuous-wave FOPA is shown. Light from the pump laser is in this case passed through a phase modulator that serves to spectrally broaden the pump wave in order to avoid SBS, though this can be omitted if other SBS-suppression methods are used. SBS-suppression is discussed further in Chapter 3. The pump light is amplified by a high-power EDFA to the required power levels. An optional optical bandpass filter serves to remove out-of-band ASE noise originating in the EDFA. A coupler, preferably a low-loss WDM coupler, combines the pump with the signal and injects them into the nonlinear fiber wherein the parametric interaction takes place. Since parametric amplification is polarization-dependent, one must ensure that the

polarization of the waves are aligned in the HNLF, and with its principal axis, so that the drift of relative polarization states between the waves are minimized. Here a manual polarization controller is used. Finally, the pump is removed by one or more optical filters and the signal/idler retrieved. OBPF2 could thus be either a bandpass filter selecting the signal/idler, as in this case, or a notch filter rejecting the pump. The dual-pumped case is similar.

Perhaps the most important part of the FOPA design is to ensure that the phase matching condition is fulfilled. This requires the pump wavelength (for single-pumped FOPAs) or average pump wavelength (for dual-pumped FOPAs) to be in the anomalous dispersion regime, but close to the ZDW. Thus, a nonlinear fiber with a ZDW in or near the C-band is needed for a gain over the C-band. A single-pumped FOPA can only be perfectly phase-matched for two signal wavelengths (the signal and idler wavelengths), but can exhibit a rather wide spectrum around these wavelengths where the phase-matching is good enough to provide substantial net gain. A dual-pumped FOPA on the other hand can exhibit almost perfect phase-matching over a large range of wavelengths between the two pumps. The gain spectrum is essentially dependent on the GVD of the HNLF, but also on the pump powers. Extensive discussions on how the FOPA gain spectrum is synthesized can be found in the literature, e.g. in [19, 42, 44]. Figure 2.4 shows example gain spectra for a single-pumped and a dual-pumped FOPA. Notable is that both the single-pumped and dual-pumped case have the same maximum gain, if pumped with the same amount of total pump power. The HNLF parameters are the same in both cases. How the gain and gain spectrum is computed is discussed further in the section below.

Many demonstrations of dual-pumped FOPAs exist in the literature [45–47]. We will limit the discussion to single-pumped FOPAs in the remainder of the thesis, as that is what has been investigated in all appended papers except Paper [E]. The main advantages of dual-pumped FOPAs over single-pumped are spectrally flat and wide gain [48, 49], potential polarization independence through the use of orthogonally polarized pumps [50], and the suppression of idler spectral broadening by phase modulating the two pumps synchronously, either in-phase or out-of-phase [51]. For the purpose of investigating the properties of phase-sensitive amplification, the main topic of this thesis, such benefits are of secondary importance; hence single-pumped FOPAs form the basis for this work.

2.5.2 The parametric gain

We have established that the gain of a parametric amplifier is dependent on the phase-matching, i.e. the GVD values of the HNLF at the pump, signal and idler

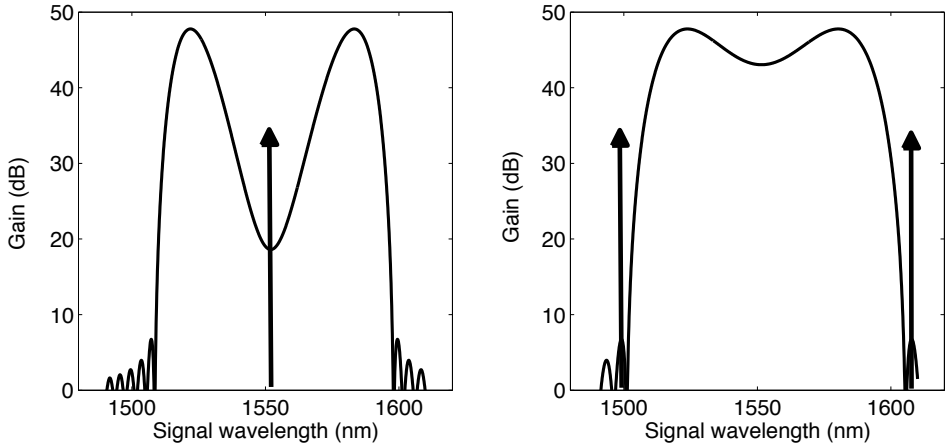

Figure 2.4: Example gain spectra for a single-pumped (left) and dual-pumped (right) FOPA in a fiber of length 500 m, $\gamma = 11$ $(\mathrm{W{\cdot}km})^{-1}$ and total pump power 1 W. The arrows indicate the wavelengths of the pumps.

wavelengths, and that for a single-pumped FOPA, perfect phase-matching is only possible at two distinct signal wavelengths, with a gain spectrum around these wavelengths. In this section, we introduce an analytical expression for the small-signal gain and use this to introduce the *transfer-matrix model* for the parametric gain, a usable model to compute e.g. the impact of varying dispersion in HNLFs. Furthermore, we discuss the case of *pump depletion*, i.e. where the gain saturates, and the simpler analytical expression no longer are valid, meaning that one has to resort to a numerical solution of the so-called *three-wave model*. Neither of these models include noise (which we will discuss in Chapter 4), nor do they account for higher-order FWM (i.e. other FWM processes than the best phase-matched one, including those involving the generated components) and other concurrent nonlinear effects (e.g. Raman) that occurs simultaneously in the HNLF. For such a complete description, one has to resort to a full numerical solution of the propagation equation (the so-called Nonlinear Schrödinger Equation) [27, 42].

Exponential and quadratic gain

In addition to the phase-matching, the gain value that can be attained is dependent on the nonlinear phase shift in the fiber, i.e. on the $2\gamma P_p L$-product. This can be seen from Eq. 2.17, in which we reached the conclusion that the growth rate of the signal and idler power along the fiber is directly dependent on $2\gamma P_p$ (in the single-pumped case). We can easily identify that in the ideal case of perfect phase matching, where the relative phase is $\pi/2$ and does not change during propagation,

the growth of the signal power (i.e. the gain) is exponentially dependent on $2\gamma P_p L$. In the absence of perfect phase matching, one needs to consider the change of the relative phase during propagation, but it is nevertheless quite straightforward to derive an expression for the gain in terms of the phase mismatch parameter κ (Eq. 2.25) [19,27,42,52], assuming no pump depletion and a "small" signal, meaning that we can neglect signal and idler SPM and XPM throughout the propagation, as

$$G = \left(1 + \left[\frac{\gamma P_p}{g}\sinh\left(gL_{\text{eff}}\right)\right]\right), \tag{2.27}$$

where

$$g^2 = \left[\left(\gamma P_p\right)^2 - \left(\kappa/2\right)^2\right]. \tag{2.28}$$

Two special cases can be identified, $\kappa = 0$ (perfect phase-matching), and $\kappa = -2\gamma P_P$ (no relative phase-shift due to dispersion, i.e. signal and pump wavelength are the same). In the first case, Eq. 2.27 can be shown in the case of large nonlinear phase-shift (and thus gain) to simplify to (using the Taylor expansion of the sinh-function) [19]

$$G_{\text{exp}} \approx \frac{1}{4}\exp\left[2\gamma P_p L_{\text{eff}}\right]. \tag{2.29}$$

Since the gain is approximately exponentially dependent on the nonlinear phase-shift, we refer to this case as *exponential gain*. The other limit case is valid when the pump and signal are close in wavelength, so that any dispersive contribution to the phase-mismatch is negligible. Then, Eq. 2.27 can be shown in the case of large nonlinear phase-shift to simplify to [19]

$$G_{\text{quad}} \approx \left(2\gamma P_p L_{\text{eff}}\right)^2. \tag{2.30}$$

In this case, the gain is approximately quadratically dependent on the nonlinear phase-shift, so we call this case *quadratic gain*. Using Eq. 2.29-2.30, one can with relatively good accuracy calculate the gain in a real single-pumped FOPA at a given pump power. Figure 2.5 shows the gain spectrum for an example single-pumped FOPA with the exponential and quadratic gain regimes indicated.

Transfer matrix-description

While Eqs. 2.27-2.28 are useful, they will only give the power gain of a uniform FOPA in the exponential and quadratic gain regimes. Moreover, if one wishes to consider a phase-sensitive case, i.e. a non-zero idler at the input, a more accommodating model is needed. Also, in that case, the full output field, rather than just the

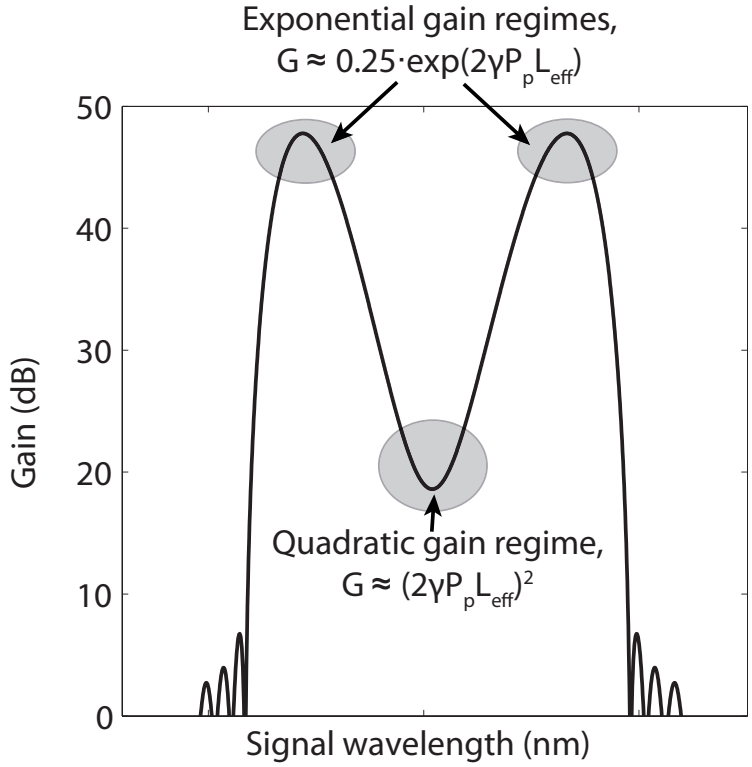

Figure 2.5: Calculated gain for a single-pumped FOPA with the exponential and quadratic gain regime indicated.

power, might be interesting. In fact, instead of deriving an expression for the power gain from Eqs. 2.16-2.18 , one can just as easily derive one for the complex field, that contains both amplitude and phase information. The input-output relation for the signal and idler in an unsaturated FOPA can be written in matrix form (in the lossless case) [53, 54]

$$\begin{bmatrix} A_s(L) \\ A_i^*(L) \end{bmatrix} = \mathbf{T} \begin{bmatrix} A_s(0) \\ A_i^*(0) \end{bmatrix}, \tag{2.31}$$

where the transfer matrix:

$$\mathbf{T} = \begin{bmatrix} \cosh(gL) - i\frac{\kappa}{2g}\sinh(gL) & i\frac{\gamma P_p}{g}\sinh(gL) \\ -i\frac{\gamma P_p}{g}\sinh(gL) & \cosh(gL) + i\frac{\kappa}{2g}\sinh(gL) \end{bmatrix}. \tag{2.32}$$

This is a simple relation that enables an analytical analysis of FOPAs in many different cases. It can account for different pump powers and different phase-matching (dispersion). It will prove very useful in Chapter 4, where we will use it to analyze phase-sensitive FOPAs, but it can also be applied to cases where one wants to consider several cascaded FOPAs. There may be no idler at the input of such a

cascade, but there is of course an idler at the input of every subsequent part. One application of this is analysis of non-uniform FOPAs, e.g. where the HNLF has a varying dispersion.

Dispersion-fluctuations

We can observe that if an output signal/idler pair from one FOPA is the input to another FOPA with another transfer matrix, it follows from matrix algebra that the two matrices can be multiplied to form the combined transfer matrix. Hence, we can divide a transfer matrix into many factors, each representing an arbitrarily short section of the propagation through the FOPA. The transfer matrix-method can thus be used to analyze FOPAs with varying dispersion, and thus phase-matching, by dividing it into many short segments of constant dispersion. Not only is this useful because real FOPAs implemented with HNLF always will suffer from some amount of dispersion-fluctuations due to manufacturing tolerances [55–57], in section 3.2 and Papers [I, J], we use the transfer-matrix method to analyze SBS-suppressed HNLFs that intentionally has a large non-uniformity.

Three-wave model and gain saturation

However, one aspect that the transfer-matrix model does not account for is when the signal and idler grows large enough to be comparable with the pump. This will affect the parametric interaction in two ways. First, the pump will be depleted and lose power. Second, the assumption that signal and idler SPM/XPM can be neglected no longer holds. Both of these effects will affect the relative phase, and therefore the strength, and eventually also direction of the power flow. Simply put, as the signal and idler grow and the pump is depleted, the gain per unit length decreases until some point where the direction of power flow reverses and the pump starts growing again. Note that this usually does not mean that the pump is completely depleted. If the FOPA is long enough, this oscillation of power between pump and signal/idler can continue over several periods. This phenomenon is illustrated in Fig. 2.6, showing the pump and signal power evolution along the fiber propagation in an example FOPA. In this example, the maximal small-signal gain if calculated with Eq. 2.29 would be 168 dB, which clearly is not possible in practice. Hence, the amplifier will be saturated.

Gain saturation also means that if the input signal power is increased to levels beyond the small-signal regime, the FOPA gain starts decreasing from the value found from e.g. Eq. 2.27 (i.e. saturating) and eventually become negative ("signal" is pumping the "pump"). Fig. 2.7 plots output pump and signal powers as input signal power is increased. Initially, the amplifier operates linearly, but as the pump

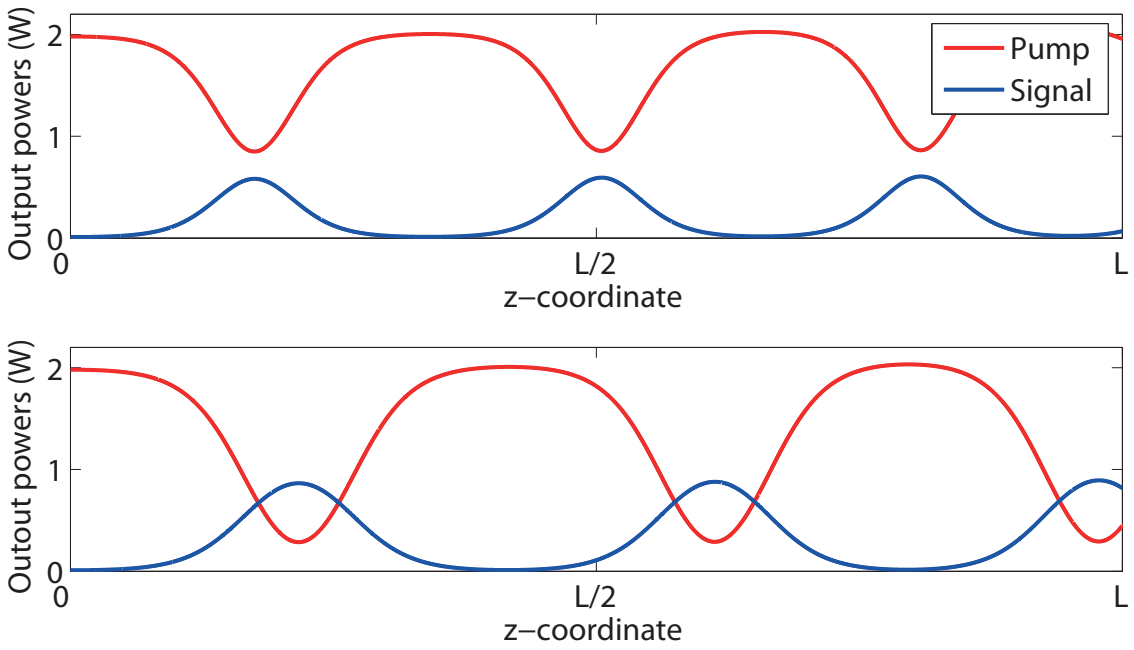

Figure 2.6: Pump and signal power evolution along the propagation for a FOPA where input pump and signal power is 2 W and 10 mW, respectively. The phase matching differs between the two cases, leading to different maximal pump depletion as well as different periodicity.

depletes, the output signal power saturates and reaches a regime where output signal power does not depend greatly on input signal power.

To account for these effects, a full solution of Eqs. 2.11-2.14 is necessary. It is usually most straightforward to solve them numerically, but analytical solutions in terms of elliptical functions are possible [43], though quite involved. This is often called the three-wave model, since, in the single-pumped case, we have three waves coupled through parametric interaction (and hence three coupled differential equations). Of course, those solutions are fully consistent with the transfer matrix-model in the small-signal case.

It should be noted that in practice, large pump depletion and/or large signal/idler powers usually also means much larger higher-order FWM (the generation of additional frequency components). This is not accounted for in the three-wave model and may affect experimental results if the higher-order components are non-negligible. In such a case, one can either resort to a more involved multi-wave model with a larger system of coupled differential equations, or a full numerical solution of the NLSE. Fig. 2.8 shows an example optical output spectrum of a saturated FOPA with higher-order FWM products, and a power imbalance between signal and idler

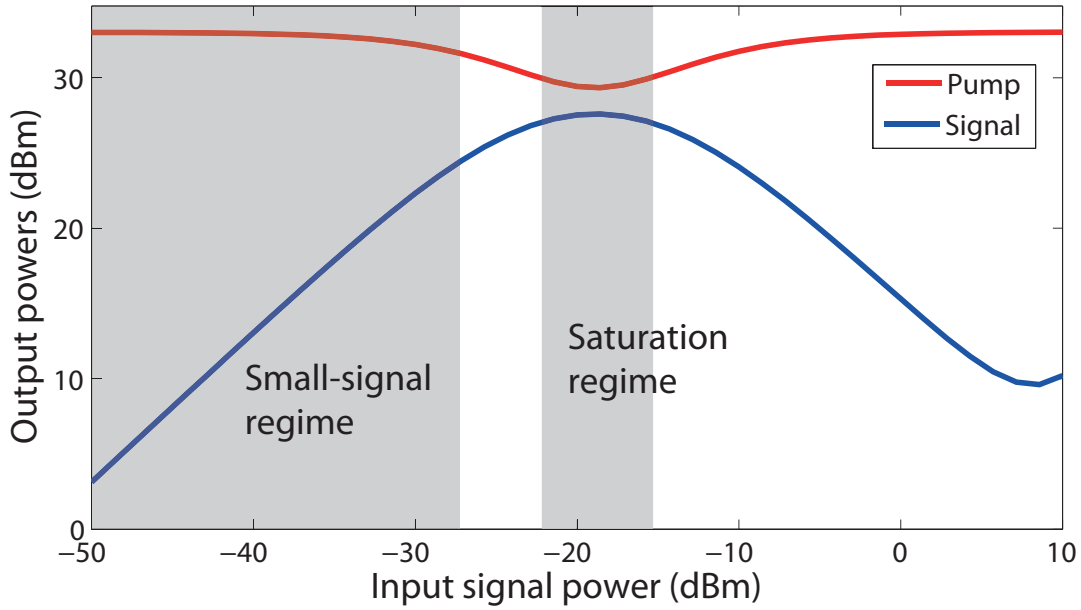

Figure 2.7: Output pump and signal powers vs. input signal powers for an example FOPA. The small-signal regime, where output signal power grows linearly with input signal power, and the saturation regime, where output signal power has minimal dependence on input signal power, are highlighted.

mainly due to the Raman effect (see next section), but also to different levels of higher-order FWM (the signal is pumping the higher-order FWM more efficiently than the idler).

2.6 Scattering effects

We have already established that the inelastic scattering processes can be described as the exchange of energy between the lightwave and vibrational modes of the medium. Unlike parametric nonlinearities, e.g. FWM, they do not require phase-matching, but rather can be considered to be automatically phase-matched thanks to the active participation of the medium, similar to amplification through stimulated emission in a medium with population inversion. In this section we elaborate further on how Raman and Brillouin scattering manifest in an optical fiber, and how these processes can be made to be stimulated.

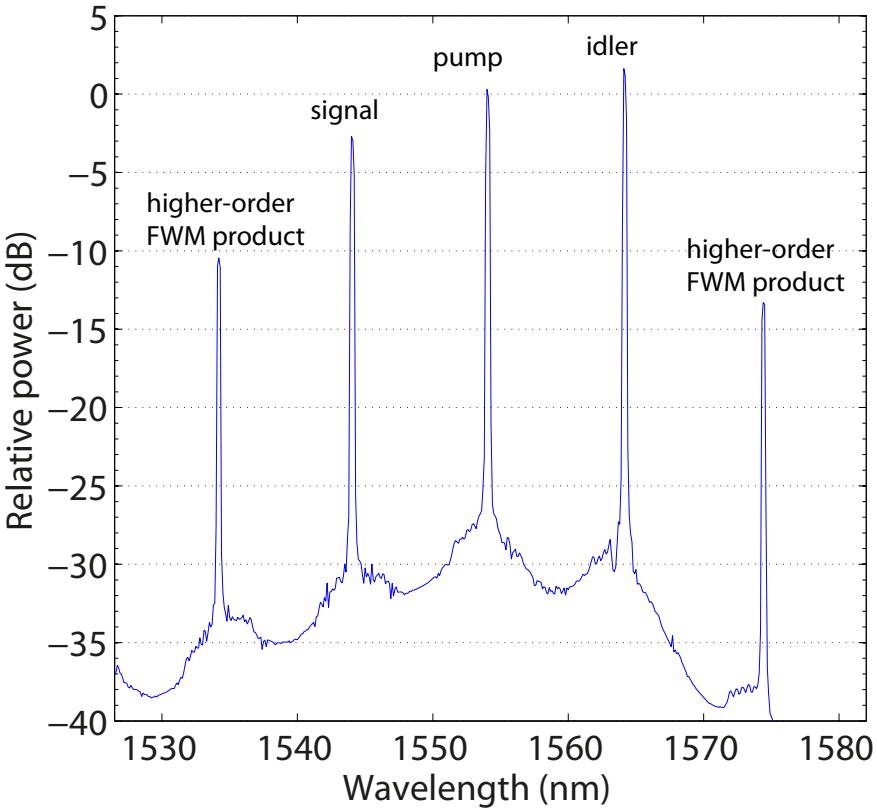

Figure 2.8: Experimentally measured optical output spectrum of a FOPA experiencing large gain saturation. The tilt in power is attributed to Raman gain and different relative strengths of the higher-order FWM-processes. (Figure from Paper [D]).

Raman scattering

Spontaneous Raman scattering was first observed by Raman in 1928 [58]. Simply put, the Raman effect is the emittance by an excited molecule of a photon of lower-frequency (Stokes-shifted) or higher-frequency (anti-Stokes-shifted) than the absorbed photon. The difference in energy is a phonon, i.e. a vibration of the molecule, and thus the energy difference is a characteristic of the material. In an optical fiber, the Raman effect becomes important if it is stimulated. Stimulated Raman scattering (SRS) was first discovered in 1962 [59] and is the process in which power from an optical wave (the pump wave) is transferred through the Raman effect to another optical wave with a lower frequency, known as the Stokes wave. If two such waves are present at the input of the fiber, and their frequency shift matches that of the material in the fiber, a chain reaction starts in which pump photons are

annihilated and Stokes photons as well as phonons are created. Since more phonons are created, the vibrational energy increases thereby stimulating the process further. Hence, the Stokes wave will be amplified. The opposite is also possible, wherein the so-called anti-Stokes wave is attenuated by a strong pump.

In a silica-based fiber, the peak frequency downshift is about 13 THz, though Raman scattering occurs over a broad spectrum. It occurs in both the forward and backward direction and can be used for signal amplification [27, 60, 61]. Similar to FWM, SRS has a very fast response time, on the order of femtoseconds, and is polarization dependent, though only in the forward direction; if the pump and signal have opposite propagation directions, the Raman process is polarization independent. Moreover, the Raman gain grows exponentially with pump power, the fiber length and the inverse of the effective area.

Brillouin scattering

Much like Raman scattering, Brillouin scattering involves the generation of a Stokes wave from a pump wave, with the difference in energy being in the form of a phonon and can occur spontaneously but also be stimulated. Stimulated Brillouin scattering (SBS) was first observed in 1964 [62] and occur in a similar fashion to SRS. SBS can become the dominant process if the pump wave exceeds a power threshold. However, unlike Raman scattering, Brillouin scattering only generates a Stokes wave in the backwards direction, relative to the pump. The frequency downshift is dictated by the speed of sound in the material, and in a silica fiber, the downshift is typically around 10 GHz with a frequency bandwidth of only tens of MHz [27, 63].

Spontaneous Brillouin scattering can also occur in the forward direction, something that is known as guided acoustic wave Brillouin scattering (GAWBS) [64]. This phenomenon is normally very weak, but e.g. in fiber Sagnac loop interferometers it can play an important role.

Since SBS limits the input power it often becomes a large limiting factor for nonlinear fiber devices that are dependent on large pump powers to drive other nonlinearities, such as the parametric devices discussed in this thesis. Fortunately, there are ways to suppress SBS. We devote Chapter 3 to SBS in nonlinear fibers, how to suppress it, and the resulting performance trade-offs.

Chapter 3

Stimulated Brillouin Scattering

In optical fibers, stimulated Brillouin scattering (SBS) typically manifests as a threshold power, above which any increase in the input power (e.g. of the pump in a parametric amplifier) will be backscattered, limiting the available usable power. In this chapter, we discuss the Brillouin gain in fibers, specifically conventional HNLFs, how it can be suppressed, and what the performance penalties for parametric devices arise from these suppression methods.

SBS in an optical fiber [63] can be understood in the classical picture as follows: through the electrostriction effect an intense pump field will generate an acoustic wave in the fiber, co-propagating with the pump, but at the speed of sound v_A. This acoustic wave modulates the refractive index, forming a moving index grating. The scattering of a lightwave against a grating into a counter-propagating wave is described by the Bragg condition [27, p. 330]:

$$\Lambda = \frac{\lambda_p}{2n}. \tag{3.1}$$

Here, Λ is the period of the grating, i.e. the wavenumber of the acoustic wave, λ_p the wavelength of the pump wave and n the refractive index of the fiber. Since the grating is moving at the speed of sound, typically around 6 km/s in silica, the scattered wave will be downshifted through the Doppler effect. The frequency downshift is given by

$$\nu_B = \frac{2v_A n}{\lambda_p}, \tag{3.2}$$

and using 6 km/s and 1.5 for v_A and n, respectively, we find a downshift of 11.6 GHz at a pump wavelength of 1550 nm. The backscattered wave will also interfere with the pump, which strengthens the grating even further, resulting in even

stronger scattering. The backscattering process occurs over a spectrum of downshift frequencies around the peak downshift, the so-called Brillouin spectrum, $\Delta\nu_B$, which typically is Lorentzian with a bandwidth of around 50-100 MHz and is related to the lifetime of the acoustic phonons.

If the input wave exceeds a certain threshold power, known as the SBS threshold of the fiber, all or almost all of the additional pump power above this threshold is transferred to the Stokes wave. The Stokes wave is seeded from noise and subsequently stimulates the process. Moreover, a wave that exceeds the SBS threshold and is backscattered to a significant degree will have substantial amplitude noise. For this reason it is crucial to avoid SBS on data signals.

3.1 The Brillouin gain

When an input pump wave is backscattered through SBS, the backscattered wave is downshifted in frequency by the SBS downshift ν_B, which is in the 9-12 GHz range in typical silica fibers. Since the backscattered wave is seeded from noise (vacuum fluctuations), it will have a spectral width that corresponds to that of the Brillouin gain. Normally, this spectrum has a Lorentzian shape, with a bandwidth $\Delta\nu_B$ of tens of MHz [27, pp. 330-333]. Since the Brillouin gain bandwidth is so narrow, in most cases two separate optical input waves will undergo SBS independently of each other[1], as the frequency separation of two optical waves is often much larger than $\Delta\nu_B$.

For a wave that has a spectral width below that of $\Delta\nu_B$, the SBS threshold, $P_{\text{threshold}}$ can be shown to be approximated by [27, 65]

$$P_{\text{threshold}} \approx \frac{21kA_{\text{eff}}}{g_B L_{\text{eff}}}. \tag{3.3}$$

Here, k is a polarization factor varying between 1 and 2 and g_B the Brillouin gain coefficient. The gain coefficient is dependent on, among other parameters, the speed of sound, the material density and the phonon lifetime [27, p. 331], some of which can be affected by the doping levels in the fiber. Of course, it also varies with the downshift frequency and has its maximum at $\nu = \nu_B$, which is the value we consider here. Neglecting loss in the fiber, the power of the backscattered wave P_{bs} will grow with (backwards) distance at a rate given by

$$\frac{dP_{bs}}{dz'} = g_B P_p P_{bs}, \tag{3.4}$$

[1]Of course SBS of one wave will affect the other if they are otherwise coupled, e.g. by parametric interaction.

where $z' = -z$ is the negative coordinate along the fiber. This means exponential growth, as long as the pump is undepleted, i.e. before reaching the SBS threshold.

Eq. 3.3 shows that the SBS threshold scales inversely with effective fiber length, meaning that the relevant measure for parametric amplification, and most other nonlinearities, the nonlinear phase shift, given by the $\gamma P_p L_{\text{eff}}$-product, will be limited to the same value regardless of fiber length when the pump power P_p is SBS-limited, since an increase in fiber length will lower the SBS threshold and thus the usable pump power. The same holds true for the effective area; increasing the nonlinearity by decreasing it will lower the SBS threshold by the same amount. However, if the nonlinear index n_2 increase, the strength of the Kerr nonlinearity relative to SBS will increase. The larger nonlinear index is one of the main reasons for using fibers made from non-silica glasses. There are thus not so many options available to improve the Kerr-to-SBS ratio in conventional silica fibers.

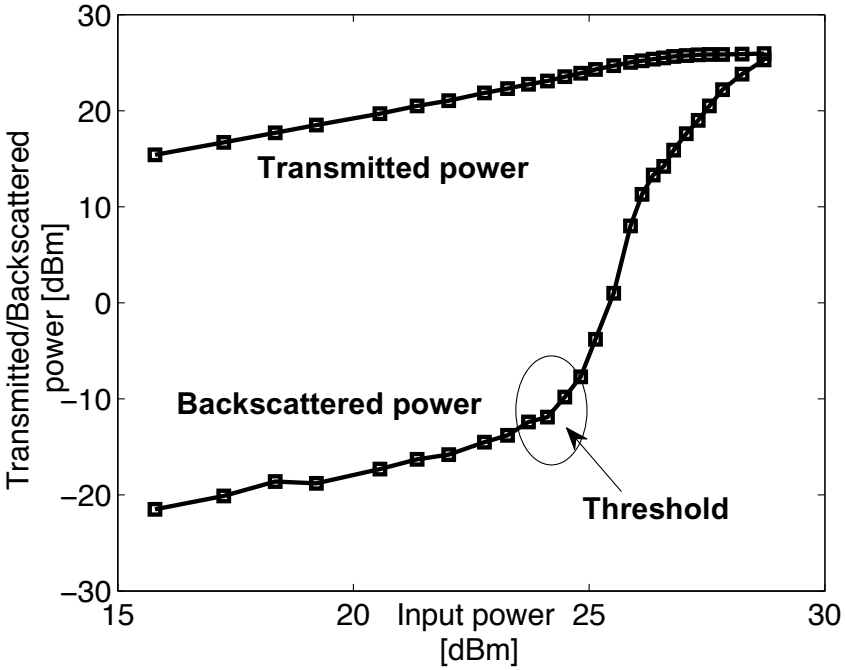

Figure 3.1: Measured backscattered and transmitted power through an 150 m HNLF as function of input power. For low input powers, the backscattered power is dominated by Rayleigh scattered light, typically about 40 dB lower than the input power.

Fig. 3.1 shows the measured backscattered and transmitted power as a function of the input power in a typical HNLF of 150 m length. From a measurement such as the one in Fig. 3.1, different definitions of the threshold exist, e.g. where the

backscattered power has increased a certain amount (3 dB, 10 dB, etc.) above the Rayleigh-only case, or alternatively where the transmitted power has saturated by a certain amount.

For a standard HNLF of 1 km, the threshold is on the order of only about 20-40 mW. Since the SBS threshold in a typical HNLF will limit the pump to powers much below what is needed for e.g. efficient FWM, there is a need to suppress SBS.

3.2 Suppression techniques and performance trade-offs

One can consider manufacturing fibers with improved Kerr-to-SBS ratio by reduced g_B, and/or increased nonlinear index n_2. This is typically accomplished by increasing the GeO_2 doping level of the core and/or by introducing another dopant such as Al_2O_3 [66–68]. Increased GeO_2 doping increases n_2, thereby increasing the Kerr-to-SBS ratio, but unfortunately also significantly increases the fiber attenuation. Introducing Al_2O_3 doping modifies the strength of the coupling between the acoustic and optical field, lowering g_B. Again, the main drawback is most notably severely increased fiber attenuation.

To increase the SBS threshold in HNLFs, one needs to reduce the exponential growth of the backscattered wave found from Eq. 3.4. Assuming a given g_B in the fiber, an increase in threshold can in principle be achieved by either:

1. Broaden the spectral width $\Delta\nu_p$ of the pump to cover a bandwidth larger than $\Delta\nu_B$, by means of e.g. phase modulation.

2. Modify the fiber to be non-uniform, so that downshift frequency ν_B changes along the fiber, leading to a broadening of the average Brillouin gain spectrum $\Delta\nu_B$.

3. Simply block the propagation of the backscattered wave at some point in the fiber, by e.g. an in-line isolator or a narrow band-stop filter, thereby forcing the backscattered wave to start building up from zero again.

The first corresponds to dividing the pump into several spectral components that undergo SBS independently. The latter two effectively amounts to reducing the length of fiber in which a seeded backscattered wave participates in stimulating SBS further. All three methods essentially means dividing a single SBS process into many, either in the frequency or spatial domain.

Pump spectral broadening

In the case of a pump with a broader spectrum than the Brillouin gain linewidth, the SBS threshold will be reduced. It can be shown [27, p. 333] that the threshold is increased by a factor

$$\frac{P_{\text{threshold,mod}}}{P_{\text{threshold}}} = \frac{\Delta\nu_B + \Delta\nu_p}{\Delta\nu_B}, \tag{3.5}$$

if the pump linewidth is also Lorentzian, and it remains a reasonable approximation also in other cases.

This is the most commonly used method for SBS suppression, usually by external phase modulation with several radio frequency (RF) tones [18,69], though it can also be accomplished with external modulation using electrical white noise [70] or pseudo-random data [71], as well as by direct modulation of the laser current [71]. When phase modulating with RF tones, the pump wave is spread out over 3^N frequency components, (neglecting higher-order sidebands) where N is the number of RF tones used. If the separation between frequency components is larger than $\Delta\nu_B$, the threshold will be reduced by a factor of 3^N, with carefully chosen frequencies and amplitudes of the RF tones [69], as each sideband experiences SBS independently. Each added RF tone thus increases the threshold by a factor of 3 (4.7 dB), at the expense of a pump spectral broadening, by a factor of $(3^N - 1) \cdot f_1$, where $f_1 > \Delta\nu_B$ is the lowest-frequency RF tone. Fig. 3.2 shows the measured optical spectrum of a wave modulated with one and two RF tones, respectively. Here, it can also be seen that it is difficult in practice to achieve sidebands that are perfectly equal in amplitude.

To increase the threshold more than 100 times (20 dB), five tones are needed (in theory providing 24 dB threshold increase), which typically means a pump spectral broadening of about 25 GHz [72]. Often, one desires to have the smallest spectral increase for a given amount of suppression. Then, modulation with white noise is preferable, since it is then, in principle, possible to achieve a pump spectrum that is flat over the desired spectral width.

While this suppression method is straightforward, in many applications the pump broadening is undesirable, particularly in FWM, where the generated idler phase includes the sum of the pump phases (Eq. 2.19). Even more problematic are applications where phase tracking of input waves are needed, such as for phase-sensitive processes. In that case, PM with a few RF tones is usually preferred over the other modulation signals, since the perturbation frequencies are few and known, so one can e.g. perform measurements at other frequencies than those affected, such as the noise figure measurements in Papers [C] and [H], or filter out those frequencies in software as was done for the transfer function measurements in Papers [B] and [D].

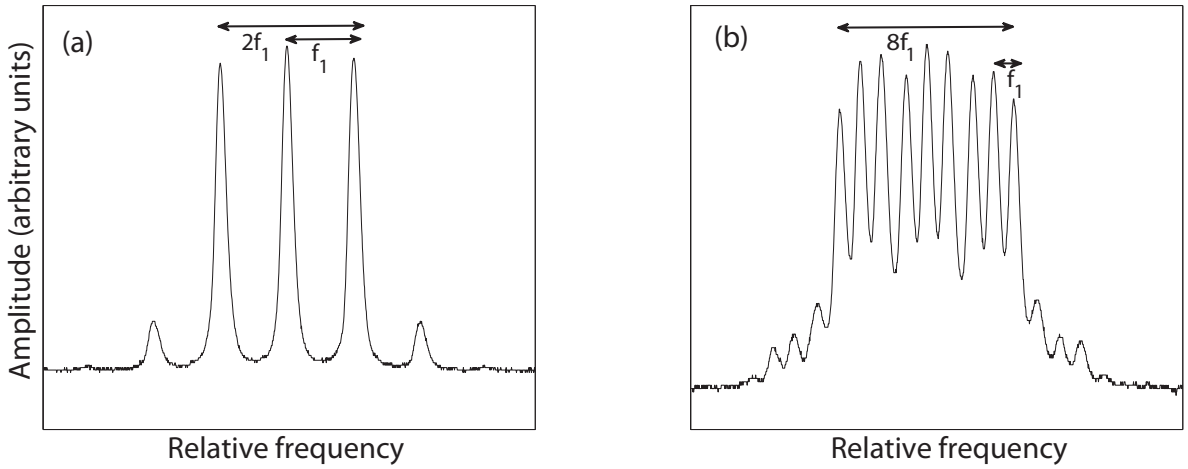

Figure 3.2: Measured optical spectra of a wave modulated with (a): one RF tone at frequency f_1, (b): two RF tones at frequencies f_1 and $f_2 \approx 3f_1$. In (a), the spectrum contains three sidebands separated by f_1 with a total width of approximately $2f_1$. In (b), the spectrum contains nine sidebands separated by f_1 with a total width of approximately $8f_1$. In both cases, weaker higher-order sidebands are also visible.

Fiber strain gradients

There are many ways of imposing a non-uniformity on the fiber, either during manufacturing or afterwards. One can can use different dopant concentrations [73] or different core geometries [74], or impose a temperature gradient [75] on the fiber. The most investigated method for HNLFs, however, is to impose a strain gradient along the fiber [68, 76, 77], Papers [I, J]. A strain gradient is practical, since it only requires spooling of the fiber once. A temperature gradient on the other hand, requires active heating and/or cooling. Regardless of method, it could either be a continuous or stepwise gradient along the fiber, or even be accomplished by concatenating different fibers, though then coupling/splicing losses become an issue.

In all these cases, the SBS is suppressed because the Brillouin gain spectrum shifts along the fiber, making a Stokes wave generated in one end not participate in the SBS process further down the fiber, where it is outside the Brillouin gain bandwidth. Ideally, the gradient is such that the SBS downshift frequency is uniformly distributed over all its values along the fiber. It does not have to be linearly varying along the fiber, but for practical reasons, this is usually the case. Fig. 3.3 shows the measured Brillouin gain spectrum of an HNLF with and without a strain gradient applied. A broadening of the Brillouin gain spectrum 10-dB bandwidth of

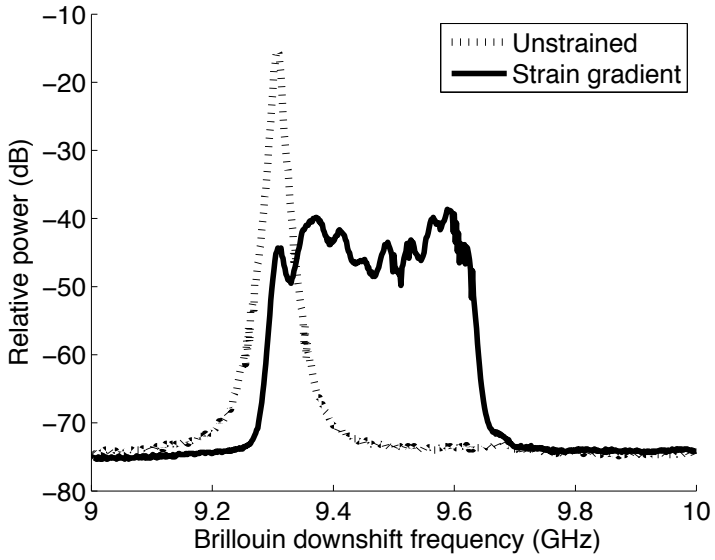

Figure 3.3: Measured Brillouin gain spectrum of an HNLF without strain (dashed) and with a linear strain gradient. (From Paper [I].)

from about 20 MHz to about 300 MHz was observed.

The fundamental problem when using these methods to suppress SBS in HNLFs for parametric amplifier-applications is that the change in SBS downshift is accompanied by a change in dispersion, leading to a dispersion gradient along the fiber that all these methods are marred by. The HNLF in Fig. 3.3 showed a ZDW gradient over about 10 nm with the strain gradient applied. Nevertheless, a dispersion gradient does not have to be an issue for some applications. It is well established that a zero-dispersion variation impairs the phase-matching of FWM, and thus the gain spectrum of parametric amplifiers [56, 78]. However, as is discussed in Paper [I], by shifting the pump wavelength far enough from the ZDW, the influence of the dispersion variation is reduced, at the expense of total bandwidth. Thus, the same maximal gain is achievable as in the case without ZDW variations, but over a much smaller bandwidth (assuming the same pump power), which may be an acceptable trade-off to increase the SBS threshold. It can also be noted that strain gradients have been used to reduce existing dispersion variations in HNLFs [79].

However, there has recently been an effort to develop HNLFs designed to have small dispersion variations after being strained, either by designing them to have an initial variation in dispersion and subsequently strained to simultaneously increase the SBS threshold and cancel the initial dispersion variations [80], or by designing them to be dispersion-robust when the geometry varies [81–83]. Increased PMD due

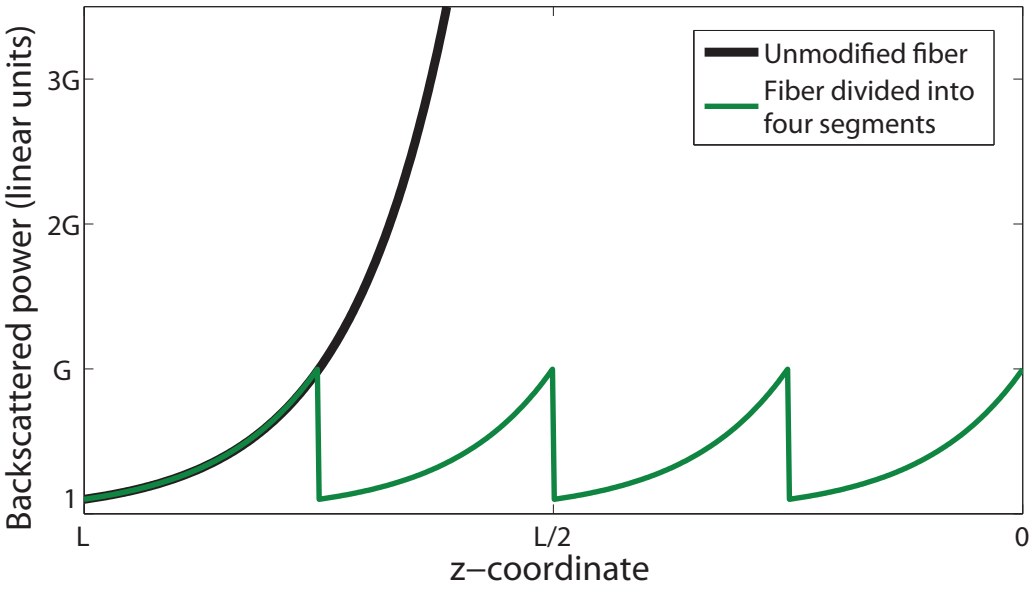

Figure 3.4: SBS backscattered power (relative) along the fiber z-coordinate, (backwards direction) illustrating the benefit of segmenting the fiber into independent parts.

to the straining remains an issue, however [83].

In-line isolators

First demonstrated in [84], and for an HNLF in [85], the SBS can be reduced by periodically blocking the backscattered wave in the fiber by using isolators (or circulators), forcing it to start growing again from a very low level. Since the power of the backscattered wave grows exponentially along the fiber, this can mean a large difference in total backscattered power. The principle is shown in Fig. 3.4. In this example, the backscattered wave (with relative power of unity at the fiber end) grows by a factor of G over a fiber length of L/4. Hence, the backscattered wave (and thus depletion of the pump) becomes G^3 times larger in the case of no blocking of the backscattered wave compared to the case where it is blocked at three points along the fiber (effectively dividing the fiber into four sections). Assuming lossless isolators and fibers, the threshold of the cascade will then be equal to the threshold of a single piece, since they operate independently in terms of SBS, i.e. the threshold will scale with the number of isolators plus one, assuming that they are uniformly distributed in a uniform fiber. However, the insertion loss and input/output coupling or splicing loss that isolators have must of course be considered. In Paper [J], an

HNLF cascade of four pieces was constructed where the threshold of each individual HNLF piece compared with the preceding was lowered (by increasing the length) by approximately the loss of the isolator before it. This design yielded approximately a 5 dB larger net threshold, to be compared with the theoretical 6 dB, had the lengths perfectly matched the isolator losses. Another issue is that inserting components, especially if they are pigtailed with SMF, may perturb e.g. the phase matching in FWM [85]. In Paper [J], this issue was addressed by using isolators with very short (a few cm) pigtails. In addition to the isolators, the HNLF segments used in Paper [J] had a strain gradient applied, which increased the SBS threshold by about 6 dB. Hence, the total net threshold increase was 11 dB, which enabled a parametric net gain of 10 dB without any pump spectral broadening.

Chapter 4

Phase-sensitive amplification

A phase-sensitive process is one where a property other than the phase (e.g. the amplitude) is affected by the input phase. The most obvious example is an interferometer where two lightwaves are combined and through constructive or destructive interference the output power is affected by the input phase. However, a regular interferometer does not provide any gain. As we know from Chapter 2, nonlinear devices, on the other hand, can through nonlinear processes generate new frequency components and provide signal gain. We have also discussed how these processes are inherently phase-sensitive, in that they are sensitive to the relative phase of the interacting lightwaves, which is what leads to the phase-matching condition. Usually though, they are often phase-insensitive (PI) with respect to the phases of the waves at the input. However, under some input conditions, nonlinear processes such as parametric amplification can typically be made phase-sensitive (PS), meaning that it is dependent on the value of the relative phase of the interacting waves (e.g. pump and signal) *at the input*, or alternatively, if e.g. the pump is considered to have a fixed phase, it becomes dependent on the absolute signal phase. Normally, one considers the signal phase to be the variable, and thereby assumes that the pump waves are perfectly phase stable. Thus, the idler needs to be phase-correlated (and frequency-locked) to the signal (and in practice also the pumps) by some other process before the phase-sensitive amplifier (PSA). This is what makes PS amplification challenging to achieve. In the discussion in this chapter, unless stated otherwise, we will assume that the pump phase is fixed, giving a relative phase that is equal to $\theta_s + \theta_i$. (Compare Eq. 2.19).

Throughout this chapter we will discuss PS amplification based on parametric amplification (i.e. FWM) in optical fibers. In addition to FWM, PSA is also possible through nonlinear fiber interferometers, with many important experimental

demonstrations [86–90]. However, such a device is completely frequency degenerate, i.e. pump and signal are indistinguishable, making them less interesting in practice. It should be mentioned that there have been many experimental demonstrations of PSA in $\chi^{(2)}$-media [91–94], including using cascaded SHG-DFG rather than parametric amplification [95–97]. However, such PSAs have not been demonstrated with particularly large gain, as can routinely be achieved in fibers. The work in this thesis that involve PSA is based only on FWM in fibers.

We begin this chapter by describing the basic concepts behind phase-sensitive amplification, and how it can be implemented in optical fibers in section 4.1 and the concept of squeezing is also introduced. In section 4.2 we build on the mathematical descriptions of parametric gain established in Chapter 2 to develop expressions for how a PSA affects the signal amplitude and phase. PSAs in saturation is an interesting topic since it is well known that a saturated FOPA can operate as an amplitude limiter, thereby reducing amplitude noise [20, 22, 98–100]. How this can be exploited in together with phase squeezing in PSA is discussed in section 4.3. Finally, a very important property of PSA that has been the subject of several earlier investigations [87, 88, 101–103], is the possibility of noiseless amplification, i.e. an amplifier with a 0 dB noise figure (NF). This topic will be addressed in section 4.4.

4.1 Basic concept

Consider the dependence on the relative phase in conventional parametric gain in section 2.4.1. This quantity controls the magnitude and direction of the power flow, as seen in Eq. 2.16-2.17. In the phase-insensitive case, where there is no idler at the input, a vacuum fluctuation will seed the idler at the correct frequency, with a phase giving the optimal condition ($\theta_{\text{rel}} = \pi/2$). During propagation, the relative phase will subsequently drift from this value if the phase-matching is not perfect. The idler thus tracks changes in the input signal and pump phase, so that the relative phase remains constant at a given point in the amplifier (e.g. the output). If we instead have an idler at the input, we can control the parametric process by controlling the idler phase (or that of any other wave). Since we have a device whose gain varies strongly with the signal phase, the output signal will have almost only the phase(s) giving the maximal gain. Recall that changing the relative phase from $\pi/2$ to $-\pi/2$ changes sign but not magnitude of the right hand side of Eq. 2.17, i.e. the signal/idler growth rate. As an example, if the gain varies between ± 20 dB for different phases, an input signal giving $\theta_{\text{rel}} = \pi/2$ will yield a 40 dB larger output signal than a signal giving $\theta_{\text{rel}} = -\pi/2$. Of course, other signal phases will end up at powers in between these extremes. By considering all input signal

phases a linear combination of these two orthogonal states, we can understand *phase squeezing* in the classical (wave) picture. A signal of an arbitrary input phase will at the output have a part at the in-phase (max. gain) quadrature, and a part at the orthogonal (max. attenuation) quadrature that usually can be neglected, due to the large difference in gain, resulting in a constant output phase. Since only the in-phase part of the input signal will contribute significantly to the output signal, the output power will be dependent on how large a fraction of the input signal is in the in-phase quadrature - i.e. the output power depends on the input phase. Essentially, we have transferred a variation in phase to one in amplitude. The main application of this phenomenon is reduction of phase noise [90], Paper [E], but it has also been suggested for dispersion compensation and pulse compression [104, 105], Paper [G].

We often call the reduction of noise in either phase or amplitude *squeezing*. Fig. 4.1 illustrates this concept. As described above, squeezing can be interpreted classically as interference of two waves. In the quantum-mechanical (photon) interpretation phase-sensitive amplifiers can also produce squeezed states of light [106, 107]. They are so called, since the interaction will "squeeze" the uncertainty, or noise, in one quadrature at the expense of the other. Such non-classical light can for instance exhibit amplitude noise below the otherwise fundamental shot-noise limit. Fundamentally, squeezed states is a quantum-mechanical phenomenon, originating in the interaction of correlated wave functions (i.e. photons). Here, the uncertainty in the two quadratures are quantum uncertainties, i.e. the product of them are limited by the Heisenberg uncertainty relation [106, p. 210]. A squeezed state is generated from a coherent state (a state of highly correlated photons exhibiting Poisson statistics, first introduced by Glauber in 1963 [108]) or from the vacuum state through a nonlinear interaction. Experimental amplitude-squeezed light has been presented at a noise level 10 dB below the otherwise fundamental shot noise limit [109], using PSA in a nonlinear crystal, but generation of amplitude-squeezed light has been demonstrated in a fiber-based PSA as well [110].

4.1.1 Implementations of phase-sensitive amplifiers in fibers

Figure 4.2 shows the frequency allocation in different implementations of PSA in optical fibers [111]. In the first case, a so-called 1-mode PSA [112, 113], the signal and idler are degenerate and is in the frequency domain symmetrically surrounded by two CW pumps. A clear advantage of this scheme is of course that no generation of an idler (i.e. with the data of the signal) is necessary, however, two frequency- and phase-locked pumps must somehow be generated. If the signal and one of the pumps

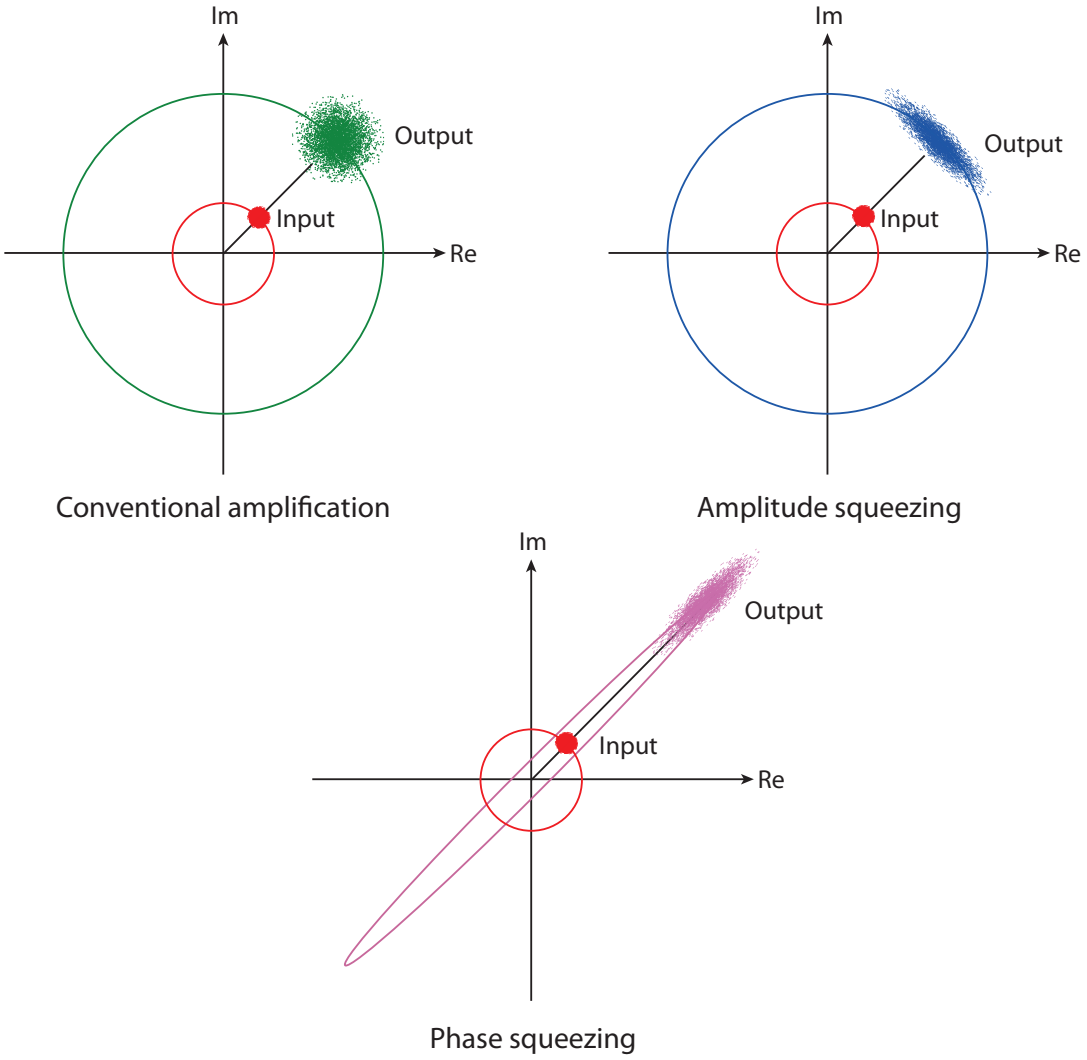

Figure 4.1: A noisy signal in the complex plane is amplified conventionally, with amplitude squeezing (e.g. in a saturated FOPA), and with phase squeezing (in a PSA). In the first two cases, the phase is preserved as shown (the red input circle is translated to a larger circle), whereas in the phase-squeezing case, the phase is not preserved and the input circle is translated to an ellipse.

originate from two separate, free-running lasers, the second pump must be locked with the phase $\theta_{p_2} = 2\theta_s - \theta_{p_1}$. It should be pointed out that if θ_s only includes the phase of the optical carrier of the signal (as is the normal case; otherwise the pump would need to carry data), the PSA will be phase-sensitive with respect to the added phase modulation and/or phase noise of the signal; hence such a PSA would be useful to reduce (squeeze) phase noise of a signal with binary phase-encoded

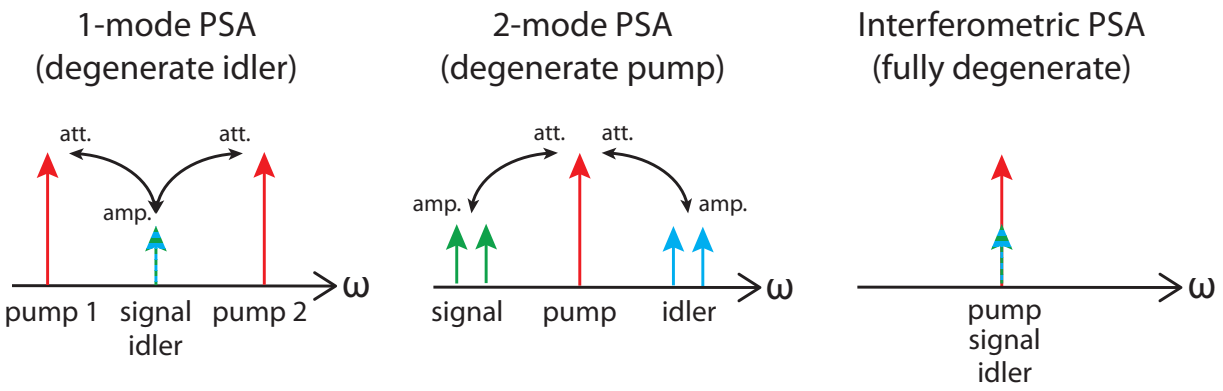

Figure 4.2: Different PSA schematics possible in optical fibers illustrated in the frequency domain. Power flow can go either from or to the pump(s) depending on the relative phase.

data. Multiple-level phase-modulated data will be destroyed of course, as the PSA will amplify only one quadrature. Finally, we mention that the degenerate-idler PSA scheme can also be implemented in the vector configuration, where the pumps have orthogonal polarizations, and the signal and idler are degenerate in frequency but not in polarization. However, we will limit the discussion in this chapter to scalar FWM, where all waves have parallel polarization, and will not consider vector schemes further.

The second case shows so-called 2-mode PSA [112,113], wherein a non-degenerate signal-idler pair symmetrically surrounds a pump in the frequency-domain. As indicated in the figure, multiple signal-idler pairs can be simultaneously phase-sensitively amplified in this case [114]. However, an idler carrying the same data as the signal, must in the normal case be generated. Additionally, the pump must be phase-locked with respect to the signal and idler. If the idler is an identical copy of the signal, then this scheme behaves much in the same way as the degenerate-idler scheme, with amplification of a single signal (and idler) quadrature. However, if the idler is the conjugate of the signal, the absolute dependence on the signal (i.e. data) phase will cancel out when the phases are summed, and the PSA will amplify all signal phases, but still be able to amplify with a quantum-limited NF of 1, as the signal will be amplified more efficiently than uncorrelated noise (refer to section 4.4 for a more elaborate discussion on this topic). The non-degenerate idler scheme can also be implemented with two pumps, and the signal idler pair must then have the same average frequency as that of the pump pair.

Finally, the third case shows a fully degenerate, interferometric PSA [86]. It

involves only two waves, pump and signal, that share the same frequency, and must be phase-locked. By injecting them into the two ports of a Sagnac loop nonlinear interferometer, the waves will experience a phase-shift due to SPM and the gain and phase-sensitivity arises by constructive/destructive interference between pump and signal at the output port [115]. Since this configuration requires generation of a CW pump of the same frequency as the signal, it is very similar to homodyne coherent detection. The loop mirror configuration is, however, sensitive to guided acoustic-wave Brillouin scattering (GAWBS) [54], which can make them unstable. Moreover, the small-signal gain in such a device is quadratic with respect to the nonlinear phase shift, whereas in FWM it can be made exponential, meaning that less pump power is needed to reach a certain gain.

Generation of phase-locked waves

Common for all three configurations detailed above, and indeed for all kinds of phase-sensitive amplifiers, is the need to generate phase-locked waves. In earlier proof-of-concept experiments, this has usually been done by generating sidebands from a single laser through electro-optic modulation [101, 116, 117]. Then, phase-locked CW components are obtained, that subsequently can be split, in order to impose data modulation on some, amplify some, etc. However, the drawback of this method is that the frequency separation is limited by the bandwidth of the electro-optic modulators (tens of GHz). To overcome this bandwidth limitation, the use of a phase-insensitive parametric amplifier to generate the locked waves was proposed in [118]. This is the so-called *copier-PSA*-configuration used in Papers [A-D, F-H], the principle of which is shown in Fig. 4.3 (top). It is further detailed in the next section of this chapter. Another important advantage of using a copier to generate the waves is that it is capable of copying also signal data, a very important feature that enables low-noise amplification of arbitrary signals. It can thus both be used to generate correlated CW waves that subsequently are modulated, as is possible with modulator-generated sidebands, but also for direct generation of a data-carrying idler.

In Paper [E], which is based on the degenerate-idler PSA configuration, a similar method to generate the phase-locked pump is used. This is work is, to the best of our knowledge, the first demonstration of a full "black-box" PSA, meaning that the only input is a free-running, data-carrying signal. In order to generate the locked pump, the signal is combined with the free-running pump in a first-stage phase-insensitive parametric amplifier, but the signal acts as pump in this stage. Since the signal carries binary phase-shift-keyed (PSK) data modulation, the data is "stripped" [119, 120], and the generated idler is phase-locked with respect to

the signal carrier (actually two times this phase), and the phase conjugate of the other pump, thus any dependence on the free-running lasers will cancel out when these three wave interact in the PSA. In subsequent work, this method has also been extend to signals with quartenary PSK data modulation by using higher-order FWM products [121,122], but it is inherently limited to M-ary PSK signals, more advanced modulation formats (e.g. quadrature amplitude modulation (QAM)) cannot be modulation-stripped in this manner. The principle (for binary PSK) is illustrated in Fig. 4.3.

To be able to exploit the often weak generated FWM component as a PSA pump in Paper [E], injection locking was used to recover its SNR. Injection locking of lasers is a way of making a slave laser track a master by injecting power from the master laser into it. It is normally capable of tracking phase and amplitude variations of the master up to the MHz level easily [123, 124], making it possible to lock to a free-running laser. It thus serves two purposes; low-pass filtering the phase, so that only the desired (relatively slow) phase variations originating from the laser linewidth remains, and to amplify the master without adding any significant amplitude noise. Another application of injection locking in the PSA context is pump recovery after transmission, e.g. a weak pump tracking the signal phase is generated at the transmitter and co-propagates with the signal. To use the pump in a PSA after transmission, simple amplification is not sufficient, as it would give a much to low optical signal-to-noise ratio (OSNR) of the pump. This was proposed in Paper [H] and subsequently experimentally demonstrated in [125].

In the case where the generated correlated waves are separated for individual processing prior to the PSA, some active phase-locking must also be done to cancel the relative drift they will experience from thermal and acoustic drifts. Fortunately, such slow drifts can be canceled by phase-locked loops are relatively straightforward to construct. They are based on lock-in amplification of a weak dithering tone and piezo-electric transducers (PZT) to stretch the fiber in order to cancel such drifts.

4.1.2 Copier-PSA implementation

Throughout this thesis, the copier-PSA configuration is used. In essence, this is a single parametric amplifier that is "split" into a phase-insensitive part (where an idler is generated) and a phase-sensitive part that is analyzed. It is based on the realization that all parametric amplifiers are phase-sensitive internally as soon as the idler has formed. By deliberately modifying the waves in a so-called *mid-stage*, the PSA behavior can be analyzed. Moreover, a very tangible benefit can be had in terms of noise performance if there is a large loss in the mid-stage, as we will see in section 4.4. Figure 4.4 illustrates the copier-PSA configuration schematically, with

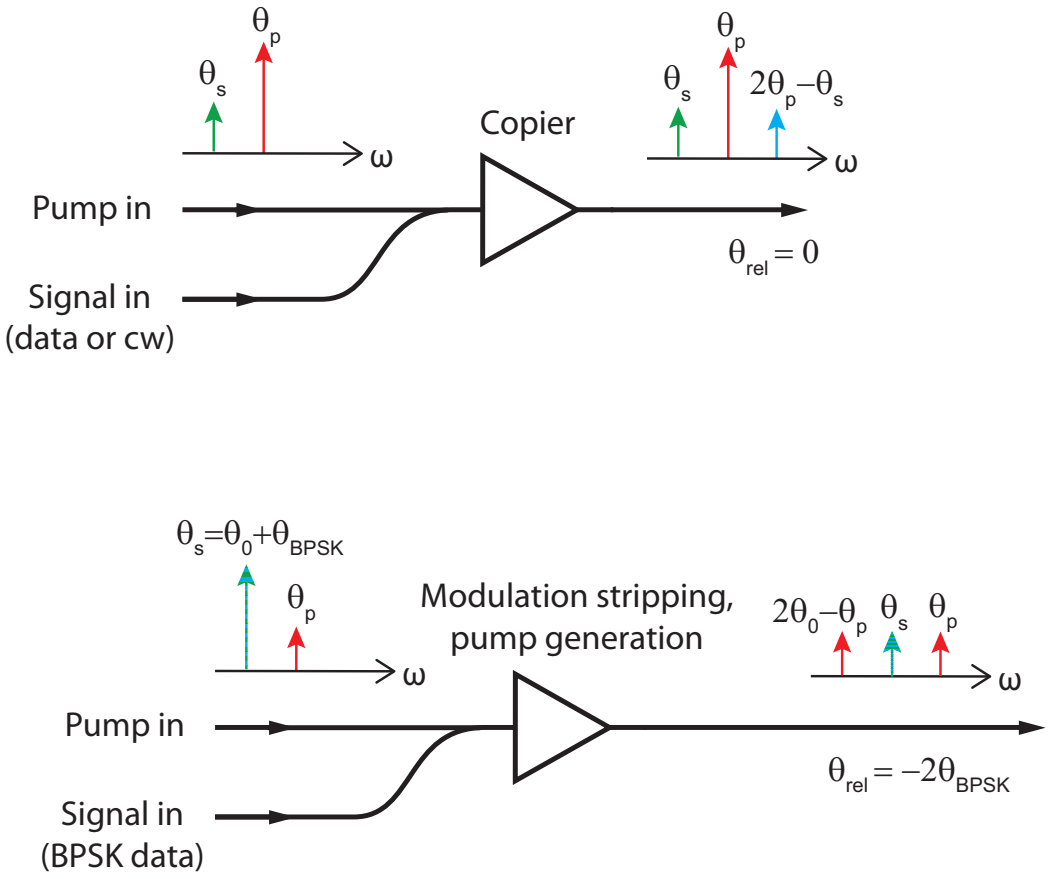

Figure 4.3: Generation of phase-locked waves using first-stage FWM. The frequency allocation and phases of interacting waves are shown. Top: a conjugate copy of the signal, carrying both pump and signal phase information is generated in a "copier" (conventional parametric amplifier). This wave triplet has a constant relative phase. Bottom: A pump is generated from a signal carrying binary PSK data by modulation stripping through phase-doubling by FWM. The generated wave triplet has a relative phase of two times the signal data, meaning that the two phase states of the signal can be amplified in a PSA.

the signal and idler being modified in some manner in the mid-stage.

The copier-PSA implementation is of course a practical one in the sense that the copier generates a correlated wave triplet, since the idler is carrying the phase of the pump and signal. Otherwise, generating waves that is completely frequency- and phase stable with respect to each other is a challenging proposition indeed. It should be emphasized that since the first stage generates a conjugated idler, the relative phase remains constant, regardless of the signal phase at the copier input.

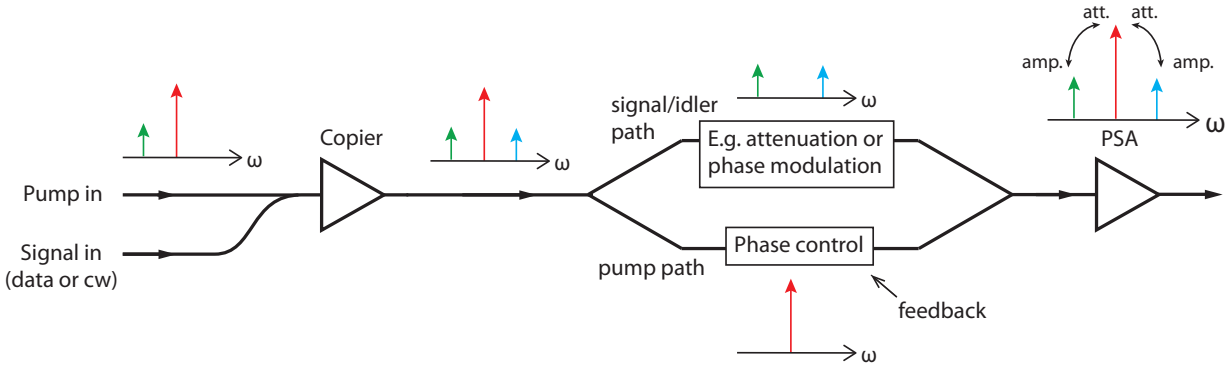

Figure 4.4: Schematic copier-PSA setup in the single-pumped non-degenerate idler configuration. The signal and idler are modified in the mid-stage, and some phase control feedback mechanism is necessary to keep pump and signal/idler stably phase-locked at the PSA input.

The full copier+PSA system is thus phase-insensitive (and has a quantum-limited NF of 3 dB, for example). In PSA experiments described in Papers [A-D, F, G], the phases of the signal and idler was modified in the mid-stage, and the PSA was phase-sensitive with respect only to the added phase modification in the mid-stage. In Papers [A, G], this modification was static, while in the others it was dynamic.

A similar method was used in Paper [E] to generate the pumps. Here, the implementation was of the non-degenerate idler variety, hence, two pumps needed to be generated from a data-carrying signal. With the additional step of modulation stripping through FWM, two CW pumps could be generated.

4.2 Phase dependence of phase-sensitive amplifiers

Considering the transfer-matrix description of a FOPA in Eq. 2.31, we observe that it can be written on the form

$$\begin{aligned} A_{s,out} &= \mu A_{s,in} + \nu A^*_{i,in} \\ A^*_{i,out} &= \nu^* A_{s,in} + \mu^* A^*_{i,in} \end{aligned}, \tag{4.1}$$

with the complex coefficients μ and ν fulfilling the relation

$$|\mu|^2 - |\nu|^2 = 1. \tag{4.2}$$

This is called a two-mode squeezing transformation, and is known to produce squeezed states [106, 111]. From Eq. 4.1, it is also easy to see that when there is no idler at the input, one that is proportional to the signal conjugate will be generated, while the signal field is merely scaled (and undergoes a constant phase rotation), i.e. it is phase-preserved. When both signal and idler are present, the output complex signal field will be a linear combination of both input fields, and thus the phase will not be preserved. Furthermore, if the input signal and idler power are equal, and $|\mu| \approx |\nu|$, as is the case for large gL, i.e. large small-signal gains, the output signal field amplitude will be twice as large in the case of idler present as compared to the case without idler. The fields are added coherently, meaning that in the case of high gain the output signal power will then be four times (6 dB) larger in the phase sensitive case, despite only having twice (3 dB) the total input power (signal+idler). This is valid not only at the perfectly phase-matched signal/idler wavelengths, but for all signal/idler wavelengths where the gain is large.

In Paper [B], explicit expressions for the output signal power and phase in terms of $|\mu|$, $|\nu|$, and the signal and idler power and phases were published for the first time, to the best of our knowledge. The full derivation of these expressions can be found in Appendix A, together with some limit cases of practical interest. The main conclusions that follow are:

- The output signal power is periodic in the signal phase with a period of π.
- The extremas of the gain with respect to the signal phase are $G_{\mathrm{max,min}} = (|\mu| \pm |\nu|)^2$, hence $G_{\mathrm{min}} = 1/G_{\mathrm{max}}$.
- The output signal power is 6 dB larger in the presence of an input idler of equal size and proper phase, if the gain is large, compared with the case without input idler, i.e. $G_{\mathrm{max}} = 4 \cdot G_{\mathrm{PIA}}$.
- The output signal phase has a one-to-one relation with the input phase in the limit of no gain, and the output signal phase dependence on the input phase is successively reduced as the gain increases.
- The output signal phase has a one-to-one relation with the input signal phase in the limit of no input idler, and the output signal phase dependence on the input phase is minimized when the input signal and idler are equal in power.
- In the high-gain limit, the output signal phase reduces to two discrete phase states, as long as the input signal and idler have the same power.

In Paper [A], the phase-to-amplitude transfer functions of a PSA were experimentally measured, using static phase-shifts and direct measurement of the signal

power. In Paper [B], the phase-to-phase transfer functions were experimentally measured, using dynamic phase-shifts in the mid-stage, and a self-homodyne approach, where the signal laser is tapped and used as local oscillator. In both cases, the measurement included the dependence on pump power and signal-to-idler power ratio.

4.3 Saturation effects in phase-sensitive amplifiers

With an established theory for the phase-dependence of PSAs in the undepleted-pump approximation, it follows to ask what will happen when this assumption no longer holds. As we saw in Chapter 2, the phase-matching condition will be affected by the growth in power of the signal and idler, leading to a more complex interaction between the waves that requires resorting to the three-wave model, rather than the simpler transfer-matrix. How are the phase-to-amplitude and phase-to-phase transfer functions affected? It is reasonable to assume that different signal phases will be affected vastly different, since the small-signal gain varies so much with the phase.

Moreover, it is well-known that a saturated phase-insensitive parametric amplifier works well as an amplitude limiter, i.e. a regenerator, since the power response becomes flat over a range of input signal powers, and thanks to the ultrafast response time it will saturate for individual pulses rather than average power, which has been used for amplitude regeneration of both amplitude- [20, 98] and phase-encoded data [22, 99, 100].

A PSA will convert any phase noise (PN) to amplitude noise (AN) since its gain is phase-dependent. In regenerating the optical phase using PSAs one may therefore want to operate the PSA in saturation. To enable this, the PSA must be saturated over the range of phases for which one wishes to squeeze both PN and AN. However, a large saturation also means a reduction in the FWM efficiency and thus, in the phase squeezing. Hence, this raises the question of what level of saturation is optimal, and how the phase-to- phase transfer function behaves as the amplifier is saturated. In Paper [E] good performance was achieved by operating the PSA in gain saturation in order to both reduce the inherent PN to AN conversion as well as to suppress any existing amplitude noise on the input signal by amplitude limiting, as had previously been suggested [126, 127]. Paper [D] investigates how an increase in signal and idler power beyond the small-signal condition affects the transfer functions experimentally as well as using numerical solutions of the three-wave model.

4.4 Noise in parametric amplifiers and PSAs

The main interest for investigating the noise properties of PSAs is their ability to amplify a signal without adding noise. Normally, FOPAs, like any other amplifier, add noise to the signal being amplified. This is usually quantified by the noise figure (NF), defined as

$$\mathrm{NF} = \frac{\mathrm{SNR_{in}}}{\mathrm{SNR_{out}}}, \tag{4.3}$$

i.e. the degradation of the SNR, as measured in the electrical domain, after the amplifier, if $\mathrm{SNR_{in}}$ is shot-noise limited when detected and converted into a photocurrent. The input and output SNR are thus electrical SNR:s measured with an ideal detector. The noise photons have a random phase, and it is the beating between signal and noise photons on the photodetector that will limit the SNR after the amplifier. When discussing the noise figure, one usually assumes that the noise bandwidth is small enough to neglect the beating between the noise photons. In an EDFA, the noise photons originates from spontaneous emission of photons from the excited Erbium ions, photons that subsequently are amplified. The noise is therefore called amplified spontaneous emission (ASE). The lowest NF that has been experimentally demonstrated in an EDFA is of 3.1 dB [128]. It can be shown that the quantum limited noise figure for an amplifier with high gain is 3 dB [129, p. 195]. In a FOPA, the fundamental noise source is similar to the ASE in EDFAs, but there are no excited particles involved, rather, the noise originates from vacuum fluctuations. Such fluctuations can be amplified by the FOPA. Therefore, ASE in a parametric amplifier is often called amplified quantum noise (AQN).

A phase-sensitive FOPA (or any PSA) on the other hand, has a quantum-limited NF of 0 dB *for the in-phase component* (the out-of-phase component has a NF of at least its attenuation). Sub-3 dB NFs have been measured in both PSAs implemented in $\chi^{(2)}$ (Lithium niobate) [92] and $\chi^{(3)}$ (fibers) [88] media. The difference in NF between phase-insensitive and phase-sensitive amplifiers can be understood from a semiclassical approach [130], where the input signal and idler fields of Eq. 2.31 are considered to be the sum of the signal field and an uncorrelated vacuum noise field, which is assumed to be a stochastic complex quantity with a Gaussian distribution and an expectation value of 0 for the amplitude, and $hf_{s,i}/2$ for the power, where h denotes Planck's constant and $f_{s,i}$ the signal and idler frequency. In Paper [D], this is used to derive the NF of a FOPA, giving the well-known 3 dB NF in the high-gain regime for a FOPA without idler at the input (the signal is amplified a factor G, while the fluctuations are amplified 2G). The NF is found to be 0 dB when considering both the input signal and input idler as part of the "signal", i.e. the enumerator, in the SNR, and -3 dB when only considering the signal. Intuitively,

this can be understood by realizing that the vacuum fluctuations will only be phase-insensitively amplified, while the signal will be phase-sensitively amplified, i.e. with 6 dB larger gain, as discussed earlier in this chapter. Hence, the signal is amplified 4G while the fluctuations are amplified 2G [112], giving the SNR improvement.

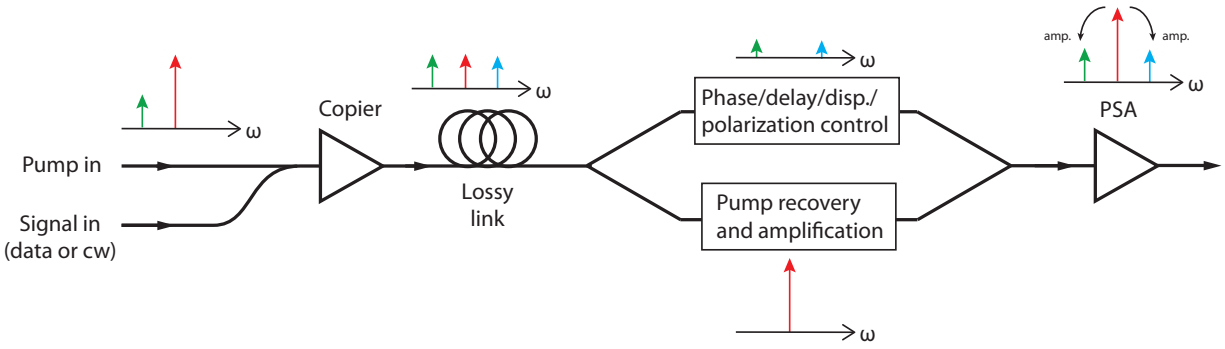

Figure 4.5: Basic principle of a copier-loss-PSA transmission link.

Importantly, the copier-PSA structure can be used to gain a practical benefit of the NF advantage of PSA. If there is a large loss (much larger than the copier gain) in the mid-stage between the copier and the PSA, any introduced correlated fluctuations in the copier will be insignificant compared with the introduced vacuum fluctuation in the loss element (e.g. a transmission fiber). Then, the PSA (if ideal) will amplify the signal-idler pair without added noise, giving the entire link a 6 dB SNR benefit compared to the same link with two PI amplifiers, and since the idler is the generated conjugate of the signal input to the copier, both signal quadratures will be amplified by the PSA [131]. Such a link has an increased information capacity compared to a conventional PI-based link [132]. Fig. 4.5 illustrates the copier-loss-PSA concept. To make it work after a real transmission link, the pump needs to be recovered and reamplified. Furthermore, control of phase, relative delay and polarization is necessary, as well as accurate dispersion compensation. In Paper [H], a proof-of-concept experiment demonstrates the link SNR benefit of the copier-loss-PSA scheme. Subsequently, it has been demonstrated with an actual 80 km SMF link in [125].

In addition to the quantum limited NF, the NF of a FOPA will typically be degraded by a number of other effects [103, 133]. One is the unavoidable Raman scattering of the FOPA pump. In addition, if the pump is noisy, this will further degrade the noise performance of the FOPA, since amplitude variations of the pump is transferred to the signal by the near-instantaneous gain of the FOPA. The pump is typically amplified by an high-power EDFA, giving it a limited OSNR. Imper-

fect filtering of pump ASE also degrades the FOPA NF. Even if the pump is not amplified, it will have a limited relative-intensity noise (RIN), meaning its intensity is fluctuating. Despite these imperfections, NFs close to the quantum limit are achievable in FOPAs.

Chapter 5

Future applications and outlook

While phase-sensitive optical parametric amplifiers have been the subject of experimental investigations for at least two decades, they still remain an exotic device, seemingly far from practical applications. However, while more work is undoubtedly necessary, one can now envision new developments and novel applications that may lift the PSA from research curiosity to commercial applications. Certainly, one can easily imagine technological developments that can make PSAs simpler and cheaper to build, such as lasers of suitable characteristics with large output power, obviating the need for pump amplification. However, we might also need to raise our perspective from the telecom- and optical fiber-centric view we take in this thesis. The PSAs of the future may well be implemented in other nonlinear media, such as silicon, and primarily used for non-telecom-applications such as scientific tools or for military or space communications. While speculative to some degree, in this chapter we discuss current implementation issues and potential future developments and applications for PSAs.

5.1 PSA applications

We have in this thesis discussed the phase-regenerative property of PSAs. As shown in Paper [D], it is possible to simultaneously reduce both amplitude and phase noise (up to a certain degree) by operating the PSA in saturation. It has also been shown to be able to scale beyond binary PSK to higher-order (M-ary) PSK data modulation by using cascaded FWM [121, 122]. However, like for most other all-optical signal processing, the chief competitor is digital signal processing (DSP) in software, which obviously always is a very flexible solution. DSP together with coherent detection

has also been the main focus of optical transmission research in the past few years. The inherent advantages of all-optical signal processing over DSP is speed and power consumption. Unlike silicon chips, the processing speed (i.e. the possible symbol rate) of optical signal processing can be increased virtually arbitrarily. Moreover, doing so will not affect the power consumption of the optical device. So far, the speed of the electronics and the symbol rate of optical communications systems have kept pace, with a large part of the increase in data rates coming from additional WDM channels and recently the use of multilevel modulation. Should a time come, however, where it proves to be easier and/or more cost efficient to increase the symbol rate, all-optical regeneration might be beneficial or even necessary.

The most spectacular ability of PSAs is undoubtedly their capability of noiseless amplification. In Paper [H], it has been shown that the copier - link - PSA configuration is likely the most practical way to exploit this capability, primarily since it can noiselessly amplify arbitrary signal formats and unlike many other PSA configurations only require comparatively slow phase-tracking. Recent developments have shown that the required pump recovery is achievable using an injection-locked laser [134]. However, in fiber-optic communications they must also compete with distributed amplification, in which the transmission fiber is the amplification medium as well (usually by Raman amplification). Copier-PSA is, in principle, compatible with distributed amplification and would then outperform all other amplification schemes (Paper [C]); unfortunately keeping the waves phase-synchronized throughout the entire fiber is not likely to be practical. A hybrid approach using the copier - link - PSA configuration together with conventional distributed Raman amplification in the link might very well be an attractive option for ultra-long span single-hop links.

Another potential development may come from current research that is looking to develop novel kinds of transmission fibers (photonic bandgap fibers) with significantly reduced attenuation and nonlinearity compared with current silica fibers [135]. Should such fibers become a reality, distributed amplification will no longer be viable, nor will current EDFAs be usable, since the fibers will have their low-loss window in the 2000 nm-wavelength range. Hence, new kinds of amplifiers are required; PSAs (as well as PI-FOPAs) have no inherently limited wavelength range of operation.

Moreover, there are other specialty applications in which high-fidelity amplification and/or amplification of very low-power signals are required because high-power laser sources are unavailable or because signal absorption is large or because signal powers must be kept low because of nonlinearities or damage thresholds. Any such application may benefit from the ultra-low noise amplification potentially offered by PSAs, since PSAs can, with suitable choice of gain medium, be made to operate

at nearly any wavelength. Application examples may include few-photon-detection, medical applications and bio-photonics, spectroscopy, LIDAR (LIght Detection And Ranging)-type sensing etc. It is also interesting to consider that if the signal and idler are unequally attenuated during the propagation, the PSA will significantly improve the SNR of the lower-power one [136].

Finally, we point out another important capability of non-degenerate PSAs, namely that the NF improvement can scale further by using additional idlers. A PSA employing two pumps and a set of four correlated signal-idlers (four-sideband interaction [48]) would in principle exhibit a noise figure of -9 dB when considering the signal only. Such a four-mode PSA has been experimentally verified in a recent experiment [137].

5.2 PSA platforms

Presently, silica-based nonlinear fibers are the preferred nonlinear medium for parametric amplification and nonlinear signal processing mainly because of their low attenuation. This gives HNLFs a very competitive nonlinearity coefficient over attenuation (γ/α) figure-of-merit when compared with other nonlinear optical media [17, 138]. Additionally, which in many cases may be equally important, HNLFs have very low coupling/splicing loss, allowing for large net efficiencies, and makes them capable of handling large optical powers, and allows them to be easily integrated in fiber-based systems. In this thesis, we have made the case for FWM in HNLF as a good way of implementing a PSA. However, we should also recognize that HNLF have a number of limitations and disadvantages compared with other nonlinear platforms. Since HNLF is made from silica, which intrinsically has a very low Kerr nonlinearity, the nonlinearity coefficient is not particularly large in HNLF, thereby making a fairly large length required. This is disadvantageous because nonuniformities along the fiber may be a limitation (dispersion variations, PMD), and because of walk-off time and/or latency. The lengths required also means that the nonlinear device necessarily will be large in size, at least compared to many other optical components. As we have discussed, SBS also remains a substantial issue in HNLFs.

So-called holey fibers, microstructured fibers or photonic crystal fibers [30], either made from silica or from other types of nonlinear glasses, e.g. Chalcogenide, Tellurite, lead-silicate or bismuth-oxide [139], as well as e.g. silicon nanowires typically outperform silica-based HNLFs in terms of nonlinearity as well as Kerr-to-SBS ratio, in many cases by orders of magnitude. With a large enough reduction in attenuation/coupling loss, they can become the medium of choice. Silicon in partic-

ular is interesting, and has been the topic of many recent experiments [35, 140–142], in no small part due to its potential for on-chip integration. However, silicon is not particularly suitable for operation in the 1550 nm-wavelength regime, due to large two-photon absorption [140], but may be suitable in e.g. the 2 μm-wavelength regime and beyond, where silica fibers on the other hand have large attenuation. PCFs, can, in principle, be tailor-made to operate at any wavelength, by designing them with the desired single-mode cut-off wavelength and GVD, by proper choice of glass and microstructure design.

The above are all $\chi^{(3)}$-media, but $\chi^{(2)}$-media should also be considered, especially when using quasi-phase-matching techniques. This is likely required for $\chi^{(2)}$-media to be competitive, so as to avoid phase matching through birefringence, which is often impractical in many applications. In particular, quasi-phase-matched (periodically poled) Lithium-niobate crystals (PPLN) have already been used to implement PSAs through cascaded SHG/DFG [95–97].

One may expect that many of the platforms discussed may be suitable for PSA implementations, albeit for different applications. For instance, we can consider that the copier-link-PSA configuration means having two different devices at two different locations. The nonlinear medium does not have to be the same for the two, even though the wavelengths obviously must be compatible with both. Indeed, they can and should be analyzed separately when choosing platform.

5.3 Issues and future developments

In Paper [C], a number of future developments were identified to be required for PSAs to be more practically viable. Remarkably, significant steps have been taken towards most of them. We now have nonlinear fibers that are less susceptible to SBS (Papers [I-J]), even though their gain bandwidth remains limited. Recently developed HNLFs that allow strain gradients without noticeable GVD variations [81–83] addresses this issue. Injection-locking-based pump recovery as well as the required phase, delay and dispersion control [143] has been proven to be possible in an actual transmission experiment through 80 km of fiber [125]. Nevertheless, many issues still remain.

In order to make PSAs less complex it would be desirable to obviate the need for auxiliary high-power EDFAs to boost the pump to sufficiently large powers. The development of lasers with large enough output power with otherwise maintained qualities (single-mode, relatively narrow linewidth, low intensity noise) is thus beneficial for PSAs. Otherwise, the required components are mostly passive optics that should be relatively simple to implement inexpensively. No fast electronics are

required, and the phase locking circuit can be built at low cost.

Another major issue that remains to be addressed is the polarization dependence that PSAs normally exhibit. While parametric amplifiers can be made polarization independent by using orthogonal dual-pumps [40, 41, 50], this may not always be a good choice, since the FWM efficiency is lower and having two pumps means additional complexity especially for PSAs where all waves must be phase-locked. Moreover, it is difficult in practice to maintain the orthogonality of the pumps, due to the PMD in the fiber, giving an unwanted polarization dependence. Polarization-diversity techniques might thus be necessary in order to construct polarization-independent PSAs.

In the longer term, we should acknowledge that PSAs remain an immature technology at present, an neither their main applications nor their implementation platform is written in stone today. The application will also dictate the wavelength range of interest and other performance requirements, and hence implementation and nonlinear platform. It thus remains clear that further research on PSA should be conducted with an open mind regarding platforms, and any developments addressing the various limitations on different nonlinear media, as those discussed above can only further the developments of PSAs towards practical applications.

Chapter 6

Summary of papers

The thesis includes ten appended papers, which are outlined below. Papers [A-D] concerns mainly the investigation of fundamental characteristics of phase-sensitive fiber optic parametric amplifiers, while Papers [E-H] are focused on different applications of PSAs in a communications context, based on the fundamental characteristics that are unique to PSAs. These applications include simultaneous phase- and amplitude regeneration, modulation signal enhancement, short-pulse amplification and ultra-low noise amplification. Additionally, Papers [I-J] addresses the topic of stimulated Brillouin scattering suppression in the nonlinear fibers constituting the parametric amplifiers.

Paper A: Detailed characterization of a fiber-optic parametric amplifier in phase-sensitive and phase-insensitive operation

Due to the stringent requirement of phase control of the ingoing waves, phase-sensitive amplifiers are very difficult to implement and characterize. Here, a first-stage FOPA is used to generate a set of phase-correlated waves, and through an intermediate optical processor the amplitude and phase of the waves can be changed. The second-stage FOPA that operates in phase-sensitive mode can thus be characterized. A symmetric gain bandwidth of 24 nm and a maximum gain of 33 dB was measured, showing that a phase-sensitive FOPA can have performance similar to their phase-insensitive counterparts. We also investigated PSA gain and attenuation versus input phase, pump power, signal power and signal-to-idler power ratio.

My contribution: J. Kakande and myself came up with the idea for the experi-

ments and set them up and conducted them jointly. I presented the work at ECOC 2009, and contributed in writing the subsequent paper.

Paper B: Phase-to-phase and phase-to-amplitude transfer characteristics of a non-degenerate-idler phase-sensitive amplifier

In this paper, the phase-to-phase and phase-to-amplitude transfer functions of a phase-sensitive FOPA are experimentally measured and compared with theory. The experimental results were obtained by imposing a linear phase modulation onto the signal and idler wave simultaneously, and detecting the input and output signal using a self-homodyne coherent receiver. We also measure the phase-to-phase transfer functions for different gains and signal-to-idler power ratios and find that the phase-squeezing capability is significantly impaired if the gain is too low or the signal-to-idler power ratio too large.

My contribution: I came up with the idea for the experiment, set up the experiment together with Z. Tong and conducted the measurements and wrote the paper.

Paper C: Ultra-low noise, broadband phase-sensitive optical amplifiers and their applications (Invited paper)

In this invited paper many aspects of our work based on the copier-PSA scheme is reviewed. This includes gain, noise performance, and phase-transfer functions. A record-low 1.1 dB noise figure was measured at 26 dB gain. Potential applications as well as practical challenges are also discussed.

My contribution: Z. Tong and myself jointly designed and built the copier-PSA setup. I performed the phase measurements and contributed in writing the paper.

Paper D: Phase and amplitude transfer characteristics of a phase-sensitive parametric amplifier operating in gain saturation

Here, the work on phase-to-phase and phase-to-amplitude transfer functions is extended to PSAs in the gain saturation regime. This enables a suppression of the inherent phase-to-amplitude conversion, and indeed of simultaneous reduction in phase- and amplitude deviations of a signal. However, the phase-to-phase transfer

characteristics becomes impaired when operating in saturation, and we evaluate the impact of this on the noise reduction using the numerical three-wave model. The validity of this model was shown by comparing it to experimental transfer functions with very good agreement.

My contribution: I designed and set up the experiment, performed the measurements and the numerical simulations, and wrote the paper.

Paper E: All-optical phase- and amplitude regenerator for next-generation telecommunications systems

Phase noise is a major limitation in data transmission using (differential) phase shift keying ((D)PSK). This could be mitigated by using phase regenerators in the transmission link. Here, the first such phase regenerator based on the phase-squeezing capability of phase-sensitive amplifiers (PSAs) in a black-box configuration is presented. The carrier is recovered from the incoming DPSK signal in an auxiliary four-wave mixing stage, and subsequently used to injection lock a laser. This component thus carries the phase of the signal laser and the auxiliary pump (but not the data). The signal was phase regenerated with a very low amplitude penalty by operating the PSA in saturation. The large reduction of phase noise was quantified through differential eye diagrams, coherently measured constellation diagrams and Bit-Error-Ratio (BER) measurements.

My contribution: I built the constellation diagram analysis together with M. Sjödin, performed the constellation measurements and assisted in performing the other measurements.

Paper F: Optical modulation signal enhancement using a phase sensitive amplifier

A method using a phase-sensitive amplifier as a modulation signal enhancer is proposed and demonstrated. Using the phase-to-phase and phase-to-amplitude characteristics of the PSA, it can generate both phase- and amplitude modulated signals from low-extinction inputs, for instance providing a phase-excursion amplification. High-extinction amplitude modulation can also be generated.

My contribution: I invented the concept. I designed and set up the experiment, performed the measurements and wrote the paper.

Paper G: Short-pulse amplification in a phase-sensitive amplifier

The amplification of picosecond-pulses in a PSA is demonstrated in this paper. We investigate the tolerance on residual delay and dispersion on the signal and idler, important for copier-PSA-based transmission links. Moreover, the PSAs ability to selectively amplify one of the quadratures of the signal and the effect this has on dispersively broadened pulses, is discussed and we show an experimental demonstration of this effect for the first time.

My contribution: The question of dispersion tolerance between copier and PSA arose during Z. Tong's work on such links. I designed and set up the experiment, performed the measurements and wrote the paper.

Paper H: Towards ultrasensitive optical links enabled by low-noise phase-sensitive amplifiers

The noiseless amplification of the PSA can provide a practical benefit in a copier-PSA configuration as well if the loss between the copier and PSA is sufficiently large. Then, a copier-loss-PSA link will outperform the same link implemented with phase-insensitive amplifiers, despite the copier-PSA being phase-insensitive as a whole. Here, this is demonstrated experimentally for the first time with a near-6 dB link NF advantage and a 5.5 dB sensitivity improvement. The modulation format independence and compatibility with WDM signals is also shown.

My contribution: The copier-PSA setup was jointly designed by Z. Tong and myself. I contributed in writing the paper.

Paper I: Tension-optimized highly nonlinear fibers for parametric applications

It is known that applying a tension gradient to a fiber will increase its SBS threshold. However, the dispersion will then also change along the fiber. Here, this is investigated for a highly nonlinear fiber. We found a variation in SBS frequency over 300 MHz and zero-dispersion wavelength of 11.5 nm for this particular fiber, and calculate what this means when using this fiber in parametric applications.

My contribution: I devised and performed the experiments with the exception of the localized measurements, performed the theoretical calculations and wrote the paper.

Paper J: Fiber optic parametric amplifier with 10 dB net gain without pump dithering"

An SBS-suppressed HNLF cascade using four HNLFs with strain gradients and three optical isolators was designed and constructed. The effective total threshold increase was about 11 dB. A record net CW parametric gain without any pump spectral broadening for SBS suppression of 10 dB was measured in this cascade. We also verified its performance as a wavelength converter of phase-encoded data. When using pump spectral broadening, such a wavelength converted signal will be significantly degraded because of the pump-to-idler phase transfer, but in the HNLF cascade we achieved 9.3 dB net conversion efficiency with no appreciable penalty found.

My contribution: I planned the HNLF-cascade concept and the experiment. Together with S.L.I. Olsson, I performed the characterization of the HNLF pieces and designed the cascade. I advised on the construction and measurement of the cascade and the wavelength conversion experiment and wrote the paper.

References

[1] K. Kao and G. Hockham, "Dielectric-fibre surface waveguides for optical frequencies," in *Proceedings of the Institution of Electrical Engineers*, pp. 1151–1158, 1966.

[2] F. P. Kapron, D. B. Keck, and R. D. Maurer, "Radiation losses in glass optical waveguides," *Applied Physics Letters*, vol. 17, no. 10, pp. 423–425, 1970.

[3] D. B. Keck, R. D. Maurer, and P. Schultz, "On the ultimate lower limit of attenuation in glass optical waveguides," *Applied Physics Letters*, vol. 22, no. 7, pp. 307–309, 1973.

[4] T. Maiman, "Stimulated optical radiation in ruby," *Nature*, vol. 187, pp. 493–494, 1960.

[5] R. H. Kingston, "Parametric amplification and oscillation at optical frequencies," *Proceedings of the IRE*, vol. 50, no. 4, p. 472, 1962.

[6] N. M. Kroll, "Parametric Amplification in Spatially Extended Media and Application to the Design of Tuneable Oscillators at Optical Frequencies," *Physical Review*, vol. 127, pp. 1207–1211, Aug. 1962.

[7] J. A. Armstrong, N. Bloembergen, J. Ducuing, and P. S. Pershan, "Interactions between light waves in a nonlinear dielectric," *Physical Review*, vol. 127, no. 6, pp. 1918–1938, 1962.

[8] R. H. Stolen, "Phase-matched-stimulated four-photon mixing in silica-fiber waveguides," *IEEE Journal of Quantum Electronics*, vol. 11, no. 3, pp. 100–103, 1975.

[9] R. H. Stolen and J. E. Bjorkholm, "Parametric amplification and frequency conversion in optical fibers," *IEEE Journal of Quantum Electronics*, vol. 18, no. 7, pp. 1062–1072, 1982.

[10] P. A. Andrekson, N. A. Olsson, J. R. Simpson, T. Tanbun-Ek, R. A. Logan, and M. Haner, "16 Gbit/s all-optical demultiplexing using four-wave mixing," *Electronics Letters*, vol. 27, no. 11, pp. 922–924, 1991.

[11] P. A. Andrekson, "Picosecond optical sampling using four-wave mixing in fibre," *Electronics Letters*, vol. 27, no. 16, pp. 1440–1441, 1991.

[12] S. Watanabe, T. Naito, and T. Chikama, "Compensation of chromatic dispersion in a single-mode fiber by optical phase conjugation," *IEEE Photonics Technology Letters*, vol. 5, no. 1, pp. 92–95, 1993.

[13] F. S. Yang, M. E. Marhic, and L. G. Kazovsky, "CW fibre optical parametric amplifier with net gain and wavelength conversion efficiency > 1," *Electronics Letters*, vol. 32, no. 25, pp. 2336–2338, 1996.

[14] M. J. Holmes, D. L. Williams, and R. J. Manning, "Highly nonlinear optical fiber for all optical processing applications," *IEEE Photonics Technology Letters*, vol. 7, no. 9, pp. 1045–1047, 1995.

[15] M. Onishi, T. Okuno, T. Kashiwada, S. Ishikawa, N. Akasaka, and M. Nishimura, "Highly nonlinear dispersion-shifted fibers and their application to broadband wavelength converter," *Optical Fiber Technology*, vol. 4, no. 2, pp. 204–214, 1998.

[16] M. Onishi, "Highly nonlinear optical fibers and their applications," *European Conference on Optical Communication (ECOC)*, vol. 2, p. 216, 1999.

[17] M. Hirano, T. Nakanishi, T. Okuno, and M. Onishi, "Silica-Based Highly Nonlinear Fibers and Their Application," *IEEE Journal of Selected Topics in Quantum Electronics*, vol. 15, no. 1, pp. 103–113, 2009.

[18] J. Hansryd and P. A. Andrekson, "Broad-band continuous-wave-pumped fiber optical parametric amplifier with 49-dB gain and wavelength-conversion efficiency," *IEEE Photonics Technology Letters*, vol. 13, no. 3, pp. 194–196, 2001.

[19] J. Hansryd, P. A. Andrekson, M. Westlund, J. Li, and P.-O. Hedekvist, "Fiber-based optical parametric amplifiers and their applications," *IEEE Journal of Selected Topics in Quantum Electronics*, vol. 8, no. 3, pp. 506–520, 2002.

[20] K. Inoue, "Optical level equalisation based on gain saturation in fibre optical parametric amplifier," *Electronics Letters*, vol. 36, no. 12, pp. 1016–1017, 2000.

[21] S. Radic, C. J. McKinstrie, R. M. Jopson, J. C. Centanni, and A. R. Chraplyvy, "All-optical regeneration in one- and two-pump parametric amplifiers using highly nonlinear optical fiber," *IEEE Photonics Technology Letters*, vol. 15, no. 7, pp. 957–959, 2003.

[22] M. Sköld, J. Yang, H. Sunnerud, M. Karlsson, S. Oda, and P. A. Andrekson, "Constellation diagram analysis of DPSK signal regeneration in a saturated parametric amplifier," *Optics Express*, vol. 16, no. 9, pp. 5974–5982, 2008.

[23] C.-S. Bres, N. Alic, E. Myslivets, and S. Radic, "Scalable Multicasting in One-Pump Parametric Amplifier," *Journal of Lightwave Technology*, vol. 27, no. 3, pp. 356–363, 2009.

[24] N. Alic, E. Myslivets, S. Moro, B. P.-P. Kuo, R. M. Jopson, C. J. McKinstrie, and S. Radic, "Microsecond Parametric Optical Delays," *Journal of Lightwave Technology*, vol. 28, no. 4, pp. 448–455, 2010.

[25] G.-W. Lu and T. Miyazaki, "Optical phase erasure based on FWM in HNLF enabling format conversion from 320 Gb/s RZ-DQPSK to 160-Gb/s RZ-DPSK," *Optics Express*, vol. 17, no. 16, pp. 13346–13353, 2009.

[26] C. M. Caves, "Quantum limits on noise in linear amplifiers," *Physical Review D*, vol. 26, no. 8, pp. 1817–1839, 1982.

[27] G. P. Agrawal, *Nonlinear Fiber Optics, 4th Ed.* Academic Press, 2007.

[28] N. Sugimoto, T. Nagashima, T. Hasegawa, and S. Ohara, "Bismuth-based optical fiber with nonlinear coefficient of 1360 W-1km-1," *Optical Fiber Communication Conference (OFC)*, p. PDP26, 2004.

[29] F. Poletti, P. Petropoulos, N. G. R. Broderick, and D. J. Richardson, "Design of Highly Nonlinear Bismuth-Oxide Holey Fibres with Zero Dispersion and Enhanced Brillouin Suppression," *European Conference on Optical Communication (ECOC)*, p. Tu.4.3.2, 2006.

[30] P. Russell, "Photonic Crystal Fibers," *Science*, vol. 299, pp. 358–362, Jan. 2003.

[31] N. G. R. Broderick, T. M. Monro, P. J. Bennett, and D. J. Richardson, "Nonlinearity in holey optical fibers: measurement and future opportunities," *Optics Letters*, vol. 24, no. 20, pp. 1395–1397, 1999.

[32] B. J. Eggleton, C. Kerbage, P. Westbrook, R. Windeler, and A. Hale, "Microstructured optical fiber devices," *Optics Express*, vol. 9, no. 13, pp. 698–713, 2001.

[33] A. Camerlingo, X. Feng, F. Poletti, G. M. Ponzo, F. Parmigiani, P. Horak, M. N. Petrovich, P. Petropoulos, W. H. Loh, and D. J. Richardson, "Near-zero dispersion, highly nonlinear lead-silicate W-type fiber for applications at 155m," *Optics Express*, vol. 18, no. 15, pp. 15747–15756, 2010.

[34] R. Boyd, *Nonlinear Optics*. San Diego, CA: Academic Press, 1992.

[35] X. Liu, R. M. Osgood, Y. A. Vlasov, and W. M. J. Green, "Mid-infrared optical parametric amplifier using silicon nanophotonic waveguides," *Nature Photonics*, vol. 4, no. 8, pp. 557–560, 2010.

[36] M. Karlsson and H. Sunnerud, "Effects of Nonlinearities on PMD-Induced System Impairments," *Journal of Lightwave Technology*, vol. 24, no. 11, pp. 4127–4137, 2006.

[37] M. Farries and D. Payne, "An optical fibre switch employing a Sagnac interferometer," *Applied Physics Letters*, vol. 55, no. 25, pp. 25–26, 1989.

[38] A. Hasegawa and F. Tappert, "Transmission of stationary nonlinear optical pulses in dispersive dielectric fibers. I. Anomalous Dispersion," *Applied Physics Letters*, vol. 23, no. 3, pp. 142–144, 1973.

[39] A. R. Chraplyvy, "Limitations on lightwave communications imposed by optical-fiber nonlinearities," *Journal of Lightwave Technology*, vol. 8, no. 10, pp. 1548–1557, 1990.

[40] R. M. Jopson and R. E. Tench, "Polarisation-independent phase conjugation of lightwave signals," *Electronics Letters*, vol. 29, no. 25, pp. 2216–2217, 1993.

[41] K. Inoue, "Polarization independent wavelength conversion using fiber four-wave mixing with two orthogonal pump lights of different frequencies," *Journal of Lightwave Technology*, vol. 12, no. 11, pp. 1916–1920, 1994.

[42] M. E. Marhic, *Fiber optical parametric amplifiers, oscillators and related devices*. Cambridge University Press, 2008.

[43] G. Cappellini and S. Trillo, "Third-order three-wave mixing in single-mode fibers: exact solutions and spatial instability effects," *Journal of the Optical Society of America B*, vol. 8, no. 4, pp. 824–838, 1991.

[44] M. E. Marhic, Y. Park, F. S. Yang, and L. G. Kazovsky, "Broadband fiber-optical parametric amplifiers and wavelength converters with low-ripple Chebyshev gain spectra," *Optics Letters*, vol. 21, no. 17, pp. 1354–1356, 1996.

[45] F. S. Yang, M.-C. Ho, M. E. Marhic, and L. G. Kazovsky, "Demonstration of two-pump fibre optical parametric amplification," *Electronics Letters*, vol. 33, no. 21, pp. 1812–1813, 1997.

[46] S. Radic, C. J. McKinstrie, R. M. Jopson, J. C. Centanni, Q. Lin, and G. P. Agrawal, "Record performance of parametric amplifier constructed with highly nonlinear fibre," *Electronics Letters*, vol. 39, no. 11, pp. 838–839, 2003.

[47] J. M. C. Boggio, S. Moro, E. Myslivets, J. R. Windmiller, N. Alic, and S. Radic, "155-nm Continuous-Wave Two-Pump Parametric Amplification," *IEEE Photonics Technology Letters*, vol. 21, no. 10, pp. 612–614, 2009.

[48] C. J. McKinstrie, S. Radic, and A. R. Chraplyvy, "Parametric amplifiers driven by two pump waves," *IEEE Journal of Selected Topics in Quantum Electronics*, vol. 8, no. 3, pp. 538–547, 2002.

[49] C. J. McKinstrie, S. Radic, and A. R. Chraplyvy, "Correction to "parametric amplifiers driven by two pump waves"," *IEEE Journal of Selected Topics in Quantum Electronics*, vol. 8, no. 4, pp. 956–956, 2002.

[50] K. K.-Y. Wong, M. E. Marhic, K. Uesaka, and L. G. Kazovsky, "Polarization-independent two-pump fiber optical parametric amplifier," *IEEE Photonics Technology Letters*, vol. 14, no. 7, pp. 911–913, 2002.

[51] S. Radic, C. J. McKinstrie, R. M. Jopson, J. C. Centanni, A. R. Chraplyvy, C. G. Jorgensen, K. Brar, and C. Headly, "Selective suppression of idler spectral broadening in two-pump parametric architectures," *IEEE Photonics Technology Letters*, vol. 15, no. 5, pp. 673–675, 2003.

[52] M. E. Marhic, N. Kagi, T. K. Chiang, and L. G. Kazovsky, "Broadband fiber optical parametric amplifiers," *Optics Letters*, vol. 21, no. 8, pp. 573–575, 1996.

[53] C. J. McKinstrie, M. Yu, M. G. Raymer, and S. Radic, "Quantum noise properties of parametric processes," *Optics Express*, vol. 13, no. 13, pp. 4986–5012, 2005.

[54] M. Vasilyev, "Distributed phase-sensitive amplification," *Optics Express*, vol. 13, no. 19, pp. 7563–7571, 2005.

[55] N. Kuwaki and M. Ohashi, "Evaluation of longitudinal chromatic dispersion," *Journal of Lightwave Technology*, vol. 8, no. 10, pp. 1476–1481, 1990.

[56] M. Karlsson, "Four-wave mixing in fibers with randomly varying zero-dispersion wavelength," *Journal of the Optical Society of America B*, vol. 15, no. 8, pp. 2269–2275, 1998.

[57] T. Okuno, T. Nakanishi, M. Hirano, and M. Onishi, "Practical considerations for the application of Highly Nonlinear Fibers," in *Optical Fiber Communication Conference (OFC)*, p. OTuJ1, IEEE, 2007.

[58] C. Raman and K. Krishnan, "A new type of secondary radiation," *Nature*, vol. 121, pp. 501–502, 1928.

[59] E. Woodbury and W. Ng, "Ruby Laser Operation in the Near IR," *Proceedings of the IRE*, vol. 50, no. 11, p. 2367, 1962.

[60] R. H. Stolen and E. P. Ippen, "Raman gain in glass optical waveguides," *Applied Physics Letters*, vol. 22, no. 6, pp. 276–278, 1973.

[61] M. N. Islam, "Raman amplifiers for telecommunications," *IEEE Journal of Selected Topics in Quantum Electronics*, vol. 8, pp. 548–559, May 2002.

[62] R. Chiao, C. Townes, and B. Stoicheff, "Stimulated Brillouin Scattering and Coherent Generation of Intense Hypersonic Waves," *Physical Review Letters*, vol. 12, pp. 592–595, May 1964.

[63] E. P. Ippen and R. H. Stolen, "Stimulated Brillouin scattering in optical fibers," *Applied Physics Letters*, vol. 21, no. 11, pp. 539–540, 1972.

[64] R. Shelby, M. Levenson, and P. Bayer, "Guided acoustic-wave Brillouin scattering," *Physical Review B*, vol. 31, no. 8, pp. 5244–5252, 1985.

[65] R. G. Smith, "Optical Power Handling Capacity of Low Loss Optical Fibers as Determined by Stimulated Raman and Brillouin Scattering," *Applied Optics*, vol. 11, no. 11, pp. 2489–2494, 1972.

[66] T. Nakanishi, M. Tanaka, T. Hasegawa, M. Hirano, T. Okuno, and M. Onishi, "Al2O3-SiO2 core highly nonlinear dispersion-shifted fiber with Brillouin gain suppression improved by 6.1 dB," *European Conference on Optical Communication (ECOC)*, p. PDP Th4.2.2, 2005.

[67] M. D. Mermelstein, "SBS threshold measurements and acoustic beam propagation modeling in guiding and anti-guiding single mode optical fibers," *Optics Express*, vol. 17, no. 18, pp. 16225–16237, 2009.

[68] L. Grüner-Nielsen, S. Dasgupta, M. D. Mermelstein, D. Jakobsen, S. Herstrøm, M. E. Pedersen, E. Lim, S. Alam, F. Parmigiani, D. J. Richardson, and B. Pálsdóttir, "A silica based highly nonlinear fibre with improved threshold for stimulated Brillouin scattering," in *European Conference on Optical Communication (ECOC)*, p. Tu.4.D.3, 2010.

[69] S. K. Korotky, P. B. Hansen, L. Eskildsen, and J. J. Veselka, "Efficient phase modulation scheme for suppressing stimulated Brillouin scattering," *Tech. Digest International Conference on Integrated Optics and Optical Fibre Communications*, vol. 2, pp. 110–111, paper WD2, 1995.

[70] A. Mussot, M. Le Parquier, and P. Szriftgiser, "Thermal noise for SBS suppression in fiber optical parametric amplifiers," *Optics Communications*, vol. 283, no. 12, pp. 2607–2610, 2010.

[71] M.-C. Ho, M. E. Marhic, K. K.-Y. Wong, and L. G. Kazovsky, "Narrow-linewidth idler generation in fiber four-wave mixing and parametric amplification by dithering two pumps in opposition of phase," *Journal of Lightwave Technology*, vol. 20, no. 3, pp. 469–476, 2002.

[72] T. Torounidis, P. A. Andrekson, and B.-E. Olsson, "Fiber-optical parametric amplifier with 70-dB gain," *IEEE Photonics Technology Letters*, vol. 18, no. 10, pp. 1194–1196, 2006.

[73] K. Shiraki, M. Ohashi, and M. Tateda, "SBS threshold of a fiber with a Brillouin frequency shift distribution," *Journal of Lightwave Technology*, vol. 14, no. 1, pp. 50–57, 1996.

[74] K. Shiraki, M. Ohashi, and M. Tateda, "Suppression of stimulated Brillouin scattering in a fibre by changing the core radius," *Electronics Letters*, vol. 31, no. 8, pp. 668–669, 1995.

[75] J. Hansryd, F. Dross, M. Westlund, P. A. Andrekson, and S. N. Knudsen, "Increase of the SBS threshold in a short highly nonlinear fiber by applying a temperature distribution," *Journal of Lightwave Technology*, vol. 19, no. 11, pp. 1691–1697, 2001.

[76] K. Byron, M. Bedgood, A. Finney, C. McGauran, S. Savory, and I. Watson, "Shifts in zero dispersion wavelength due to pressure, temperature and strain

in dispersion shifted singlemode fibres," *Electronics Letters*, vol. 28, no. 18, pp. 1712–1714, 1992.

[77] J. M. C. Boggio, J. D. Marconi, and H. L. Fragnito, "Experimental and numerical investigation of the SBS-threshold increase in an optical fiber by applying strain distributions," *Journal of Lightwave Technology*, vol. 23, no. 11, pp. 3808–3814, 2005.

[78] M. Farahmand and M. de Sterke, "Parametric amplification in presence of dispersion fluctuations," *Optics Express*, vol. 12, no. 1, pp. 136–142, 2004.

[79] E. Myslivets, C. Lundström, J. Aparicio, S. Moro, A. O. J. Wiberg, C.-S. Bres, N. Alic, P. A. Andrekson, and S. Radic, "Spatial Equalization of Zero-Dispersion Wavelength Profiles in Nonlinear Fibers," *IEEE Photonics Technology Letters*, vol. 21, no. 24, pp. 1807–1809, 2009.

[80] M. Takahashi, M. Tadakuma, and T. Yagi, "Dispersion and Brillouin Managed HNLFs by Strain Control Techniques," *Journal of Lightwave Technology*, vol. 28, no. 1, pp. 59–64, 2010.

[81] B. P.-P. Kuo and S. Radic, "Highly nonlinear fiber with dispersive characteristic invariant to fabrication fluctuations," *Optics Express*, vol. 20, no. 7, pp. 7716–7725, 2012.

[82] B. P. P. Kuo, M. Hirano, and S. Radic, "Continuous-wave, short-wavelength infrared mixer using dispersion-stabilized highly-nonlinear fiber," *Optics Express*, vol. 20, no. 16, pp. 18422–18431, 2012.

[83] B. P. P. Kuo, J. M. Fini, L. Grüner-Nielsen, and S. Radic, "Dispersion-stabilized highly-nonlinear fiber for wideband parametric mixer synthesis," *Optics Express*, vol. 20, pp. 18611–18619, Aug. 2012.

[84] Y. Takushima and T. Okoshi, "Suppression of simulated Brillouin scattering using optical isolators," *Electronics Letters*, vol. 28, no. 12, pp. 1155–1157, 1992.

[85] K. K.-Y. Wong, K. Shimizu, K. Uesaka, G. Kalogerakis, M. E. Marhic, and L. G. Kazovsky, "Continuous-wave fiber optical parametric amplifier with 60-dB gain using a novel two-segment design," *IEEE Photonics Technology Letters*, vol. 15, no. 12, pp. 1707–1709, 2003.

[86] M. E. Marhic, C. H. Hsia, and J.-M. Jeong, "Optical amplification in a nonlinear fibre interferometer," *Electronics Letters*, vol. 27, no. 3, pp. 210–211, 1991.

[87] W. Imajuku and A. Takada, "In-line optical phase-sensitive amplifier with pump light source controlled by optical phase-lock loop," *Journal of Lightwave Technology*, vol. 17, no. 4, pp. 637–646, 1999.

[88] W. Imajuku, A. Takada, and Y. Yamabayashi, "Low-noise amplification under the 3 dB noise figure in high-gain phase-sensitive fibre amplifier," *Electronics Letters*, vol. 35, no. 22, pp. 1954–1955, 1999.

[89] W. Imajuku, A. Takada, and Y. Yamabayashi, "Inline coherent optical amplifier with noise figure lower than 3 dB quantum limit," *Electronics Letters*, vol. 36, no. 1, pp. 63–64, 2000.

[90] K. Croussore and G. Li, "Phase and amplitude regeneration of differential phase-shift keyed signals using phase-sensitive amplification," *IEEE Journal of Selected Topics in Quantum Electronics*, vol. 14, no. 3, pp. 648–658, 2008.

[91] J. Levenson, I. Abram, and T. Rivera, "Quantum optical cloning amplifier," *Physical Review*, vol. 70, no. 3, pp. 267–270, 1993.

[92] J. A. Levenson, I. Abram, T. Rivera, and P. Grangier, "Reduction of quantum noise in optical parametric amplification," *Journal of the Optical Society of America B*, vol. 10, no. 11, pp. 2233–2238, 1993.

[93] K. Bencheikh, O. Lopez, I. Abram, and J. A. Levenson, "Improvement of photodetection quantum efficiency by noiseless optical preamplification," *Applied Physics Letters*, vol. 66, no. 4, pp. 399–401, 1995.

[94] D. J. Lovering, J. A. Levenson, P. Vidakovic, J. Webjörn, and P. S. J. Russell, "Noiseless optical amplification in quasi-phase-matched bulk lithium niobate," *Optics Letters*, vol. 21, no. 18, pp. 1439–1441, 1996.

[95] K. J. Lee, F. Parmigiani, S. Liu, J. Kakande, P. Petropoulos, K. Gallo, and D. Richardson, "Phase sensitive amplification based on quadratic cascading in a periodically poled lithium niobate waveguide," *Optics Express*, vol. 17, no. 22, pp. 20393–20400, 2009.

[96] B. J. Puttnam, D. Mazroa, S. Shinada, and N. Wada, "Large Phase Sensitive Gain in Periodically Poled Lithium–Niobate With High Pump Power," *IEEE Photonics Technology Letters*, vol. 23, no. 7, pp. 426–428, 2011.

[97] B. J. Puttnam, D. Mazroa, S. Shinada, and N. Wada, "Phase-squeezing properties of non-degenerate PSAs using PPLN waveguides," *Optics Express*, vol. 19, no. 26, pp. B131–B139, 2011.

[98] Y. Su, L. Wang, A. Agarwal, and P. Kumar, "All-optical limiter using gain flattened fibre parametric amplifier," *Electronics Letters*, vol. 36, no. 13, pp. 1103–1105, 2000.

[99] M. Matsumoto, "Regeneration of RZ-DPSK signals by fiber-based all-optical regenerators," *IEEE Photonics Technology Letters*, vol. 17, no. 5, pp. 1055–1057, 2005.

[100] M. Matsumoto and T. Kamio, "Nonlinear Phase Noise Reduction of DQPSK Signals by a Phase-Preserving Amplitude Limiter Using Four-Wave Mixing in Fiber," *IEEE Journal of Selected Topics in Quantum Electronics*, vol. 14, no. 3, pp. 610–615, 2008.

[101] O.-K. Lim, V. S. Grigoryan, M. Shin, and P. Kumar, "Ultra-Low-Noise Inline Fiber-Optic Phase-Sensitive Amplifier for Analog Optical Signals," *Optical Fiber Communication Conference (OFC)*, p. OML3, 2008.

[102] Z. Tong, A. Bogris, C. Lundström, C. J. McKinstrie, M. Vasilyev, M. Karlsson, and P. A. Andrekson, "Noise Figure Measurements in Phase-Insensitive and Phase-Sensitive Fiber Parametric Amplifier Cascade," *Optical Fiber Communication Conference (OFC)*, p. OWT4, Jan. 2010.

[103] Z. Tong, A. Bogris, M. Karlsson, and P. A. Andrekson, "Full characterization of the signal and idler noise figure spectra in single-pumped fiber optical parametric amplifiers," *Optics Express*, vol. 18, no. 3, pp. 2884–2893, 2010.

[104] R.-D. Li, P. Kumar, W. L. Kath, and J. N. Kutz, "Combating dispersion with parametric amplifiers," *IEEE Photonics Technology Letters*, vol. 5, no. 6, pp. 669–672, 1993.

[105] R.-D. Li, P. Kumar, and W. L. Kath, "Dispersion compensation with phase-sensitive optical amplifiers," *Journal of Lightwave Technology*, vol. 12, no. 3, pp. 541–549, 1994.

[106] R. Loudon, *The quantum theory of light.* Oxford University Press, 2000.

[107] D. F. Walls, "Squeezed states of light," *Nature*, vol. 306, no. 10, pp. 141–146, 1983.

[108] R. Glauber, "Coherent and Incoherent States of the Radiation Field," *Physical Review*, vol. 131, pp. 2766–2788, Sept. 1963.

[109] H. Vahlbruch, M. Mehmet, S. Chelkowski, B. Hage, A. Franzen, N. Lastzka, S. Gossler, K. Danzmann, and R. Schnabel, "Observation of squeezed light with 10-dB quantum-noise reduction," *Physical Review Letters*, vol. 100, no. 3, pp. 033602–033606, 2008.

[110] D. Levandovsky, M. Vasilyev, and P. Kumar, "Amplitude squeezing of light by means of a phase-sensitive fiber parametric amplifier," *Optics Letters*, vol. 24, no. 14, pp. 984–986, 1999.

[111] C. J. McKinstrie and S. Radic, "Phase-sensitive amplification in a fiber," *Optics Express*, vol. 12, no. 20, pp. 4973–4979, 2004.

[112] C. J. McKinstrie, "Everything You Always Wanted to Know About Cascaded Parametric Amplifiers, but Were Afraid to Ask," *Optical Fiber Communication Conference (OFC)*, p. OTh1C.5, 2012.

[113] C. J. McKinstrie and J. Gordon, "Field fluctuations produced by parametric processes in fibers," *IEEE Journal of Selected Topics in Quantum Electronics*, vol. 18, no. 2, pp. 958–969, 2012.

[114] R. Tang, P. S. Devgan, V. S. Grigoryan, P. Kumar, and M. Vasilyev, "In-line phase-sensitive amplification of multi-channel CW signals based on frequency nondegenerate four-wave-mixing in fiber," *Optics Express*, vol. 16, no. 12, pp. 9046–9053, 2008.

[115] N. J. Doran and D. Wood, "Nonlinear-optical loop mirror," *Optics Letters*, vol. 13, no. 1, pp. 56–58, 1988.

[116] I. Bar-Joseph, A. A. Friesem, R. G. Waarts, and H. H. Yaffe, "Parametric interaction of a modulated wave in a single-mode fiber," *Optics Letters*, vol. 11, no. 8, pp. 534–536, 1986.

[117] R. Tang, P. Devgan, P. L. Voss, V. S. Grigoryan, and P. Kumar, "In-line frequency-nondegenerate phase-sensitive fiber-optical parametric amplifier," *IEEE Photonics Technology Letters*, vol. 17, no. 9, pp. 1845–1847, 2005.

[118] R. Tang, J. Lasri, P. Devgan, V. S. Grigoryan, P. Kumar, and M. Vasilyev, "Gain characteristics of a frequency nondegenerate phase-sensitive fiber-optic parametric amplifier with phase self-stabilized input," *Optics Express*, vol. 13, no. 26, pp. 10483–10493, 2005.

[119] I. Kim, K. Croussore, X. Li, and G. Li, "All-Optical Carrier Synchronization Using a Phase-Sensitive Oscillator," *IEEE Photonics Technology Letters*, vol. 19, no. 13, pp. 987–989, 2007.

[120] G.-W. Lu and T. Miyazaki, "Optical Phase Add–Drop for Format Conversion Between DQPSK and DPSK and its Application in Optical Label Switching Systems," *IEEE Photonics Technology Letters*, vol. 21, no. 5, pp. 322–324, 2009.

[121] J. Kakande, A. Bogris, R. Slavík, F. Parmigiani, D. Syvridis, P. Petropoulos, and D. J. Richardson, "First Demonstration of All-Optical QPSK Signal Regeneration in a Novel Multi-Format Phase Sensitive Amplifier," in *European Conference on Optical Communication (ECOC)*, p. PDP, 2010.

[122] J. Kakande, R. Slavík, F. Parmigiani, A. Bogris, D. Syvridis, L. Grüner-Nielsen, R. Phelan, P. Petropoulos, and D. J. Richardson, "Multilevel quantization of optical phase in a novel coherent parametric mixer architecture," *Nature Photonics*, vol. 5, pp. 748–752, Oct. 2011.

[123] A. Bordonalli, C. Walton, and A. J. Seeds, "High-performance phase locking of wide linewidth semiconductor lasers by combined use of optical injection locking and optical phase-lock loop," *Journal of Lightwave Technology*, vol. 17, no. 2, pp. 328–342, 1999.

[124] J. Pezeshki, M. Saylors, H. Mandelberg, and J. Goldhar, "Amplitude modulation transfer in an injection-locked DFB semiconductor laser," *IEEE Photonics Technology Letters*, vol. 17, no. 11, pp. 2433–2435, 2005.

[125] B. Corcoran, S. L. I. Olsson, C. Lundström, M. Karlsson, and P. A. Andrekson, "Phase-Sensitive Optical Pre-Amplifier Implemented in an 80km DQPSK Link," *Optical Fiber Communication Conference (OFC)*, p. PDP5A.4, 2012.

[126] K. Croussore, I. Kim, C. Kim, Y. Han, and G. Li, "Phase-and-amplitude regeneration of differential phase-shift keyed signals using a phase-sensitive amplifier," *Optics Express*, vol. 14, no. 6, pp. 2085–2094, 2006.

[127] A. Bogris and D. Syvridis, "RZ-DPSK signal regeneration based on dual-pump phase-sensitive amplification in fibers," *IEEE Photonics Technology Letters*, vol. 18, no. 20, pp. 2144–2146, 2006.

[128] R. Laming, M. Zervas, and D. Payne, "Erbium-doped fiber amplifier with 54 dB gain and 3.1 dB noise figures," *IEEE Photonics Technology Letters*, vol. 4, no. 12, pp. 1345–1347, 1992.

[129] G. P. Agrawal, *Lightwave technology: telecommunication systems*. Wiley Interscience, 2005.

[130] Z. Tong, A. Bogris, C. Lundström, C. J. McKinstrie, M. Vasilyev, M. Karlsson, and P. A. Andrekson, "Modeling and measurement of the noise figure of a cascaded non-degenerate phase-sensitive parametric amplifier," *Optics Express*, vol. 18, no. 14, pp. 14820–14835, 2010.

[131] Z. Tong, C. J. McKinstrie, C. Lundström, M. Karlsson, and P. A. Andrekson, "Noise performance of optical fiber transmission links that use non-degenerate cascaded phase-sensitive amplifiers," *Optics Express*, vol. 18, no. 15, pp. 15426–15439, 2010.

[132] C. J. McKinstrie and N. Alic, "Information efficiencies of parametric devices," *IEEE Journal of Selected Topics in Quantum Electronics*, vol. 18, no. 2, pp. 794–811, 2012.

[133] P. Kylemark, M. Karlsson, and P. A. Andrekson, "Gain and wavelength dependence of the noise-figure in fiber optical parametric amplification," *IEEE Photonics Technology Letters*, vol. 18, no. 11, pp. 1255–1257, 2006.

[134] S. L. I. Olsson, B. Corcoran, C. Lundström, E. Tipsuwannakul, S. Sygletos, A. D. Ellis, Z. Tong, M. Karlsson, and P. A. Andrekson, "Optical injection-locking-based pump recovery for phase-sensitively amplified links," in *Optical Fiber Communication Conference (OFC)*, p. OW3C.3, 2012.

[135] "ModeGap - Multi-mode capacity enhancement with PBG fiber." `http://www.modegap.eu/`.

[136] Z. Tong, C. Lundström, M. Karlsson, M. Vasilyev, and P. A. Andrekson, "Noise performance of a frequency nondegenerate phase-sensitive amplifier with unequalized inputs," *Optics Letters*, vol. 36, no. 5, pp. 722–724, 2011.

[137] T. Richter, B. Corcoran, S. L. I. Olsson, C. Lundström, M. Karlsson, C. Schubert, and P. A. Andrekson, "Experimental Characterization of a Phase-Sensitive Four-Mode Fiber-Optic Parametric Amplifier," *To be presented at the European Conference on Optical Communication (ECOC)*, 2012.

[138] S. Radic, "Parametric Signal Processing," *IEEE Journal of Selected Topics in Quantum Electronics*, vol. 18, no. 2, pp. 670–680, 2012.

[139] X. Feng, A. K. Mairaj, D. W. Hewak, and T. M. Monro, "Nonsilica glasses for holey fibers," *Journal of Lightwave Technology*, vol. 23, pp. 2046–2054, June 2005.

[140] S. Zlatanovic, J. Park, F. Gholami, J. Chavez Boggio, S. Moro, N. Alic, S. Mookherjea, and S. Radic, "Mid-Infrared Wavelength Conversion in Silicon Waveguides Pumped by Silica-Fiber-Based Source," *IEEE Journal of Selected Topics in Quantum Electronics*, vol. 18, no. 2, pp. 612–620, 2012.

[141] S. Zlatanovic, J. S. Park, S. Moro, J. M. C. Boggio, I. B. Divliansky, N. Alic, S. Mookherjea, and S. Radic, "Mid-infrared wavelength conversion in silicon waveguides using ultracompact telecom-band-derived pump source," *Nature Photonics*, vol. 4, no. 8, pp. 561–564, 2010.

[142] L. K. Oxenlowe, J. Hua, M. Galili, M. Pu, H. Hu, H. C. Hansen Mulvad, K. Yvind, J. Hvam, A. T. Clausen, and P. Jeppesen, "Silicon Photonics for Signal Processing of Tbit/s Serial Data Signals," *IEEE Journal of Selected Topics in Quantum Electronics*, vol. 18, pp. 996–1004, Feb. 2012.

[143] M. A. F. Roelens, S. Frisken, J. Bolger, D. Abakoumov, G. Baxter, S. Poole, and B. J. Eggleton, "Dispersion Trimming in a Reconfigurable Wavelength Selective Switch," *Journal of Lightwave Technology*, vol. 26, no. 1, pp. 73–78, 2008.

Chapter A

Appendix

In this Appendix we derive the expressions for the phase-to-phase and phase-to-power transfer functions of a single-pumped non-degenerate-idler PSA in the small-signal regime. We also highlight some limit cases. Henceforth, we shall refer to the case of no input idler as PI-case, and the case of equal input signal and idler power and phase ($P_{s,\text{in}} = P_{i,\text{in}}$, $\theta_{s,\text{in}} = \theta_{i,\text{in}}$) as the ideal PS-case. We also consider the nonlinear fiber to be lossless, but one can easily account for loss by replacing L by L_{eff} throughout the Appendix.

A.1 General phase-to-power and phase-to-phase transfer functions of a fiber PSA

Starting from Eq. 4.1 we know that:

$$P_{s,\text{out}} = |A_{s,\text{out}}|^2 = |\mu A_{s,\text{in}} + \nu A^*_{i,\text{in}}|^2. \tag{A.1}$$

By rewriting the signal and idler fields in terms of their powers P and phases θ (relative to that of the pump), such that:

$$A_{s,i} = \sqrt{P_{s,i}} \cdot \exp\left(i\theta_{s,i}\right) \tag{A.2}$$

we can easily find a general expression for the output signal power as

$$P_{s,\text{out}} = |\mu|^2 P_{s,\text{in}} + |\nu|^2 P_{i,\text{in}} + 2|\mu||\nu|\sqrt{P_{s,\text{in}} P_{i,\text{in}}} \cdot \cos\left(\Delta_\theta\right) \tag{A.3}$$

with $\Delta_\theta = \theta_\mu - \theta_\nu + \theta_{s,\text{in}} + \theta_{i,\text{in}}$, where we have defined $\theta_{\mu,\nu}$ as the phase angles of the complex transfer functions. We may observe that the first two terms of the right

hand side of Eq. A.3 corresponds to the PI-gain of the signal and PI-wavelength conversion of the idler, respectively. These two terms cannot be negative. The last term is responsible for the additional coherent gain or attenuation when both signal and idler are present at the input, and is the phase-dependent term. This term can be both positive and negative. It is also immediately apparent that in the PI-case, any dependence on the signal phase vanishes, as should be expected, and the PI-gain is $|\mu|^2$. Finally, one may easily find that if $P_{s,\mathrm{in}} = P_{i,\mathrm{in}}$, then the signal gain $G = P_{s,\mathrm{out}}/P_{s,\mathrm{in}}$ is

$$G = |\mu|^2 + |\nu|^2 + 2|\mu||\nu| \cdot \cos(\Delta_\theta) \tag{A.4}$$

with extremas $G_{\mathrm{max,min}} = (|\mu| \pm |\nu|)^2$, and hence $G_{\mathrm{min}} = 1/G_{\mathrm{max}}$ for all μ and ν.

From Eq. 2.32 we have the expressions for the transfer coefficients μ and ν as:

$$\mu = \cosh(gL) - i\frac{\kappa}{2g}\sinh(gL) \tag{A.5}$$

and

$$\nu = i\frac{(\gamma P_p)}{g}\sinh(gL) \tag{A.6}$$

with the phase angles of μ and ν, respectively, being $\theta_\mu = -\frac{\kappa \tanh(gL)}{2g}$ and $\theta_\nu = \pi/2$. Furthermore[1],

$$|\mu|^2 = 1 + \frac{(\gamma P_p)^2}{g^2}\sinh^2(gL) \tag{A.7}$$

and

$$|\nu|^2 = \frac{(\gamma P_p)^2}{g^2}\sinh^2(gL). \tag{A.8}$$

Hence, μ and ν fulfills the relation $|\mu|^2 - |\nu|^2 = 1$.

Starting out by rewriting the right hand side of Eq. A.3 using a standard trigonometric identity as

$$\begin{aligned} P_{s,\mathrm{out}} &= |\mu|^2 P_{s,\mathrm{in}} + |\nu|^2 P_{i,\mathrm{in}} \\ &+2|\nu|\sqrt{P_{s,\mathrm{in}}P_{i,\mathrm{in}}} \cdot \left[|\mu|\cos(\theta_\mu) \cdot \cos(-\theta_\nu + \theta_s + \theta_i) + |\mu|\sin(\theta_\mu) \cdot \sin(-\theta_\nu + \theta_s + \theta_i)\right], \end{aligned} \tag{A.9}$$

realizing that $|\mu|\cos\theta_\mu = \mathrm{Re}(\mu)$ and $|\mu|\sin\theta_\mu = \mathrm{Im}(\mu)$, and inserting the expressions for μ and ν we find that we can write the full expression for the output power in

[1]While the result for $|\mu|^2$ may not be immediately obvious, it can be found by inserting the expressions for κ (Eq. 2.24) and g (Eq. 2.28) into Eq. A.5 and using the relation $\cosh^2(x) = 1 - \sinh^2(x)$.

the general case as:

$$\begin{aligned} P_{s,\text{out}} &= P_{s,\text{in}} + (P_{s,\text{in}} + P_{i,\text{in}})\,\frac{(\gamma P_p)^2}{g^2}\sinh^2(gL) \\ &\quad + 2\sinh(gL)\frac{(\gamma P_p)}{g}\sqrt{P_{s,\text{in}}P_{i,\text{in}}}\cdot \\ &\quad \cdot\left(\frac{\kappa}{2g}\sinh(gL)\cos\left(\theta_{s,\text{in}}+\theta_{i,\text{in}}\right)+\cosh(gL)\sin\left(\theta_{s,\text{in}}+\theta_{i,\text{in}}\right)\right). \end{aligned} \tag{A.10}$$

To retrieve the output signal phase we start from the expression for the output signal field:

$$\begin{aligned} A_{s,\text{out}} &= \mu A_{s,\text{in}} + \nu A^*_{i,\text{in}} \\ &= |\mu|e^{i\theta_\mu}\sqrt{P_{s,\text{in}}}e^{i\theta_{s,\text{in}}} + |\nu|e^{i\theta_\nu}\sqrt{P_{i,\text{in}}}e^{-i\theta_{i,\text{in}}}. \end{aligned} \tag{A.11}$$

Thus, the general expression for the output signal phase becomes:

$$\begin{aligned} \tan(\theta_{s,\text{out}}) &= \frac{\text{Im}(A_{s,\text{out}})}{\text{Re}(A_{s,\text{out}})} \\ &= \frac{|\mu|\sqrt{P_{s,\text{in}}}\sin\left(\theta_\mu+\theta_{s,\text{in}}\right)+|\nu|\sqrt{P_{i,\text{in}}}\sin\left(\theta_\nu-\theta_{i,\text{in}}\right)}{|\mu|\sqrt{P_{s,\text{in}}}\cos\left(\theta_\mu+\theta_{s,\text{in}}\right)+|\nu|\sqrt{P_{i,\text{in}}}\cos\left(\theta_\nu-\theta_{i,\text{in}}\right)}. \end{aligned} \tag{A.12}$$

Clearly, the output phase is dependent on the transfer coefficients as well as the signal and idler input powers and phases. In the PI-case, the terms containing the idler power vanishes and all that remains is:

$$\begin{aligned} \theta_{s,out} &= \arctan\left[\frac{|\mu|\sqrt{P_{s,\text{in}}}\sin\left(\theta_\mu+\theta_{s,\text{in}}\right)}{|\mu|\sqrt{P_{s,\text{in}}}\cos\left(\theta_\mu+\theta_{s,\text{in}}\right)}\right] \\ &= \theta_\mu + \theta_{s,\text{in}}, \end{aligned} \tag{A.13}$$

i.e. the output signal phase is equal to the input signal phase (plus a constant phase shift). We can also see that in the ideal PS-case, the dependence on input signal/idler power vanishes, meaning that in the general case, the output phase is only dependent on the ratio between signal and idler power and not the absolute power (as long as we remain in the small-signal regime).

Inserting the expressions for μ and ν into Eq. A.12 and following the same method as above to rewrite in terms of the real and imaginary parts of μ and ν, we

find that the output phase is given by

$$\tan(\theta_{s,\mathrm{out}}) = \frac{\sqrt{P_{s,\mathrm{in}}}\left[\cosh(gL)\sin(\theta_{s,\mathrm{in}}) - \frac{\kappa}{2g}\sinh(gL)\cos(\theta_{s,\mathrm{in}})\right] + \sqrt{P_{i,\mathrm{in}}}\left[\frac{\gamma P_p}{g}\sinh(gL)\cos(\theta_{i,\mathrm{in}})\right]}{\sqrt{P_{s,\mathrm{in}}}\left[\cosh(gL)\cos(\theta_{s,\mathrm{in}}) + \frac{\kappa}{2g}\sinh(gL)\sin(\theta_{s,\mathrm{in}})\right] + \sqrt{P_{i,\mathrm{in}}}\left[\frac{\gamma P_p}{g}\sinh(gL)\sin(\theta_{i,\mathrm{in}})\right]}. \tag{A.14}$$

A.2 Special cases

Perfect phase-matching (Exponential gain regime)

In the case of perfect phase matching, $\kappa = 0$ and $g = \gamma P_p$ so that $\mu = \cosh(gL)$ and $\nu = i\sinh(gL)$. Then, the output signal power of Eq. A.10 simplifies to

$$\begin{aligned} P_{s,\mathrm{out}} = \quad & P_{s,\mathrm{in}} + (P_{s,\mathrm{in}} + P_{i,\mathrm{in}})\sinh^2(gL) \\ & + \sinh(2gL)\sqrt{P_{s,\mathrm{in}}P_{i,\mathrm{in}}}\cdot\sin(\theta_{s,\mathrm{in}} + \theta_{i,\mathrm{in}}), \end{aligned} \tag{A.15}$$

where the relation $2\cosh(x)\cdot\sinh(x) = \sinh(2x)$ was used.

In the ideal PS-case, this simplifies further to:

$$P_{s,\mathrm{out}} \quad = \quad P_{s,\mathrm{in}}\left[1 + 2\sinh^2(gL) + \sinh(2gL)\cdot\sin(2\theta_{s,\mathrm{in}})\right], \tag{A.16}$$

which may be expressed in exponential functions as

$$P_{s,\mathrm{out}} = \frac{P_{s,\mathrm{in}}}{2}\left[e^{2gL} + e^{-2gL} + \left(e^{2gL} - e^{-2gL}\right)\cdot\sin(2\theta_{s,\mathrm{in}})\right]. \tag{A.17}$$

It is then readily seen that the maximum and minimum values of the gain $G = P_{\mathrm{s,out}}/P_{\mathrm{s,in}}$ is $G_{\mathrm{max,min}} = \exp(\pm 2gL)$, respectively.

The phase-to-phase transfer function, in the case of ideal phase matching, simplifies to

$$\tan(\theta_{s,\mathrm{out}}) = \frac{\sqrt{P_{s,\mathrm{in}}}\left[\cosh(gL)\sin(\theta_{s,\mathrm{in}})\right] + \sqrt{P_{i,\mathrm{in}}}\left[\sinh(gL)\cos(\theta_{i,\mathrm{in}})\right]}{\sqrt{P_{s,\mathrm{in}}}\left[\cosh(gL)\cos(\theta_{s,\mathrm{in}})\right] + \sqrt{P_{i,\mathrm{in}}}\left[\sinh(gL)\sin(\theta_{i,\mathrm{in}})\right]}, \tag{A.18}$$

which, in the ideal PS-case, may be further simplified as

$$\tan(\theta_{s,\mathrm{out}}) = \frac{\left[\cosh(gL)\sin(\theta_{s,\mathrm{in}})\right] + \left[\sinh(gL)\cos(\theta_{s,\mathrm{in}})\right]}{\left[\cosh(gL)\cos(\theta_{s,\mathrm{in}})\right] + \left[\sinh(gL)\sin(\theta_{s,\mathrm{in}})\right]}. \tag{A.19}$$

In the limit of large gain, i.e. $gL >> 1$, $\cosh(gL) \approx \sinh(gL) >> 1$. Then, the dependence on the gL-product vanishes in Eq. A.19, and all that remains is

$$\tan(\theta_{s,\text{out}}) = 1 \tag{A.20}$$

with solutions $\theta_{s,\text{out}} = \pi/4, 5\pi/4, ...$ Conversely, in the unity-gain limit, i.e. $gL \to 0$, $\cosh(gL) = 1$ and $\sinh(gL) = 0$. Then, one finds from Eq. A.19 that $\theta_{s,\text{out}} \to \theta_{s,\text{in}}$.

Quadratic gain-regime

In the quadratic gain regime, $\kappa = 2\gamma P_p$ and $g = 0$. Using the Taylor series expansions of the hyperbolic functions, we can find that $\mu = 1 - i\gamma P_p L$ and $\nu = i\gamma P_p L$. Then, the output signal power becomes

$$\begin{aligned} P_{s,\text{out}} =& P_{s,\text{in}} + (P_{s,\text{in}} + P_{i,\text{in}}) \cdot (\gamma P_p L)^2 + 2\sqrt{P_{s,\text{in}} P_{i,\text{in}}} \cdot \\ & \cdot \left[(\gamma P_p L) \cdot \sin(\theta_{s,\text{in}} + \theta_{i,\text{in}}) + (\gamma P_p L)^2 \cdot \cos(\theta_{s,\text{in}} + \theta_{i,\text{in}}) \right] \\ =& P_{s,\text{in}} + (P_{s,\text{in}} + P_{i,\text{in}}) \cdot (\gamma P_p L)^2 + 2\sqrt{P_{s,\text{in}} P_{i,\text{in}}} \cdot \\ & (\gamma P_p L) \cdot \sqrt{1 + (\gamma P_p L)^2} \cdot \sin(\theta_{s,\text{in}} + \theta_{i,\text{in}} + \arctan(\gamma P_p L)). \end{aligned} \tag{A.21}$$

In the ideal PS-case, this simplifies to

$$P_{s,\text{out}} = P_{s,\text{in}} \left[1 + 2(\gamma P_p L)^2 \left(1 + \sqrt{(1 + (\gamma P_p L)^{-2}} \cdot \sin(2\theta_{s,\text{in}} + \arctan(\gamma P_p L)) \right) \right]. \tag{A.22}$$

with the maximum and minimum values of the gain being $G_{\text{max,min}} = \left(\sqrt{1 + (\gamma P_p L)} \pm \gamma P_p L \right)^2$, respectively.

The phase-to-phase transfer function in the quadratic gain regime becomes

$$\tan(\theta_{s,\text{out}}) = \frac{\sqrt{P_{s,\text{in}}} \left[\sin(\theta_{s,\text{in}}) - (\gamma P_p L) \cos(\theta_{s,\text{in}}) \right] + \sqrt{P_{i,\text{in}}} (\gamma P_p L) \cos(\theta_{i,\text{in}})}{\sqrt{P_{s,\text{in}}} \left[\cos(\theta_{s,\text{in}}) + (\gamma P_p L) \sin(\theta_{s,\text{in}}) \right] + \sqrt{P_{i,\text{in}}} (\gamma P_p L) \sin(\theta_{i,\text{in}})}, \tag{A.23}$$

which, in the ideal PS-case, reduces to

$$\tan(\theta_{s,\text{out}}) = \frac{\sin(\theta_{s,\text{in}})}{\cos(\theta_{s,\text{in}}) + (2\gamma P_p L) \sin(\theta_{s,\text{in}})}. \tag{A.24}$$

Here, it is easy to see that in the limit $2\gamma P_p L \to 0$ i.e. when the gain goes toward unity, then $\theta_{s,\text{out}} \to \theta_{s,\text{in}}$, and in the limit $2\gamma P_p L >> 1$ i.e. when the gain is large, then

$$\tan(\theta_{s,\text{out}}) \to 0 \tag{A.25}$$

with solutions $\theta_{s,\text{out}} = 0, \pi, ...$